RANDOM FINITE SET INFORMATION-THEORETIC SENSOR CONTROL FOR AUTONOMOUS MULTI-SENSOR MULTI-OBJECT SURVEILLANCE

A Dissertation

Presented to the Faculty of the Graduate School

of Cornell University

in Partial Fulfillment of the Requirements for the Degree of

Doctor of Philosophy

by

Keith Allen LeGrand

August 2022

RANDOM FINITE SET INFORMATION-THEORETIC SENSOR CONTROL FOR AUTONOMOUS MULTI-SENSOR MULTI-OBJECT SURVEILLANCE

Keith Allen LeGrand, Ph.D.
Cornell University 2022

Tracking multiple moving objects in complex environments is a key objective of many robotic and aerospace surveillance systems. In the Bayesian multi-object tracking framework, noisy sensor measurements are assimilated over time to form probabilistic beliefs, namely probability densities, of the multi-object state by virtue of Bayes' rule. This dissertation shows that, using probabilistic beliefs and environmental feedback, intelligent sensors can also optimize the value of information gathered in real time by means of information-driven control. In particular, it is shown that in object tracking applications, sensor actions can be optimized based on the expected reduction in uncertainty or information gain estimated from probabilistic beliefs for future sensor measurements. When compared to traditional estimation problems, the problem of estimating the information value for multi-object surveillance is more challenging due to unknown object-measurement association and unknown object existence. The advent of random finite set (RFS) theory has provided a formalism for quantifying and estimating information gain in multi-object tracking problems. However, direct computation of many relevant RFS functions, including posterior density functions and predicted information gain functions, is often intractable and requires principled approximation.

This dissertation presents new theory, approximations, and algorithms related to autonomous multi-sensor multi-object surveillance. A new approach is presented for systematically incorporating ambiguous inclusion/exclusion type evidence, such

as the non-detection of an object within a known sensor field-of-view (FoV). The resulting state estimation problem is nonlinear and solved using a new Gaussian mixture approximation achieved through recursive component splitting. Based on this approximation, a novel Gaussian mixture Bernoulli filter for imprecise measurements is derived. The filter can accommodate "soft" data from human sources and is demonstrated in a tracking problem using only natural language statements as inputs. This dissertation further investigates the relationship between bounded FoVs and cardinality distributions for a representative selection of multi-object distributions. These new FoV cardinality distributions can be used for sensor planning, as is demonstrated through a problem involving a multi-Bernoulli process with up to one hundred potential objects.

Finally, a new tractable approximation is presented for RFS expected information gain that is applicable to sensor control in multi-sensor multi-object search-while-tracking problems. Unlike existing RFS approaches, the approximation presented in this dissertation accounts for multiple measurement outcomes due to noise, missed detections, false alarms, and object appearance/disappearance. The effectiveness of the information-driven sensor control is demonstrated through a multi-vehicle search-while-tracking experiment using real video data from a remote optical sensor.

BIOGRAPHICAL SKETCH

Keith A. LeGrand is a Ph.D. candidate in the Laboratory for Intelligent Systems and Controls (LISC) at Cornell University and a National Defense Science and Engineering Graduate (NDSEG) Fellow. Prior to that, he was a Senior Member of Technical Staff at Sandia National Laboratories in Albuquerque, New Mexico where he conducted research in inertial navigation, space systems, and multi-object tracking. He received the B.S. and M.S. degrees in Aerospace Engineering from the Missouri University of Science and Technology.

Dedicated to my family, especially my devoted and supportive wife, Samantha.

ACKNOWLEDGEMENTS

This work was supported in part by the National Defense Science and Engineering Graduate (NDSEG) fellowship, Office of Naval Research Grant N0014-19-1-2266, and the Laboratory Directed Research and Development program at Sandia National Laboratories.

TABLE OF CONTENTS

LIST OF TABLES

LIST OF FIGURES

CHAPTER 1

INTRODUCTION

Beginning with the seminal work of Rudolf Kalman in 1960 [59], state estimation theory has enabled the development of algorithms that are now ubiquitous in modern robotic and aerospace systems. In particular, the state estimation problem known as *object tracking* [7] is characterized by the estimation of the motion of remote objects that are subject to unknown random inputs. Many tracking applications also require the simultaneous estimation of multiple objects' states. Such problems are the subject of multi-object (a.k.a. multitarget) tracking theory [88, 15, 16, 9], as pioneered by Bar-Shalom in the 1970s [8, 9]. Multi-object tracking problems arise in a broad range of important and timely applications, including but not limited to space situational awareness (SSA) [26, 46, 45, 38, 39, 98, 66, 64, 63, 20], ground vehicle tracking [29, 69, 68, 13], terrain navigation [77, 78], simultaneous localization and mapping (SLAM) [44, 31], cell microscopy [52], anti-submarine warfare [30], maritime ship tracking [27], swarm control [28, 35], pedestrian tracking [87, 82, 53], audio processing [22], and cyber-security [36]. While intimately linked, multi-object tracking theory is a nontrivial generalization of traditional tracking and estimation theory. This additional complexity is partly due to the unknown origin of measurements that is fundamental to multi-object problems, and which generally requires combinatorial optimization over measurement/track assignments.

Modern surveillance systems increasingly employ autonomous and reconfigurable sensors that are able to control the quality of future measurements by deciding sensor mode and motion variables, such as translation, rotation, zoom, beam-forming, and frequency selection. In principle, a so-called intelligent sensor can automate the selection of measurements through feedback control such that it collects the most relevant and informative measurements based on the underlying estimation objective. In *information-theoretic* planning and control [48, 75, 34], sensing actions are determined based on theoretically rigorous objectives that quantify the information value of measurements under each possible sensor state. In contrast, *task-driven* control policies are developed to be tailored to a specific sensor and application and often do not generalize beyond the original scope for which they were designed.

Recently, random finite set (RFS) theory has emerged as a powerful and unifying Bayesian framework for solving multi-sensor multi-object tracking and information-driven control problems [41, 74, 75]. Central to RFS theory is the representation of state and measurement as finite sets, whose elements *and size* are random quantities. By this representation, the uncertainties associated with dynamic disturbances, object appearance/disappearance, measurement noise, spurious detections, and missed detections are all captured by set-based multi-object density functions. Equipped with the RFS, multi-object density, and the appropriate set calculus, the concepts of divergence and information gain are then elegantly lifted from traditional estimation theory to the complex multi-sensor multi-object setting, enabling, in principle, theoretically rigorous multi-sensor multi-object information-driven control [92, 11].

Despite the power of the RFS information-driven control formulation, significant challenges arise its application to real-world search-while-tracking (SWT) problems. RFS tracking algorithms are predominantly implemented in either particle [111] or Gaussian mixture (GM) form. GM implementations offer distinct advantages over the former. GM representations are not as severely limited by the curse of dimensionality, are generally more computationally efficient, and are conducive to meaningful multi-sensor fusion. Yet existing GM RFS multi-object trackers lack the ability to account for bounded sensor field-of-view (FoV) geometry and are ill-suited for incorporating soft data from human sources or other forms of imprecise information. Furthermore, while RFS information gain functions are symbolically simple expressions, no computationally practical approaches exist for accurately approximating the *expected* information gain, which is the foundation of information-driven control objectives [49, 34]. The intractability of RFS information gain expectations is further exacerbated when considering the joint information value from multiple sensors, particularly when sensor FoVs overlap. Thus, principled and accurate approximations of the expected information gain are needed to enable real-time information-driven control.

Chapter 3 presents new methods for incorporating imprecise and negative information in GM based RFS filtering. The approach recursively splits GM probability density function (pdf) components near sensor FoV boundaries such that the information content of non-detections can be leveraged in a Bayesian framework. The developed approach is more generally applicable to broad categories of inclusion/exclusion type evidence in GM RFS filtering. To demonstrate this fact, a novel GM Bernoulli filter for imprecise measurements is derived and demonstrated in a tracking problem where measurements take the form of natural language statements from human observers. The role of bounded FoV geometry is also considered in the context of object cardinality distributions. Using finite set statistics (FISST), expressions are derived for describing object cardinality probabilities within bounded FoVs, which may be used as general figures of merit or as a principled basis for sensor placement.

Chapter 4 presents a novel information-theoretic approach to single-sensor multi-object autonomous SWT. Existing RFS sensor control research has largely focused on the development of information gain functions for a variety of prior distribution classes. Yet, little attention has been given to computationally tractable techniques for accurately *forecasting* information gain in these settings. As such, this work presents a new principled approximation of the multi-object information gain *expectation*, which is shown to lead to improved tracking performance in an experiment using real video data. A new joint probabilistic representation for discovered and undiscovered objects is proposed within this framework that enables efficient SWT and more readily scales to large geographic regions compared to existing representations.

Building on the theory developed in Chapter 4, Chapter 5 presents a derivation of information gain functions and approximate expectations for autonomous *multi-sensor* multi-object SWT. The multi-sensor control problem is shown to be a nontrivial extension of the single-sensor problem, particularly when sensor FoVs are not restricted to be disjoint. Thus, additional constraints and optimization techniques are required to enable computationally practical solutions. The multi-sensor control approach is demonstrated in an SWT problem, and the performance is compared for different numbers of sensors. An analysis shows the importance of allowing dynamic sensor FoV overlap, which in many instances provides higher information value than disjoint sensor coverage.

CHAPTER 2

BACKGROUND

2.1 Notation

Throughout this dissertation, single-object states are represented by lowercase letters (e.g. $\mathbf{x}$, $\mathring{x}$), while multi-object states are represented by italic uppercase letters (e.g. X, $\mathring{X}$). Bold lowercase letters are used to denote vectors (e.g. $\mathbf{x}$, $\mathbf{y}$), and bold uppercase letters are used to denote matrices (e.g. $\mathbf{P}$, $\mathbf{\Lambda}$). The accent "$\circ$" is used to distinguish labeled states and functions (e.g. $\mathring{f}$, $\mathring{x}$, $\mathring{X}$) from their unlabeled equivalents. Spaces are represented by blackboard bold symbols (e.g. $\mathbb{X}$, $\mathbb{L}$).

For brevity, the multi-object exponential notation,

$$h^A \triangleq \prod_{a \in A} h(a) \tag{2.1}$$

where $h^{\emptyset} \triangleq 1$, is adopted throughout. For multivariate functions, the dot "$\cdot$" denotes the argument of the multi-object exponential, e.g.:

$$[g(a, \cdot, c)]^B \triangleq \prod_{b \in B} g(a, b, c) \tag{2.2}$$

The exponential notation is used to denote the product space, $\mathbb{X}^n = \prod^n (\mathbb{X} \times)$. Exponents of finite sets are used to denote finite sets of a given cardinality, e.g. $|X^n| = n$, where n is the cardinality. The set of natural numbers less than or equal to n is denoted by

$$\mathbb{N}_n \triangleq \{1, \ldots, n\} \tag{2.3}$$

The operator $\mathrm{diag}(\cdot)$ places its input on the diagonal of the zero matrix. The

Kronecker delta function is defined as

$$\delta_{\boldsymbol{a}}(\boldsymbol{b}) \triangleq \begin{cases} 1, & \text{if } \boldsymbol{b} = \boldsymbol{a} \\ 0, & \text{otherwise} \end{cases} \tag{2.4}$$

for any two arbitrary vectors $\boldsymbol{a}$, $\boldsymbol{b} \in \mathbb{R}^n$. The inner product of two integrable functions $f(\cdot)$ and $g(\cdot)$ is denoted by

$$\langle f, g \rangle = \int f(\mathbf{x}) g(\mathbf{x}) \mathrm{d}\mathbf{x} \tag{2.5}$$

2.2 Bayesian State Estimation

The Bayesian approach to state estimation is distinct from central-moment-based approaches such as the Kalman filter, extended Kalman filter (EKF), and unscented Kalman filter (UKF), in that it constructs the full posterior pdf at each time step given all available measurement information up to the present time. In the Bayesian approach, both the state $\mathbf{x}_k \in \mathbb{R}^{n_x}$ and measurement $\mathbf{z}_k \in \mathbb{R}^{n_z}$ evolve stochastically according to a sequence of conditional probability distributions [96]

$$\mathbf{x}_k \sim p_{k-1}(\mathbf{x}_k | \mathbf{x}_{k-1}) \tag{2.6}$$

$$\mathbf{z}_k \sim g_k(\mathbf{z}_k | \mathbf{x}_k) \tag{2.7}$$

for $k = 1, 2, \ldots$, where $p_{k-1}(\mathbf{x}_k | \mathbf{x}_{k-1})$ denotes the Markov state transition density and $g_k(\mathbf{z}_k | \mathbf{x}_k)$ is the measurement likelihood function.

2.2.1 Bayes Filter Recursion

Under the standard model (2.6)-(2.7), the Bayes filtering equations presented in this subsection are the general equations for computing Bayesian prior and posterior distributions for both linear/nonlinear and Gaussian/non-Gaussian state space models [96]. Assume that the initial pdf $p_0(\mathbf{x}_0)$ is known. Denote the *prior* density at time k by $p_{k|k-1}(\mathbf{x}_k, \mathbf{z}_{0:k-1})$, the *posterior* density at time $k-1$ by $p_{k-1|k-1}(\mathbf{x}_{k-1}|\mathbf{z}_{0:k-1})$. The forward prediction is given by the Chapman-Kolmogorov equation [56]

$$p_{k|k-1}(\mathbf{x}_k|\mathbf{z}_{0:k-1}) = \int p_{k-1}(\mathbf{x}_k|\mathbf{x}_{k-1})p_{k-1|k-1}(\mathbf{x}_{k-1}|\mathbf{z}_{0:k-1})\mathrm{d}\mathbf{x}_{k-1} \tag{2.8}$$

where the subscript "$k|k'$" denotes a density at time k conditioned on information up to and including time k'.

Assume that the measurement noise is white, such that

$$g_k(\mathbf{z}_k \mid \mathbf{x}_k, \mathbf{z}_{0:k-1}) = g_k(\mathbf{z}_k \mid \mathbf{x}_k) \tag{2.9}$$

Then, given a noisy measurement $\mathbf{z}_k$ at time k, the posterior density is given by Bayes' rule:

$$p_{k|k}(\mathbf{x}|\mathbf{z}_k, \mathbf{z}_{0:k-1}) = \frac{g_k(\mathbf{z}_k|\mathbf{x}_k)p_{k|k-1}(\mathbf{x}_k|\mathbf{z}_{0:k-1})}{\int g_k(\mathbf{z}_k|\mathbf{x}')p_{k|k-1}(\mathbf{x}'|\mathbf{z}_{0:k-1})\mathrm{d}\mathbf{x}'} \tag{2.10}$$

Throughout this dissertation, the abbreviation $p_k(\cdot) = p_{k|k}(\cdot)$ is frequently used when possible to do so without ambiguity. Remarkably, when both the transition density (2.6) and measurement likelihood (2.7) are linear-Gaussian, the optimal Bayes filter is algorithmically equivalent to the Kalman filter.

2.2.2 Gaussian Mixture Filters

In the general case where $p_0(\mathbf{x}_0)$ is non-Gaussian, or where the state transition or measurement are nonlinear or non-Gaussian, the resulting filtering densities will be non-Gaussian. One effective approach to non-Gaussian, nonlinear filtering is GM filtering [2]. The key principle of GM filtering is the approximation of a pdf as a weighted sum of L Gaussian mixands:

$$p(\mathbf{x}) \approx \sum_{\ell=1}^{L} w^{(\ell)} \mathcal{N}(\mathbf{x};\, \mathbf{m}^{(\ell)}, \mathbf{P}^{(\ell)}) \tag{2.11}$$

where $w^{(\ell)}$, $\mathbf{m}^{(\ell)}$, and $\mathbf{P}^{(\ell)}$ denote the weight, mean, and covariance, respectively of the ℓ^{th} component (mixand), and

$$\mathcal{N}(\mathbf{x};\, \mathbf{m},\, \mathbf{P}) \triangleq |2\pi\mathbf{P}|^{-1/2} \exp\left\{-\frac{1}{2}(\mathbf{x}-\mathbf{m})^T\mathbf{P}^{-1}(\mathbf{x}-\mathbf{m})\right\} \tag{2.12}$$

GMs are exceptionally versatile, as they are universal function approximators for valid pdfs with a finite number of discontinuities [102]. By this representation, closed-form approximate solutions of the Bayes filter can be expressed in terms of component-level filter recursions, such as the Kalman filter [102], EKF [2, 4], and sigma point filters [108].

2.2.3 Information Divergence

Many important concepts in information-driven control – namely information, entropy, and divergence – are rooted in early problems in communication theory. For instance, given a sequence of random events whose discrete outcomes are to be transmitted via digital messages, the average message length can be reduced by assigning shorter-length descriptions to higher-probability outcomes. By this approach, the average number of bits needed to describe a random event is equal to the *entropy* of the random variable distribution. The entropy is a measure of the average uncertainty of a discrete random variable and can also be extended to continuous random variables [23]. Given a continuous random variable distribution with density $p(\mathbf{x})$, its uncertainty can be quantified in terms of its *differential* *entropy*

$$\mathcal{H}[p(\mathbf{x})] \triangleq -\int p(\mathbf{x}) \log p(\mathbf{x}) \mathrm{d}\mathbf{x} \tag{2.13}$$

where the integral is taken over the distribution support. The *relative entropy*–also known as the *Kullback-Leibler divergence (KLD)* or *information divergence*–between two distributions with densities $p(\mathbf{x})$ and $q(\mathbf{x})$ is [86, 70]

$$I_{\mathrm{KL}}(p; q) = \int p(\mathbf{x}) \log \frac{p(\mathbf{x})}{q(\mathbf{x})} \mathrm{d}\mathbf{x} \tag{2.14}$$

When q and p represent prior and posterior densities, the KLD is a measure of *information gain*. By this principle, the information gain associated with sensing decisions and outcomes can be rigorously quantified and used as a basis for intelligent sensor control.

More generally, the KLD belongs to a class of divergence measures known as f-divergences, as shown by Csizár [70]. For two distributions P and Q with corresponding density functions $p(\mathbf{x}) = \mathrm{d}P/\mathrm{d}\mathbf{x}$ and $q = \mathrm{d}Q/\mathrm{d}\mathbf{x}$, the f-divergence is

$$I_f(P, Q) = \int q(\mathbf{x}) f\left(\frac{p(\mathbf{x})}{q(\mathbf{x})}\right) \mathrm{d}\mathbf{x} \tag{2.15}$$

for any convex function $f : (0, \infty) \mapsto \mathbb{R}$, where the integrand is assumed to be properly specified at points where the densities are zero [70]. Letting $f(t) = t \log t$ in (2.15), the KLD is recovered.

In some cases, the terminology "information-theoretic" is used to refer to any combinations of quantities that are in some way related to uncertainty reduction. However, this dissertation adopts the narrower definition of this terminology by which "information-theoretic" is used exclusively to describe measures and policies based on f-divergence measures, the Cauchy-Schwarz divergence (which behaves much like the KLD), or entropy reduction.

2.3 Random Finite Set Background

The pioneering efforts of Goodman and Mahler [41] in RFS theory have resulted in a robust framework for solving multi-sensor multi-object information fusion problems. In essence, RFS theory establishes multi-object analogs to random variables, density functions, moments, and other statistics, such that multi-sensor multi-object problems can be solved in a top-down fashion and with theoretic guarantees. RFS theory has enabled the development of numerous state-of-the-art multi-object filters [73, 114, 116, 89, 112, 65, 93] as well as provided a unifying theoretical basis for the reformulation and analysis of earlier non-RFS-based approaches [125].

An RFS X is a random variable that takes values on $\mathcal{F}(\mathbb{X})$, where $\mathcal{F}(\mathbb{X})$ denotes the space of finite subsets of $\mathbb{X}$. A labeled random finite set (LRFS) $\mathring{X}$ is a random variable that takes values on $\mathcal{F}(\mathbb{X}\times\mathbb{L})$, where $\mathbb{L}$ is a discrete label space. Both RFS and LRFS distributions can be described by set density functions, as established by Mahler's FISST [74, 75]. This section provides a review of key RFS concepts and notation, including an overview of the Poisson RFS, independently and identically distributed cluster (i.i.d.c.) RFS, multi-Bernoulli (MB) RFS, and generalized labeled multi-Bernoulli (GLMB) LRFS distributions used in this dissertation.

2.3.1 Poisson RFS

The Poisson RFS is fundamental to RFS multi-object tracking due to its desirable mathematical properties and its usage in modeling false alarm and birth processes. For example, the popular probability hypothesis density (PHD) filter is derived from the assumption that the multi-object state is governed by a Poisson RFS process, which, in turn, leads to a computationally efficient multi-object filtering algorithm [72, 97, 110].

The density of a Poisson-distributed RFS X is

$$f(X) = e^{-N_X}[D]^X \tag{2.16}$$

where N_X is the object cardinality mean, and $D(\mathbf{x})$ is the PHD, or intensity function, of X, which is defined on the single-object space $\mathbb{X}$. The cardinality of a Poisson RFS is, in fact, Poisson distributed:

$$|X| \sim \mathrm{Pois}_{N_X}(|X|) \triangleq \frac{{N_X}^{|X|} e^{-N_X}}{|X|!} \tag{2.17}$$

where "$|\cdot|$" denotes the cardinality of its argument. Each element $\mathbf{x} \in X$ is independently and identically distributed (i.i.d.) according to the normalized density $D(\mathbf{x})/N_X$, such that

$$\mathbf{x} \sim \frac{D(\mathbf{x})}{N_X} \quad \forall \mathbf{x} \in X \tag{2.18}$$

The PHD is an important statistic in RFS theory as its integral over a set $T \subseteq \mathbb{X}$ gives the expected number of objects in that set:

$$\mathrm{E}[|X \cap T|] = \int_T D(\mathbf{x}) \mathrm{d}\mathbf{x} \tag{2.19}$$

The PHD of a general RFS X is given in terms of its set density $f(X)$ as [72]

$$D(\mathbf{x}) = \int f(\{\mathbf{x}\} \cup X')\delta X' \tag{2.20}$$

The integral in (2.20) is a set integral, defined as

$$\int f(X)\delta X \triangleq \sum_{n=0}^{\infty} \frac{1}{n!} \int f(\{\mathbf{x}_1, \dots, \mathbf{x}_n\}) \mathrm{d}\mathbf{x}_1 \cdots \mathrm{d}\mathbf{x}_n \tag{2.21}$$

The set integral is a fundamental construct of RFS theory and enables the direct translation of the Bayes' filter recursion to the multi-object setting, as shown in [74] and discussed in Section 2.3.5. Set integration via (2.21) also presents practical challenges, since exact computation is rarely possible due to the infinite summation of nested multivariate integrals required. This challenge is a key motivation of the tractable cell multi-Bernoulli approximation introduced in Section 4.3.

2.3.2 Independent Identically Distributed Cluster RFS

The density of an i.i.d.c. RFS is

$$f(X) = |X|! \cdot \rho(|X|)[p]^X \tag{2.22}$$

where $\rho(n)$ is the cardinality probability mass function (pmf) and $p(\mathbf{x})$ is the single-object state pdf. Similar to the Poisson RFS, elements of the i.i.d.c. RFS are i.i.d. such that

$$\mathbf{x} \sim p(\mathbf{x}) \quad \forall\, \mathbf{x} \in X \tag{2.23}$$

Unlike the Poisson RFS distribution, the cardinality of an i.i.d.c. RFS is distributed according to an arbitrary pmf:

$$|X| \sim \rho(|X|) \tag{2.24}$$

This generalization of the cardinality distribution enables an extra degree of specificity and plays an important role in the development of the cardinalized probability hypothesis density (CPHD) filter, as shown in [115].

2.3.3 Multi-Bernoulli RFS

In an MB distribution, a given object's existence is modeled as a Bernoulli random variable and specified by a probability of existence. As such, the MB RFS can accurately model a variety of multi-object processes when the true existence of objects is unknown and subject to change. The density of an MB distribution is [75, p. 102]

$$f(X) = \left[1 - r^{(\cdot)}\right]^{\mathbb{N}_M} \sum_{1 \leq i_1 \neq \cdots \neq i_n \leq M} \left[\frac{r^{i_{(\cdot)}} p^{i_{(\cdot)}}(\mathbf{x}_{(\cdot)})}{1 - r^{i_{(\cdot)}}}\right]^{\mathbb{N}_n} \tag{2.25}$$

where $n = |X|$, M is the number of MB components and maximum possible object cardinality, r^i is the probability that the i^{th} object exists, and $p^i(\mathbf{x})$ is the single-object state probability density of the i^{th} object if it exists. Given an MB distribution with density (2.25), its PHD is given by

$$D(\mathbf{x}) = \sum_{j=1}^{M} r^j p^j(\mathbf{x}) \tag{2.26}$$

2.3.4 Generalized Labeled Multi-Bernoulli LRFS

The density of a GLMB distribution, as proposed in [112], is given by

$$\mathring{f}(\mathring{X}) = \Delta(\mathring{X}) \sum_{\xi \in \Xi} w^{(\xi)}(\mathcal{L}(\mathring{X}))[p^{(\xi)}]^{\mathring{X}} \tag{2.27}$$

where Ξ is a discrete space, and where each $\xi \in \Xi$ represents a history of measurement association maps, each $p^{(\xi)}(\cdot, \ell)$ is a probability density on $\mathbb{X}$, and each weight $w^{(\xi)}$ is non-negative with

$$\sum_{(I,\xi) \in \mathcal{F}(\mathbb{L}) \times \Xi} w^{(\xi)}(I) = 1$$

The label of a labeled state $\mathring{x}$ is recovered by $\mathcal{L}(\mathring{x})$, where $\mathcal{L} : \mathbb{X} \times \mathbb{L} \mapsto \mathbb{L}$ is the projection defined by $\mathcal{L}((\mathbf{x}, \ell)) \triangleq \ell$. Similarly, for LRFSs, $\mathcal{L}(\mathring{X}) \triangleq \{\mathcal{L}(\mathring{x}) : \mathring{x} \in \mathring{X}\}$. The distinct label indicator $\Delta(\mathring{X}) = \delta_{(|\mathring{X}|)}(|\mathcal{L}(\mathring{X})|)$ ensures that only sets with distinct labels are considered.

2.3.5 Multi-Object Bayes Filter

In multi-object estimation problems, single-object states evolve stochastically due to unknown inputs and random environmental phenomena. Furthermore, the number of objects itself is random due to object appearance (birth) and disappearance (death). Thus, the multi-object state can be naturally modeled as an RFS $X \in \mathcal{F}(\mathbb{X})$. Similarly, the multi-object measurement, which is corrupted by random noise, missed detections, and spurious detections, is naturally modeled as an RFS $Z \in \mathcal{F}(\mathbb{Z})$.

By these RFS definitions of measurement and state, Mahler's FISST establishes the *multi-object Bayes recursion* [74]:

$$f_{k|k-1}(X_k|Z_{0:k-1}) = \int f_{k|k-1}(X_k|X_{k-1})f_{k-1}(X_{k-1}|Z_{0:k-1})\delta X_{k-1} \tag{2.28}$$

$$f_k(X_k|Z_{0:k}) = \frac{g_k(Z_k|X_k)f_{k|k-1}(X_k|Z_{0:k-1})}{\int g_k(Z_k|X)f_{k|k-1}(X|Z_{0:k-1})\delta X} \tag{2.29}$$

where $f_{k|k-1}(X_k|X_{k-1})$ is the multi-object transition density, $g_k(Z_k|X_k)$ is the multi-object likelihood function. LRFS distributions are predicted and updated in a similar manner via the *labeled multi-object Bayes filter recursion*:

$$\mathring{f}_{k|k-1}(\mathring{X}_k|Z_{0:k-1}) = \int \mathring{f}_{k|k-1}(\mathring{X}_k|\mathring{X}_{k-1})\mathring{f}_{k-1}(\mathring{X}_{k-1}|Z_{0:k-1})\delta\mathring{X}_{k-1} \tag{2.30}$$

$$\mathring{f}_k(\mathring{X}_k|Z_{0:k}) = \frac{g_k(Z_k|\mathring{X}_k)\mathring{f}_{k|k-1}(\mathring{X}_k|Z_{0:k-1})}{\int g_k(Z_k|\mathring{X})\mathring{f}_{k|k-1}(\mathring{X}|Z_{0:k-1})\delta\mathring{X}} \tag{2.31}$$

as shown in [113, 112]. The accent "$\mathring{}$" is used to distinguish labeled states and functions from their unlabeled equivalents, where a state's label is simply a unique number or tuple to distinguish it from the states of other objects and associate track estimates over time.

Equations (2.28)-(2.29) and (2.30)-(2.31) are often referred to in the literature as the "standard" form of the unlabeled and labeled Bayes recursion, respectively.

In the standard recursion, object appearance is modeled as part of the multi-object transition density and thus is treated in the prediction stage of the Bayes recursion. This approach is often problematic in practice, as it requires maintaining a probabilistic representation of objects that may exist but are never detected.

An alternative approach is to model object appearance as part of the Bayes update and treat an object's appearance as the event of first detection, circumventing the aforementioned issues. This approach is hereon referred to as the *measurement-driven labeled Bayes filter recursion* [65], given by:

$$\mathring{f}_{\mathrm{p}}(\mathring{X}_{\mathrm{p},k}|Z_{0:k-1}) = \int \mathring{f}(\mathring{X}_{\mathrm{p},k}|\mathring{X}_{k-1})\mathring{f}(\mathring{X}_{k-1}|Z_{0:k-1})\delta\mathring{X}_{k-1} \tag{2.32}$$

$$\mathring{f}(\mathring{X}_{k}|Z_{0:k}) = \frac{g(Z_k|\mathring{X}_k)\mathring{f}_{\mathrm{p}}(\mathring{X}_{\mathrm{p},k}|Z_{0:k-1})\mathring{f}_{\mathrm{b}}(\mathring{X}_{\mathrm{b},k})}{\int g(Z_k|\mathring{X})\mathring{f}_{\mathrm{p}}(\mathring{X}_{\mathrm{p},k}|Z_{0:k-1})\mathring{f}_{\mathrm{b}}(\mathring{X}_{\mathrm{b},k})\delta\mathring{X}} \tag{2.33}$$

The function time indices have been suppressed for brevity, and $\mathring{f}_{\mathrm{p},k}(\mathring{X}_{\mathrm{p},k})$ and $\mathring{f}_{\mathrm{b},k}(\mathring{X}_{\mathrm{b},k})$ denote the density of persisting and birth objects, respectively, where the joint state $\mathring{X}_k = \mathring{X}_{\mathrm{p},k} \cup \mathring{X}_{\mathrm{b},k}$. $\mathring{f}_{k|k-1}(\mathring{X}_{\mathrm{p},k}|\mathring{X}_{k-1})$ is the multi-object transition density, $g_k(Z_k|\mathring{X}_k)$ is the multi-object measurement likelihood function, and g_k is used to denote both the single-object and multi-object measurement likelihood function. The nature of the likelihood function can be easily determined from its arguments.

2.3.6 Multi-Sensor Multi-Object Bayes Filter

Given a multi-object state realization X, the multi-sensor measurement likelihood function is denoted by $g_k(Z^{(1)}, \dots, Z^{(\mathrm{M})}|X)$. If sensor measurements are conditionally independent of the multi-object state, i.e.,

$$g_k(Z^{(1)}, \dots, Z^{(\mathrm{M})}|X) = g_k^{(1)}(Z^{(1)}|X) \cdots g_k^{(\mathrm{M})}(Z^{(\mathrm{M})}|X) \tag{2.34}$$

then the multi-sensor multi-object posterior is given by the Bayes update [75, p. 280]

$$f_{k|k}(X \mid Z_{0:k}^{(1:\mathrm{M})}) = \frac{g_k(Z^{(1)}, \ldots, Z^{(\mathrm{M})}|X) f_{k|k-1}(X)}{f_k(Z^{(1)}, \ldots, Z^{(\mathrm{M})})} \tag{2.35}$$

where $Z_{0:k}^{(1:\mathrm{M})}$ denotes the collection of all measurements up to and including time k, and where the normalization constant is given by

$$f_k(Z^{(1)}, \ldots, Z^{(\mathrm{M})}) = \int g(Z^{(1)}, \ldots, Z^{(\mathrm{M})} \mid X) f_{k|k-1}(X) \delta X \tag{2.36}$$

2.3.7 Kullback-Leibler Divergence

Like single-object distributions, the similarity of two RFS distributions may be measured by the KLD. Let f_1 and f_0 be integrable set densities where f_1 is absolutely continuous with respect to f_0. Then, the KLD is [41, p. 206]

$$I_{\mathrm{KL}}(f_1; f_0) = \int f_1(Y) \log\left(\frac{f_1(Y)}{f_0(Y)}\right) \delta Y \tag{2.37}$$

Further simplification is possible if f_0 and f_1 are Poisson with respective PHDs D_0 and D_1, in which case

$$I_{\mathrm{KL,Pois}}(f_1; f_0) = N_0 - N_1 + \int D_1(\mathbf{y}) \cdot \log\left(\frac{D_1(\mathbf{y})}{D_0(\mathbf{y})}\right) \mathrm{d}\mathbf{y} \tag{2.38}$$

where $N_0 = \int D_0(\mathbf{y})\mathrm{d}\mathbf{y}$ and $N_1 = \int D_1(\mathbf{y})\mathrm{d}\mathbf{y}$. The KLD has many practical uses in estimation theory, including as a metric for measuring the goodness of a density approximation with respect to the original density, as demonstrated in Section 4.3.1. Importantly, when f_0 and f_1 represent prior and posterior densities, respectively, the KLD is a measure of *information gain* and provides a foundation for information-driven control, as discussed in Chapters 4 and 5.

CHAPTER 3

SOFT AND NEGATIVE INFORMATION AND FIELD-OF-VIEW CARDINALITY DISTRIBUTIONS

3.1 Introduction

RFS theory has been proven a highly effective framework for developing and analyzing tracking and sensor planning algorithms in applications involving an unknown number of multiple targets (objects) [74, 112, 89, 37, 51, 12, 117]. To date, however, little attention has been given to the role that bounded FoV and negative information play in the FISST recursive updates for assimilating measurements, or lack thereof, into multi-object probability distributions. Existing algorithms typically terminate object tracks after the object is believed to have left the sensor FoV. While this approach is suitable when the FoV doubles as the tracking region of interest (ROI), it is inapplicable when the sensor FoV is much smaller than the ROI and, thus, must be moved or positioned so as to maximize information value [33, 119, 39, 18, 68, 69].

Knowledge of object presence inside the FoV is powerful evidence that can be incorporated to update the object pdf in a Bayesian framework. For example, the absence of detections, referred to as *negative information*, may suggest that the object state resides outside the FoV [60]. In contrast, binary-type sensors may produce *imprecise measurements* [41, 40, 90] that indicate the object is inside the sensor FoV but provide no further localization information. Similarly, "soft" data from human sources, such as natural language statements, can be modeled as imprecise measurements due to their inherent ambiguity [14, 93]. Particle-based filtering algorithms [5, 111, 90] can accommodate such measurements but require a large number of particles and are computationally expensive. Particle representations are also not amenable to rigorous multi-sensor fusion, since the supports of two Dirac mixtures will be disjoint in general. Another approach [101] uses GMs to model both the object pdf and the state-dependent probability of detection function. Though GMs efficiently model some detection probability functions, other simple functions, such as uniform probability densities over a 3D FoV, require problematically large numbers of components. Other approaches [1, 118] employ stochastic sampling and the expectation maximization (EM) algorithm to compute GM approximations to the posterior pdf. However, the use of intermediate particle representations and EM reconstruction can lead to information loss, and convergence is sensitive to EM initial condition specification.

This chapter presents relevant bounded FoV statistics both in the form of state densities and cardinality pmfs. Section 3.3 presents a deterministic method that partitions a GM state density along FoV bounds through recursive Gaussian splitting. By this approach, inclusion/exclusion evidence can be incorporated in single- and multi-object GM filtering densities by virtue of Bayes' rule. Section 3.4 presents an application of the splitting method to the tracking of a person in a crowded space using natural language statements and a new GM Bernoulli filter algorithm. In Section 3.5, FoV object cardinality pmfs are derived for some of the most commonly encountered RFS distributions. Section 3.6 presents an application of bounded FoV statistics to a sensor placement problem, and conclusions are made in Section 3.7.

3.2 Problem Formulation and Assumptions

This chapter considers the incorporation of bounded FoV information into algorithms for (multi-)object tracking and sensor planning when the number of objects is unknown and time-varying. Often in tracking, object detection may depend only a partial state $\mathbf{s} \in \mathbb{X}_s \subseteq \mathbb{R}^{n_s}$, where $\mathbb{X}_s \times \mathbb{X}_v = \mathbb{X} \subseteq \mathbb{R}^{n_x}$ forms the full object state space. For example, the instantaneous ability of a sensor to detect an object may depend only on the object's relative position. In that case, $\mathbb{X}_s$ is the position space, and $\mathbb{X}_v$ is composed of non-position states, such as object velocity. This nomenclature is adopted throughout the chapter while noting that the approach is applicable to other state definitions. As shown in [10], the sensor FoV can be defined as the compact subset $\mathcal{S}(\boldsymbol{q}) \subset \mathbb{X}_s$. In general, the FoV is a function of the sensor state $\boldsymbol{q}$, which, for example, may consist of the sensor position, orientation, and zoom level. However, for notational simplicity, this dependence is omitted in the remainder of this chapter.

Now, let the object state $\mathbf{x}$ consist of the kinematic variables that are to be estimated from data via filtering, such as the object position, velocity, turn rate, etc. Then, the single-object pdf is denoted by $p(\mathbf{x})$. Letting $\mathbf{s} = \text{proj}_{\mathbb{X}_s}\mathbf{x}$ denote the state elements that correspond to $\mathbb{X}_s$, an object's presence inside the FoV can be expressed by the generalized indicator function

$$1_{\mathcal{S}}(\mathbf{x}) = \begin{cases} 1, & \text{if } \mathbf{s} \in \mathcal{S} \\ 0, & \text{otherwise} \end{cases} \tag{3.1}$$

The number of objects and their kinematic states are unknown *a priori*, but can be assumed to consist of discrete and continuous variables, respectively. The collection of object states is modeled as an RFS X or LRFS $\mathring{X}$, where the single-object labeled state $\mathring{x} = (\mathbf{x}, \ell) \in \mathbb{X} \times \mathbb{L}$ consists of a kinematic state vector $\mathbf{x}$ and unique discrete label ℓ. It is assumed that the prior multi-object distribution is known, e.g., from the output of a multi-object filter, and modeled using either the RFS density $f(X)$ or LRFS density $\mathring{f}(\mathring{X})$.

In RFS-based tracking, single-object densities are, in fact, parameters of the higher-dimensional multi-object density. Non-Gaussian single-object state densities are often modeled using GMs because they admit closed-form approximations to the multi-object Bayes recursion under certain conditions [112, 110]. Therefore, in this chapter, it is assumed that single-object densities (which are parameters of the higher dimensional multi-object density) are parameterized as

$$p(\mathbf{x}) = \sum_{\ell=1}^{L} w^{(\ell)} \mathcal{N}(\mathbf{x};\, \mathbf{m}^{(\ell)},\, \mathbf{P}^{(\ell)}) \tag{3.2}$$

where L is the number of GM components and $w^{(\ell)}$, $\mathbf{m}^{(\ell)}$, and $\mathbf{P}^{(\ell)}$ are the weight, mean, and covariance matrix of the ℓ^{th} component, respectively.

In this chapter, the problem considered is forming GM Bayesian posteriors given evidence of the forms:

T1. *The existence or non-existence of a measurement is evidence of the inclusion or exclusion of the object state within a known set.* For example, the non-existence of a detection (measurement) is evidence of an object's position exclusion from the sensor FoV.

T2. *The value of the measurement is evidence of the inclusion or exclusion of the object state within a known set.* For example, the observation that a sea-level freshwater lake is frozen is evidence that the water temperature belongs to the set of temperatures below 0 °C.

Mahler's FISST provides the mathematical machinery for modeling types T1 and T2 using state-dependent probability of detection functions and generalized likelihood functions, respectively. However, in both cases, the Bayes posterior involves products of the prior GM with indicator functions such as

$$p(\mathbf{x})1_{\mathcal{S}}(\mathbf{x}) \triangleq p_{\mathcal{S}}(\mathbf{x}) \qquad \text{and} \tag{3.3}$$

$$(1 - 1_{\mathcal{S}}(\mathbf{x}))p(\mathbf{x}) \triangleq p_{\mathcal{C}(\mathcal{S})}(\mathbf{x}) \tag{3.4}$$

and thus, the resulting posterior is no longer a GM.

This chapter presents a fast GM approximation of (3.3) and (3.4), thereby enabling the assimilation of inclusion/exclusion evidence in any GM-based RFS single-object or multi-object filter. Building on these concepts, this chapter also considers the role of inclusion/exclusion evidence in object cardinality distributions and derives pmf expressions that describe the probabilities associated with different numbers of objects existing within a given set $\mathcal{S}$ (such as an FoV).

3.3 GM Approximation of FoV-Partitioned Densities

This section presents a method for partitioning the object pdf into truncated densities $p_{\mathcal{S}}(\mathbf{x})$ and $p_{\mathcal{C}(\mathcal{S})}(\mathbf{x})$, with supports $\mathcal{S} \times \mathbb{X}_v$ and $\mathcal{C}(\mathcal{S}) \times \mathbb{X}_v$, respectively. Focus is given to the single-object state density with the awareness that the method is naturally extended to RFS multi-object densities and algorithms that use GM parameterization. Consider the single-object density $p(\mathbf{x})$ parameterized by an L-component GM, as follows:

$$p(\mathbf{x}) = p_{\mathcal{S}}(\mathbf{x}) + p_{\mathcal{C}(\mathcal{S})}(\mathbf{x}) = \sum_{\ell=1}^{L} w^{(\ell)} \mathcal{N}(\mathbf{x};\, \mathbf{m}^{(\ell)}, \mathbf{P}^{(\ell)}) \tag{3.5}$$

One simple approximation of densities partitioned according to the discrete FoV geometry, referred to as FoV-partitioned densities hereon, is found by evaluating the indicator function at the component means [64], i.e.:

$$p_{\mathcal{S}}(\mathbf{x}) \approx \sum_{\ell=1}^{L} w^{(\ell)} 1_{\mathcal{S}}(\mathbf{m}^{(\ell)}) \mathcal{N}(\mathbf{x};\, \mathbf{m}^{(\ell)},\, \mathbf{P}^{(\ell)}) \tag{3.6}$$

$$p_{\mathcal{C}(\mathcal{S})}(\mathbf{x}) \approx \sum_{\ell=1}^{L} w^{(\ell)} (1 - 1_{\mathcal{S}}(\mathbf{m}^{(\ell)})) \mathcal{N}(\mathbf{x};\, \mathbf{m}^{(\ell)},\, \mathbf{P}^{(\ell)}) \tag{3.7}$$

By this approach, components whose means lie inside (outside) the FoV are preserved (pruned), or vice versa.

The accuracy of this mean-based partition approximation depends strongly on the resolution of the GM near the geometric boundaries of the FoV. Even though the mean of a given component lies inside (outside) the FoV, a considerable portion of the probability mass may lie outside (inside) the FoV, as is illustrated in Fig. 3.1a. Therefore, the amount of FoV overlap, along with the weight of the component, determines the accuracy of the approximations (3.6)-(3.7). To that end, the algorithm presented in the following subsection iteratively resolves the GM near FoV bounds by recursively splitting Gaussian components that overlap the FoV bounds.

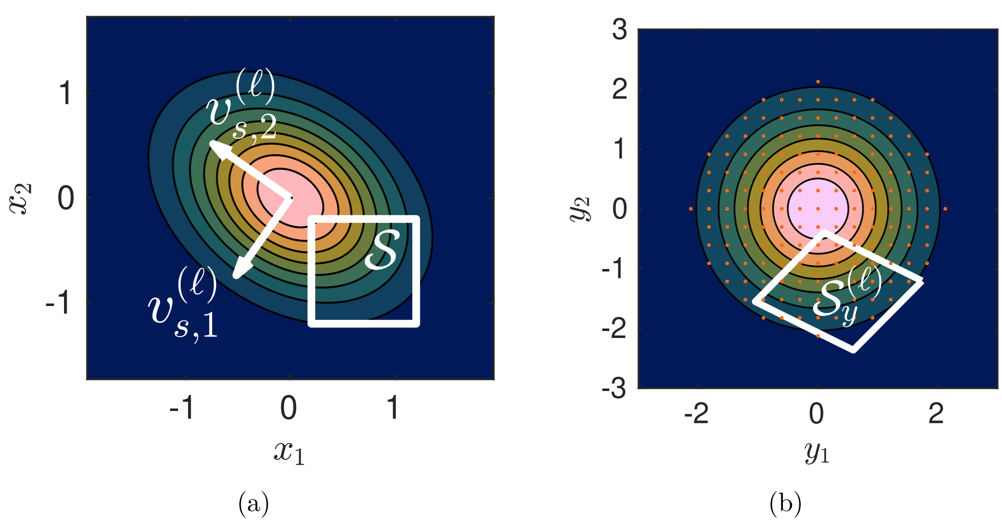

Figure 3.1: Original component density and FoV with covariance eigenvectors overlaid (a), and same component density and FoV after change of variables (b).

3.3.1 Gaussian Splitting Algorithm

The Gaussian splitting algorithm presented in this subsection forms an FoV-partitioned GM approximation of the original GM by using a higher number of components near the FoV boundaries, $\partial\mathcal{S}$, so as to improve the accuracy of the mean-based partition.

Consider for simplicity a two-dimensional example in which the original GM, $p(\mathbf{x})$, has a single component whose mean lies outside the FoV, as shown in Fig. 3.1a. The algorithm first applies a change of variables $\mathbf{x} \mapsto \mathbf{y} \in \mathbb{Y} \subseteq \mathbb{R}^{n_s}$ such that $p(\mathbf{y})$ is symmetric and has zero mean and unit variance. The basis vectors of the space $\mathbb{Y}$ correspond to the principal directions of the component's position covariance. The same change of variables is applied to the FoV bounds (Fig. 3.1b).

A pre-computed point grid is then tested for inclusion in the transformed FoV in order to decide whether to split the component, and if so, along which principal direction. For each new split component, the process is repeated–if a new component significantly overlaps the FoV boundaries, it may be further split into several smaller components, as illustrated in Fig. 3.2b. This process is repeated until stopping criteria are satisfied. After the GM splitting terminates, $p_{\mathcal{S}}(\mathbf{x})$ and $p_{\mathcal{C}(\mathcal{S})}(\mathbf{x})$ are approximated by the mean-based partition, as illustrated in Fig. 3.3.

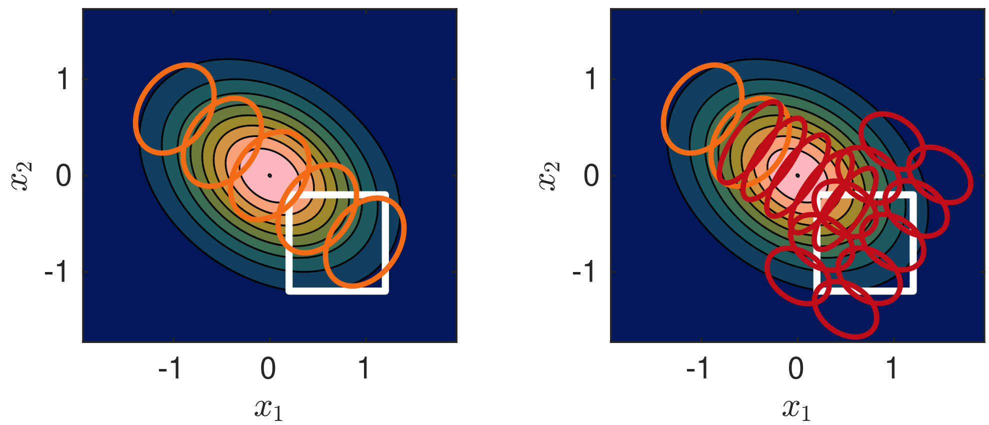

(a) (b)

Figure 3.2: 1σ contours of components after first split operation (a), and second split operation (b), where components formed in the second operation are shown in red.

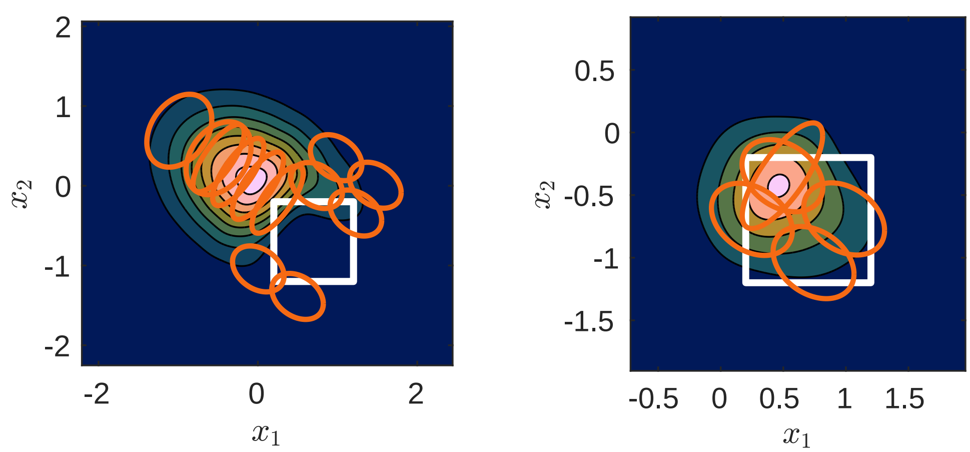

(a) (b)

Figure 3.3: The GM approximations to densities $p_{\mathcal{C}(\mathcal{S})}(\mathbf{x})$ (a), and $p_{\mathcal{S}}(\mathbf{x})$ (b) after two iterations of splitting.

3.3.2 Univariate Splitting Library

Splitting is performed efficiently by utilizing a pre-generated library of optimal split parameters for the univariate standard Gaussian $q(x)$, as first proposed in [55] and later generalized in [25]. The univariate split parameters are retrieved at run-time and applied to arbitrary multivariate Gaussian densities via scaling, shifting, and covariance diagonalization.

Generation of the univariate split library is performed by minimizing the cost function

$$J = L_2(q||\tilde{q}) + \lambda\tilde{\sigma}^2 \qquad \text{s.t.} \sum_{j=1}^{R} \tilde{w}^{(j)} = 1 \tag{3.8}$$

where

$$\tilde{q}(x) = \sum_{j=1}^{R} \tilde{w}^{(j)} \mathcal{N}(x;\, \tilde{m}^{(j)},\, \tilde{\sigma}^2) \tag{3.9}$$

for different parameter values R, λ. The regularization term λ balances the importance of using smaller standard deviations $\tilde{\sigma}$ with the minimization of the L_2 distance. While other distance measures may be used, the L_2 distance is attractive because it can be computed in closed form for GMs [25]. As an example, the optimal split parameters for $R = 4$, $\lambda = 0.001$ are provided in Table 3.1 and plotted in Fig. 3.4.

Table 3.1: Univariate split parameters for $R = 4$, $\lambda = 0.001$.

j	$\tilde{w}^{(j)}$	$\tilde{m}^{(j)}$	$\tilde{\sigma}$
1	0.10766586425362	−1.42237156603631	0.58160633157686
2	0.39233413574638	−0.47412385534547	0.58160633157686
3	0.39233413574638	0.47412385534547	0.58160633157686
4	0.10766586425362	1.42237156603631	0.58160633157686

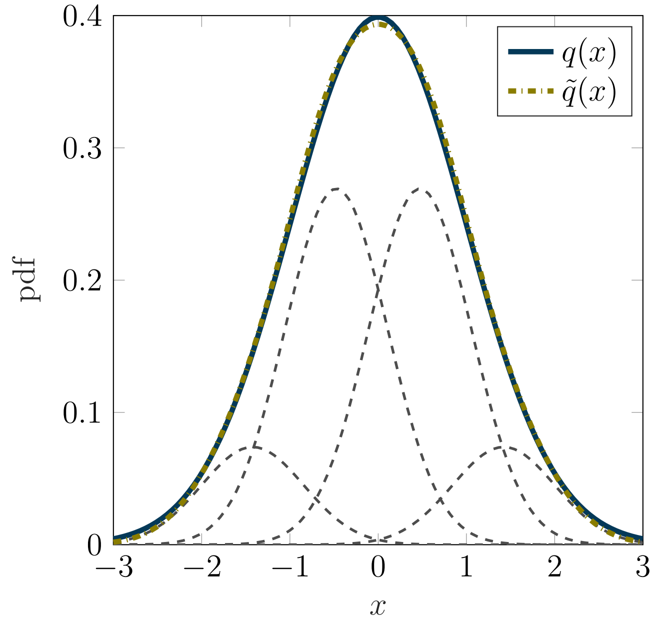

Figure 3.4: Standard univariate normal $q(x)$ and optimal GM approximation $\tilde{q}(x)$ with $R = 4$, $\lambda = 0.001$.

3.3.3 Change of Variables

The determination of which components should be split, and if so, along which direction, is simplified by first establishing a change of variables. By applying this change of variables, the split criteria and direction selection are standardized in terms of the standard unit normal distribution, as described in the following. For each component with index ℓ, the change of variables $\boldsymbol{h}^{(\ell)} : \mathbb{X}_s \mapsto \mathbb{Y}$ is applied as follows:

$$\mathbf{y} = \boldsymbol{h}^{(\ell)}(\mathbf{s}; \mathbf{m}_s^{(\ell)}, \mathbf{P}_s^{(\ell)}) \triangleq (\boldsymbol{\Lambda}_s^{(\ell)})^{-\frac{1}{2}} \boldsymbol{V}_s^{(\ell)T}(\mathbf{s} - \mathbf{m}_s^{(\ell)}) \tag{3.10}$$

where

$$\boldsymbol{V}_s^{(\ell)} = [\boldsymbol{v}_{s,1}^{(\ell)} \quad \cdots \quad \boldsymbol{v}_{s,n_s}^{(\ell)}] \tag{3.11}$$

$$(\boldsymbol{\Lambda}_s^{(\ell)})^{-1/2} = \operatorname{diag}\left(\left[\frac{1}{\sqrt{\lambda_{s,1}^{(\ell)}}} \quad \cdots \quad \frac{1}{\sqrt{\lambda_{s,n_s}^{(\ell)}}}\right]\right) \tag{3.12}$$

and $\mathbf{m}_s^{(\ell)}$ is the n_s-element position portion of the full-state mean, and the columns of $\boldsymbol{V}_s^{(\ell)}$ are the normalized eigenvectors of the position-marginal covariance $\mathbf{P}_s^{(\ell)}$, with $\boldsymbol{v}_{s,i}^{(\ell)}$ corresponding to the i^{th} eigenvalue $\lambda_{s,i}^{(\ell)}$. In the transformed space,

$$p(\mathbf{y}) = \mathcal{N}(\mathbf{y};\, \mathbf{0},\, \mathbf{I}) \tag{3.13}$$

Note that, in defining the transformation over $\mathbb{X}_s$, the same transformation can be applied to the FoV, such that

$$\mathcal{S}_y^{(\ell)} = \{\boldsymbol{h}^{(\ell)}(\mathbf{s}; \mathbf{m}_s^{(\ell)}, \mathbf{P}_s^{(\ell)}) : \mathbf{s} \in \mathcal{S}\} \tag{3.14}$$

In $\mathbb{Y}$, the Euclidean distances to boundary points of $\mathcal{S}_y^{(\ell)}$ can be interpreted as probabilistically normalized distances. In fact, the Euclidean distance of a point $\mathbf{y}$ from the origin in $\mathbb{Y}$ corresponds exactly to the Mahalanobis distance between the corresponding point $\mathbf{s}$ and the original position-marginal component.

3.3.4 Component Selection and Collocation Points

Components are selected for splitting if they have sufficient weight and significant statistical overlap of the FoV boundaries ($\partial\mathcal{S}$). For components of sufficient weight, the change of variables is applied to the FoV to obtain $\mathcal{S}_y^{(\ell)}$ per (3.14). The overlap of the original component on $\mathcal{S}$ is then equivalent to the overlap of the standard Gaussian distribution on $\mathcal{S}_y^{(\ell)}$, which is quantified using a grid of collocation points on $\mathbb{Y}$, as shown in Fig. 3.1b.

Define the collocation point $\bar{\mathbf{y}}_{i_1,\ldots i_{n_s}} \in \mathbb{Y}$ such that

$$\bar{\mathbf{y}}_{i_1,\cdots,i_{n_s}} \triangleq [\bar{y}_1(i_1) \ \ldots \ \bar{y}_{n_s}(i_{n_s})]^T, \quad (i_1,\ldots,i_{n_s}) \in G \tag{3.15}$$

$$\bar{y}_j(l) = -\zeta + 2\zeta\left(\frac{l-1}{N_g-1}\right), \qquad j \in \mathbb{N}_{n_s} \tag{3.16}$$

$$G = \{(i_1,\ldots,i_{n_s}) : i_{(\cdot)} \in \mathbb{N}_{N_g}, \, \|\mathbf{y}_{i_1,\ldots,i_{n_s}}\| \leq \zeta\} \tag{3.17}$$

where ζ is a user-specified bound for the grid, G is the set of indices of points that are within ζ of the origin, and N_g is the upper bound of the number of points per dimension. An inclusion variable is defined as

$$d^{(\ell)}_{i_1,\ldots,i_{n_s}} \triangleq 1_{\mathcal{S}^{(\ell)}_y}(\bar{\mathbf{y}}_{i_1,\ldots,i_{n_s}}) \tag{3.18}$$

With this, $\varrho_{\mathcal{S}^{(\ell)}_y} \in \{0,1\}$ is established to mark total inclusion or total exclusion as

$$\varrho_{\mathcal{S}^{(\ell)}_y} = \prod_G \delta_{d^{(\ell)}_{1,\ldots,1}}(d^{(\ell)}_{i_1,\ldots,i_{n_s}}) \tag{3.19}$$

which is equal to unity if all grid points lie inside of $\mathcal{S}^{(\ell)}_y$ or all grid points lie outside of $\mathcal{S}^{(\ell)}_y$, and is zero otherwise. If either all or no points are included, no splitting is required. Otherwise, the component is marked for splitting.

3.3.5 Position Coordinate Split Direction

Rather than split the component along each of its principal directions, a more judicious selection can be made by limiting split operations to a single direction (per component) per recursion. Thus, by performing one split per component per recursion, the component selection criteria are re-evaluated, reducing the overall number of components generated. In the aforementioned two-dimensional example, only a subset of new components generated from the first split is selected for further splitting as shown in Fig. 3.2b.

The split direction is chosen based on the relative geometry of the FoV, and thus position vectors are of interest. Choosing the best position split direction is a challenging problem. A common approach is to split along the component's covariance eigenvector with the largest eigenvalue [55]. This strategy, however, does not consider the FoV geometry and thus may increase the mixture size without improvement to the FoV-partitioned densities (3.6)-(3.7). Ref. [54] provides a more sophisticated split direction criterion based on the integral linearization errors along the covariance eigenvectors. However, in the case that the FoV does not intersect the eigenvectors, this criterion cannot distinguish the best split direction. Another approach [107] determines the split direction based on the Hessian of the underlying nonlinear transformation, evaluated at the component mean. However, for the transformations (3.3)-(3.4) considered in this chapter, the associated Hessian either vanishes (for $\mathbf{s} \notin \partial\mathcal{S}$) or is undefined (for $\mathbf{s} \in \partial\mathcal{S}$).

Ideally, splitting along the chosen direction should minimize the number of splits required in the next iteration as well as improve the accuracy of the partition approximation applied after the final iteration. The computational complexity of exhaustive optimization of the split direction would likely negate the computational efficiency of the overall algorithm. Instead, to minimize the number of splits required in the next iteration, the position split direction is chosen as the direction that is orthogonal to the most grid planes of consistent inclusion/exclusion. Introducing a convenience function $s_j^{(\ell)} : \mathbb{N}_{N_g} \mapsto \{0, 1\}$, the plane of constant $y_j = \bar{y}_j(l)$ is consistently inside or consistently outside if

$$s_j^{(\ell)}(l) = \prod_{G, i_j = l} \delta_{d^{(\ell)}_{1,\ldots,i_j,\ldots,1}}(d^{(\ell)}_{i_1,\ldots,i_j,\ldots,i_{n_s}}) \tag{3.20}$$

is equal to unity. The optimal position split direction is then given by the eigenvector $\boldsymbol{v}_{s,j^*}$, where the optimal eigenvector index is found as

$$j^* = \arg\max_j \left(\sum_{l=1}^{N_g} s_j^{(\ell)}(l) \right) \tag{3.21}$$

For notational simplicity, the implicit dependence of j^* on the component index ℓ is omitted. For example, referring back to the two-dimensional example and Fig. 3.1b, there are more rows than columns that are consistently inside or outside the transformed FoV, and thus $j^* = 2$ is chosen as the desired position split direction index. In the case where multiple maxima exist, the eigenvector with the largest eigenvalue is selected, which corresponds to the direction of the largest variance among the maximizing eigenvectors.

3.3.6 Multivariate Split of Full-State Component

Gaussian splitting must be performed along the principal directions of the full-state covariance. The general multivariate split approximation, splitting along the k^{th} eigenvector $\boldsymbol{v}_k^{(\ell)}$ is given by [25] as

$$w^{(\ell)}\mathcal{N}(\mathbf{x};\, \mathbf{m}^{(\ell)},\, \mathbf{P}^{(\ell)}) \approx \sum_{j=1}^{R} w^{(\ell,j)}\mathcal{N}(\mathbf{x};\, \mathbf{m}^{(\ell,j)},\, \mathbf{P}^{(\ell,j)}) \tag{3.22}$$

where

$$w^{(\ell,j)} = \tilde{w}^{(j)} w^{(\ell)} \tag{3.23}$$

$$\mathbf{m}^{(\ell,j)} = \mathbf{m}^{(\ell)} + \sqrt{\lambda_k^{(\ell)}}\tilde{m}^{(j)}\boldsymbol{v}_k^{(\ell)} \tag{3.24}$$

$$\mathbf{P}^{(\ell,j)} = \boldsymbol{V}^{(\ell)}\boldsymbol{\Lambda}^{(\ell)}\boldsymbol{V}^{(\ell)T} \tag{3.25}$$

$$\boldsymbol{\Lambda}^{(\ell)} = \operatorname{diag}\left([\lambda_1 \ \cdots \ \tilde{\sigma}^2\lambda_k \ \cdots \ \lambda_{n_x}]\right) \tag{3.26}$$

and the optimal univariate split parameters $\tilde{w}^{(j)}$, $\tilde{m}^{(j)}$, and $\tilde{\sigma}$ are found from the pre-computed split library given the number of split components R and regularization parameter λ. In general, the position components of the full-state eigenvectors will not perfectly match the desired position split vector due to correlations between the states. Rather, the actual full-state split is performed along $\boldsymbol{v}_{k*}^{(\ell)}$, where the optimal eigenvector index is found according to

$$k^* = \arg\max_{k} \left| \left[\boldsymbol{v}_{s,j^*}^{(\ell)T} \ \mathbf{0}^T \right] \boldsymbol{v}_k^{(\ell)} \right| \tag{3.27}$$

where, without loss of generality, a specific state convention is assumed such that position states are first in element order.

3.3.7 Split Recursion and Role of Negative Information

The splitting procedure is applied recursively, as detailed in Algorithm 1. The recursion is terminated when no remaining components satisfy the criteria for splitting. Each recursion further refines the GM near the FoV bounds to improve the approximations of (3.6)-(3.7). However, because a Gaussian component's split approximation (3.22) does not perfectly replicate the original component, a small error is induced with each split. Given enough recursions, this error may become dominant. In the author's experience, the recursion is terminated well before the cumulative split approximation error dominates.

One of the many potential applications of the recursive algorithm presented in this section involves incorporating the evidence of non-detections, or negative information, in single- and multi-object filtering. To demonstrate, a single-object filtering problem with a bounded square FoV is considered where, in three subsequent sensor reports, no object is detected. The true object position and constant velocity are unknown but are distributed according to a known GM pdf at the first time step. As the initial pdf is propagated over time, the position-marginal pdf travels from left to right, as shown in Fig. 3.5. For simplicity, the probabil-

Algorithm 1 `split_for_fov`($\{w^{(\ell)}, \mathbf{m}^{(\ell)}, \mathbf{P}^{(\ell)}\}_{\ell=1}^{L}$, $w_{\min}$, $\mathcal{S}$, R, λ)

`split` $\leftarrow \{\}$, `no_split` $\leftarrow \{\}$
if $L = 0$ **then**
  return `split`
end if
for $\ell = 1, \dots, L$ **do**
  if $w^{(\ell)} < w_{\min}$ **then**
    add $\{w^{(\ell)}, \mathbf{m}^{(\ell)}, \mathbf{P}^{(\ell)}\}$ to `no_split`
    continue
  end if
  Compute $\mathcal{S}_y^{(\ell)}$ accrd. to (3.14)
  if $\varrho_{\mathcal{S}_y^{(\ell)}} = 1$ **then**
    add $\{w^{(\ell)}, \mathbf{m}^{(\ell)}, \mathbf{P}^{(\ell)}\}$ to `no_split`
  else
    $j^* \leftarrow$ Eq. (3.21) , $k^* \leftarrow$ Eq. (3.27)
    $\{w^{(\ell,j)}, \mathbf{m}^{(\ell,j)}, \mathbf{P}^{(\ell,j)}\}_{j=1}^{R} \leftarrow$ Eq. (3.22) with $k = k^*$
    add $\{w^{(\ell,j)}, \mathbf{m}^{(\ell,j)}, \mathbf{P}^{(\ell,j)}\}_{j=1}^{R}$ to `split`
  end if
end for
`split`$\leftarrow$`split_for_fov`(`split`, $w_{\min}$, $\mathcal{S}$, R, λ)
return `split` $\cup$ `no_split`

ity of detection inside the FoV is assumed equal to one. At each time step, the GM is refined by Algorithm 1 using $w_{\min} = 0.01$, $R = 3$, and $\lambda = 0.001$. Then, the mean-based partition approximation (3.7) is applied and the updated filtering density (3.4) is found. By this approach, the number of components may increase over time but can be reduced as needed through component merging and pruning.

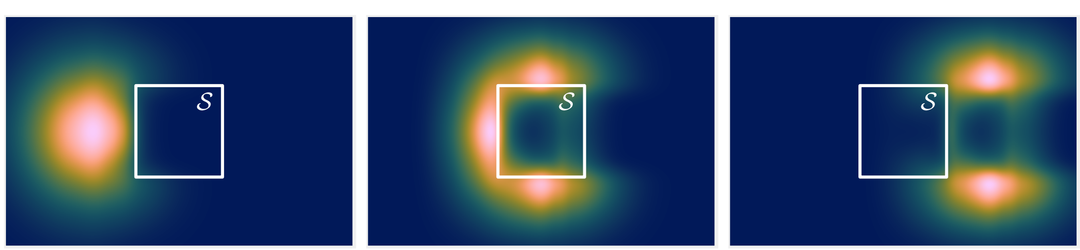

Figure 3.5: Negative information, comprising the absence of detections inside the sensor FoV $\mathcal{S}$, is used to update the object pdf as the object moves across the ROI.

3.3.8 Splitting for Multiple FoVs

The splitting approach presented in Section 3.3.7 can be extended to accommodate multiple FoVs, which may arise in multi-sensor networks or in imprecise measurements that take the form of multiple closed subsets, as is shown in Section 3.4. Consider the case where the GM is to be partitioned about the boundaries of M FoVs $\{\mathcal{S}^{(\imath)}\}_{\imath=1}^{\mathrm{M}}$. One simple approach to incorporate the multiple FoVs is to recursively apply Algorithm 1 for each FoV. Recall from Section 3.3.5, however, that the direction order in which components are split ultimately determines the total number of components generated. Thus, by the described naive approach, the resulting mixture size inherently depends on the order by which the FoVs are processed, which is undesirable.

Instead, the remainder of this subsection establishes a multi-FoV splitting algorithm that is invariant to FoV order. Given $\mathcal{S}^{(\imath)}$, denote by $\mathcal{S}_y^{(\imath,\ell)}$ the resulting transformed FoV for component ℓ via application of (3.14). Then, an inclusion variable similar to (3.18) is established as

$$d_{i_1,\dots,i_{n_s}}^{(\imath,\ell)} \triangleq 1_{\mathcal{S}_y^{(\imath,\ell)}}(\bar{\mathbf{y}}_{i_1,\dots,i_{n_s}}) \tag{3.28}$$

In each transformed FoV, grid points are either totally excluded or totally included if and only if

$$\varrho_{\{\mathcal{S}_y\}}^{(\ell)} = \prod_{\imath=1}^{\mathrm{M}} \prod_{G} \delta_{d_{1,\dots,1}^{(\imath,\ell)}}(d_{i_1,\dots,i_{n_s}}^{(\imath,\ell)}) \tag{3.29}$$

is equal to unity, which indicates that a component does not require splitting. If a component is to be split, the direction is chosen to minimize downstream mixture size, as discussed in Section 3.3.5. This is accomplished by identifying grid planes that are either consistently included/excluded in each FoV. Consistency of the plane of constant $y_j = \bar{y}_j(l)$ is indicated by

$$s_j^{(\ell)}(l) = \prod_{\imath=1}^{\mathrm{M}} \prod_{G, i_j = l} \delta_{d^{(\imath,\ell)}_{1,\ldots,i_j,\ldots,1}}(d^{(\imath,\ell)}_{i_1,\ldots,i_j,\ldots,i_{n_s}}) \tag{3.30}$$

equal to unity, where the inner product is taken over index sets in G that satisfy the condition $i_j = l$. By this multi-FoV generalized indicator function, the optimal position split direction is found via (3.21). The complete multi-FoV splitting algorithm is summarized in Algorithm 2, and an example tracking problem involving multiple FoVs is presented in the following section.

Algorithm 2 `split_for_multifov`($\{w^{(\ell)}, \mathbf{m}^{(\ell)}, \mathbf{P}^{(\ell)}\}_{\ell=1}^{L}$, $w_{\min}$, $\{\mathcal{S}^{(\imath)}\}_{\imath=1}^{\mathrm{M}}$, R, λ)

> `split` $\leftarrow \{\}$, `no_split` $\leftarrow \{\}$
> **if** $L = 0$ **then**
>   **return** `split`
> **end if**
> **for** $\ell = 1, \ldots, L$ **do**
>   **if** $w^{(\ell)} < w_{\min}$ **then**
>   add $\{w^{(\ell)}, \mathbf{m}^{(\ell)}, \mathbf{P}^{(\ell)}\}$ to `no_split`
>   **continue**
>   **end if**
>   **for** $\imath = 1, \ldots, \mathrm{M}$ **do**
>   compute $\mathcal{S}_y^{(\imath,\ell)}$ accrd. to Eq. (3.14)
>   **end for**
>   **if** $\varrho^{(\ell)}_{\{\mathcal{S}_y\}} = 1$ **then**
>   add $\{w^{(\ell)}, \mathbf{m}^{(\ell)}, \mathbf{P}^{(\ell)}\}$ to `no_split`
>   **else**
> $j^* \leftarrow$ Eq. (3.21) , $k^* \leftarrow$ Eq. (3.27)
> $\{w^{(\ell,j)}, \mathbf{m}^{(\ell,j)}, \mathbf{P}^{(\ell,j)}\}_{j=1}^{R} \leftarrow$ Eq. (3.22) with $k = k^*$
>   add $\{w^{(\ell,j)}, \mathbf{m}^{(\ell,j)}, \mathbf{P}^{(\ell,j)}\}_{j=1}^{R}$ to `split`
>   **end if**
> **end for**
> `split`$\leftarrow$`split_for_multifov`(`split`, $w_{\min}$, $\{\mathcal{S}^{(\imath)}\}_{\imath=1}^{\mathrm{M}}$, R, λ)
> **return** `split` $\cup$ `no_split`

3.4 Application to Imprecise Measurements

This section presents the application of the splitting algorithm to estimation problems involving imprecise measurements. Unlike traditional vector-type measurements, imprecise measurements are non-specific, yet still contain valuable information. Examples of imprecise measurements include natural language statements [14, 93], inference rules [75, Sec. 22.2.4], and received signal strength type measurements under path-loss uncertainty [93, 84]. This section demonstrates the estimation of a person's location and velocity as they move through a public space using imprecise natural language measurements, as originally posed in [93]. Tracking is performed using a new GM Bernoulli filter for imprecise measurements, as discussed in the following subsections.

3.4.1 Imprecise Measurements

Imprecise measurements, such as those from natural language statements, can be modeled as RFSs and specified using *generalized likelihood functions.* For example, the statement

$$S = \text{“Felice is near the taco stand”} \tag{3.31}$$

provides some evidence about Felices's location, yet is not mutually exclusive[1]. For simplicity, this chapter adopts the definition of being "near" a point $\mathbf{z}_0$ as belonging to a disc $\boldsymbol{\zeta} \subset \mathbb{Z}$ of radius l:

$$\boldsymbol{\zeta} = \{\mathbf{z} : \|\mathbf{z} - \mathbf{z}_0\| \leq l\} \tag{3.32}$$

[1] In fact, this statement can further be considered vague or fuzzy due to uncertainty in the observer's definition of "near" [41, p. 266].

Although this specific natural language statement interpretation is considered for simplicity, the presented approach does not preclude more sophisticated models, such as those in [14, 106]. The associated generalized likelihood function for this imprecise measurement is

$$\tilde{g}(\boldsymbol{\zeta}|\mathbf{x}) = P\{\mathbf{z} \in \boldsymbol{\zeta}\} = P\{\mathbf{h}(\mathbf{x}) \in \boldsymbol{\zeta}\} \tag{3.33}$$

where $\mathbf{h} : \mathbb{X} \mapsto \mathbb{Z}$ is the deterministic mapping from the state space to the measurement space [93]. Generalized likelihood functions, such as those for natural language statements, are often nonlinear in $\mathbf{x}$ and therefore result in non-Gaussian posterior single-object densities. Through the presented Gaussian splitting approach and expansion of the likelihood function about the component means, GM RFS filters can accommodate imprecise measurements, as demonstrated in the context of the RFS Bernoulli filter in the following subsection.

3.4.2 Bernoulli Filter for Imprecise Measurements

The Bernoulli filter is the Bayes-optimal filter for tracking a single object in the presence of false alarms, misdetections, and unknown object birth/death [74, Sec. 14]. A Bernoulli distribution is parameterized by a probability of object existence r and state pdf $p(\mathbf{x})$. The density of a Bernoulli RFS is [74, p. 516]

$$f(X) = \begin{cases} 1 - r, & \text{if } X = \emptyset \\ r \cdot p(\mathbf{x}), & \text{if } X = \{\mathbf{x}\} \end{cases} \tag{3.34}$$

Denote by p_b the conditional probability that the object is born given that it did not exist in the previous time step. Similarly, denote by p_S the conditional probability that the object survives to the next time step. The initial state of an object born at time k is assumed to be distributed according to the birth spatial density $b_k(\mathbf{x})$. Then, by the FISST generalized Chapman-Kolmogorov equation, the Bernoulli filter prediction equations are [74, p. 519]

$$p_{k|k-1}(\mathbf{x}) = \frac{p_b \cdot (1 - r_{k-1|k-1}) b_{k|k-1}(\mathbf{x})}{r_{k|k-1}} + \frac{p_S \cdot r_{k-1|k-1} \int \pi_{k|k-1}(\mathbf{x}|\mathbf{x}') p_{k-1|k-1}(\mathbf{x}') \mathrm{d}\mathbf{x}'}{r_{k|k-1}} \tag{3.35}$$

$$r_{k|k-1} = p_b \cdot (1 - r_{k-1|k-1}) + p_S \cdot r_{k-1|k-1} \tag{3.36}$$

where $\pi_{k|k-1}(\mathbf{x}|\mathbf{x}')$ is the single-object Markov state transition density. Suppose that the spatial density and birth density are GMs and that the transition density is linear-Gaussian:

$$p_{k-1|k-1}(\mathbf{x}) = \sum_{\ell=1}^{L_{k-1}} w_{k-1}^{(\ell)} \mathcal{N}(\mathbf{x};\, \mathbf{m}_{k-1}^{(\ell)},\, \mathbf{P}_{k-1}^{(\ell)}) \tag{3.37}$$

$$b_{k|k-1}(\mathbf{x}) = \sum_{\ell=1}^{L_{b,k}} \hat{w}_{b,k}^{(\ell)} \mathcal{N}(\mathbf{x};\, \mathbf{m}_{b,k}^{(\ell)},\, \mathbf{P}_{b,k}^{(\ell)}) \tag{3.38}$$

$$\pi_{k|k-1}(\mathbf{x}|\mathbf{x}') = \mathcal{N}(\mathbf{x};\, \mathbf{F}_{k-1}\mathbf{x}',\, \mathbf{Q}_{k-1}) \tag{3.39}$$

where $\mathbf{F}_{k-1} \in \mathbb{R}^{n_x \times n_x}$ is the discrete time state transition matrix and $\mathbf{Q}_{k-1} \in \mathbb{R}^{n_x \times n_x}$ is the process noise covariance matrix. Then, the predicted spatial density at k is the sum of two GMs, given as

$$p_{k|k-1}(\mathbf{x}) = \sum_{\ell=1}^{L_{b,k}} w_{b,k}^{(\ell)} \mathcal{N}(\mathbf{x};\, \mathbf{m}_{b,k}^{(\ell)},\, \mathbf{P}_{b,k}^{(\ell)}) + \sum_{\ell=1}^{L_{k-1}} w_{S,k|k-1}^{(\ell)} \mathcal{N}(\mathbf{x};\, \mathbf{m}_{S,k|k-1}^{(\ell)},\, \mathbf{P}_{S,k|k-1}^{(\ell)}) \tag{3.40}$$

where

$$w_{b,k}^{(\ell)} = \hat{w}_{b,k}^{(\ell)} \frac{p_b \cdot (1 - r_{k-1|k-1})}{r_{k|k-1}} \tag{3.41}$$

$$w_{S,k|k-1}^{(\ell)} = w_{k-1}^{(\ell)} \frac{p_S \cdot r_{k-1|k-1}}{r_{k|k-1}} \tag{3.42}$$

$$\mathbf{m}_{S,k|k-1}^{(\ell)} = \mathbf{F}_{k-1} \mathbf{m}_{k-1}^{(\ell)} \tag{3.43}$$

$$\mathbf{P}_{S,k|k-1}^{(\ell)} = \mathbf{F}_{k-1} \mathbf{P}_{k-1}^{(\ell)} \mathbf{F}_{k-1}^T + \mathbf{Q}_{k-1} \tag{3.44}$$

The predicted spatial density (3.40) can thus be expressed as a combined GM of the form

$$p_{k|k-1}(\mathbf{x}) = \sum_{\ell=1}^{L_{k|k-1}} w_{k|k-1}^{(\ell)} \mathcal{N}(\mathbf{x};\, \mathbf{m}_{k|k-1}^{(\ell)},\, \mathbf{P}_{k|k-1}^{(\ell)}) \tag{3.45}$$

where $\sum_{\ell=1}^{L_{k|k-1}} w_{k|k-1}^{(\ell)} = 1$.

The FoV-dependent probability of detection function is given by

$$p_{D,k}(\mathbf{x}; \mathcal{S}_k) = 1_{\mathcal{S}_k}(\mathbf{x}) p_D(\mathbf{s}) \tag{3.46}$$

where the single-argument function $p_D(\mathbf{s})$ is the corresponding probability of detection for an unbounded FoV. The measurement Υ_k is then an RFS

$$\Upsilon_k = \{\boldsymbol{\zeta}_1,\, \ldots,\, \boldsymbol{\zeta}_{M_k}\} \in \mathcal{F}(\mathfrak{Z}) \tag{3.47}$$

consisting of a (potentially empty) set of false alarms and a (potentially empty) imprecise measurement set due a true object, where $\mathfrak{Z}$ is the set of all closed subsets of $\mathbb{Z}$ and $\mathcal{F}(\mathfrak{Z})$ is the space of all finite subsets of $\mathfrak{Z}$, as shown in [74, Ch. 5]. Assume that false alarms are Poisson distributed (2.16) with rate λ_c and PHD $\lambda_c \tilde{c}(\boldsymbol{\zeta})$, where $\tilde{c}(\boldsymbol{\zeta})$ denotes the normalized density. Then, the posterior state density and probability of existence are given by

$$p_{k|k}(\mathbf{x}) = \frac{1 - p_D(\mathbf{x}; \mathcal{S}_k) + p_D(\mathbf{x}; \mathcal{S}_k) \sum_{\boldsymbol{\zeta} \in \Upsilon_k} \frac{\tilde{g}_k(\boldsymbol{\zeta}|\mathbf{x})}{\lambda_c \tilde{c}(\boldsymbol{\zeta})}}{1 - \Delta_k} p_{k|k-1}(\mathbf{x}) \tag{3.48}$$

$$r_{k|k} = \frac{1 - \Delta_k}{1 - r_{k|k-1}\Delta_k} r_{k|k-1} \tag{3.49}$$

where

$$\Delta_k = \int p_D(\mathbf{x}; \mathcal{S}_k) p_{k|k-1}(\mathbf{x}) \mathrm{d}\mathbf{x} - \sum_{\boldsymbol{\zeta} \in \Upsilon_k} \frac{\int p_D(\mathbf{x}; \mathcal{S}_k) \tilde{g}_k(\boldsymbol{\zeta}|\mathbf{x}) p_{k|k-1}(\mathbf{x}) \mathrm{d}\mathbf{x}}{\lambda_c \tilde{c}(\boldsymbol{\zeta})} \tag{3.50}$$

If $p_{k|k-1}(\mathbf{x})$ is a GM, the state-dependent probability of detection and generalized likelihood function can be expanded about the component means, giving

$$p_{k|k}(\mathbf{x}) = \sum_{\ell=1}^{L_{k|k}} w_{k|k}^{(\ell)} \mathcal{N}(\mathbf{x};\, \mathbf{m}_{k|k}^{(\ell)},\, \mathbf{P}_{k|k}^{(\ell)}) \tag{3.51}$$

$$w_{k|k}^{(\ell)} = \frac{w_{k|k-1}^{(\ell)}}{1-\Delta_k}\left[1 - p_D(\mathbf{m}_{k|k-1}^{(\ell)}; \mathcal{S}_k) + p_D(\mathbf{m}_{k|k-1}^{(\ell)}; \mathcal{S}_k) \sum_{\boldsymbol{\zeta}\in\Upsilon_k} \frac{\tilde{g}_k(\boldsymbol{\zeta}|\mathbf{m}_{k|k-1}^{(\ell)})}{\lambda_c \tilde{c}(\boldsymbol{\zeta})}\right] \tag{3.52}$$

$$\begin{aligned}\Delta_k = &\sum_{\ell=1}^{L_{k|k-1}} w_{k|k-1}^{(\ell)} p_D(\mathbf{m}_{k|k-1}^{(\ell)}; \mathcal{S}_k) \\ &- \sum_{\boldsymbol{\zeta}\in\Upsilon_k} \frac{\sum_{\ell=1}^{L_{k|k-1}} w_{k|k-1}^{(\ell)} p_D(\mathbf{m}_{k|k-1}^{(\ell)}; \mathcal{S}_k)\tilde{g}_k(\boldsymbol{\zeta}|\mathbf{m}_{k|k-1}^{(\ell)})}{\lambda_c \tilde{c}(\boldsymbol{\zeta})}\end{aligned} \tag{3.53}$$

$$\mathbf{m}_{k|k}^{(\ell)} = \mathbf{m}_{k|k-1}^{(\ell)} \tag{3.54}$$

$$\mathbf{P}_{k|k}^{(\ell)} = \mathbf{P}_{k|k-1}^{(\ell)} \tag{3.55}$$

The approximation error due to the expansion in (3.52) and (3.53) depends on the GM resolution near points of strong nonlinearity. In a high-resolution mixture containing many components with small covariance matrices, the region about each mean in which the linear approximation must be valid is correspondingly smaller compared to a low-resolution mixture [2]. Therefore, the recursive splitting method is employed to refine the mixture in nonlinear regions–specifically around $\partial\mathcal{S}_k^{(\cdot)}$ and $\partial\boldsymbol{\zeta}_{(\cdot)}$–before computing the posterior GM (3.51). Then, the resulting posterior GM is reduced using one of many available algorithms for GM reduction [124, 94, 95, 24]. This novel process, referred to as the GM Bernoulli filter for imprecise measurements, is summarized in Algorithm 3.

Algorithm 3 GM Bernoulli Filter for Imprecise Measurements

given $r_{0|0}, p_{0|0}(\mathbf{x})$
for $k = 1, \ldots, K$ **do**
  Compute $r_{k|k-1}$ accrd. to (3.36)
  Compute $\{w_{S,k|k-1}^{(\ell)}, \mathbf{m}_{S,k|k-1}^{(\ell)}, \mathbf{P}_{S,k|k-1}^{(\ell)}\}_{\ell=1}^{L_{k|k-1}}$ accrd. to (3.42)-(3.44)
  Compute $\{w_{b,k}^{(\ell)}\}_{\ell=1}^{L_{b,k}}$ accrd. to (3.41)
  $\{w_{k|k-1}^{(\ell)}, \mathbf{m}_{k|k-1}^{(\ell)}, \mathbf{P}_{k|k-1}^{(\ell)}\}_{\ell=1}^{L_{k|k-1}} \leftarrow \ldots$
    $\{w_{S,k|k-1}^{(\ell)}, \mathbf{m}_{S,k|k-1}^{(\ell)}, \mathbf{P}_{S,k|k-1}^{(\ell)}\}_{\ell=1}^{L_{k-1}} \cup \{w_{b,k|k-1}^{(\ell)}, \mathbf{m}_{b,k|k-1}^{(\ell)}, \mathbf{P}_{b,k|k-1}^{(\ell)}\}_{\ell=1}^{L_{b,k}}$
  $\{w_{k|k-1}^{(\ell)}, \mathbf{m}_{k|k-1}^{(\ell)}, \mathbf{P}_{k|k-1}^{(\ell)}\}_{\ell=1}^{L_{k|k-1}} \leftarrow \ldots$
    `split_for_multifov(`$\{w_{k|k-1}^{(\ell)}, \mathbf{m}_{k|k-1}^{(\ell)}, \mathbf{P}_{k|k-1}^{(\ell)}\}_{\ell=1}^{L_{k|k-1}}$, $w_{\min}$, $\{\mathcal{S}_k^{(\imath)}\}_{\imath=1}^{\mathrm{M}} \cup \Upsilon_k$, R, λ`)`
  Compute Δ_k accrd. to (3.53)
  Compute $r_{k|k}$ accrd. to (3.49)
  Compute $\{w_{k|k}^{(\ell)}, \mathbf{m}_{k|k}^{(\ell)}, \mathbf{P}_{k|k}^{(\ell)}\}_{\ell=1}^{L_{k|k}}$ accrd. to (3.52),(3.54),(3.55)
  $\{w_{k|k}^{(\ell)}, \mathbf{m}_{k|k}^{(\ell)}, \mathbf{P}_{k|k}^{(\ell)}\}_{\ell=1}^{L_{k|k}} \leftarrow$ `reduce(` $\{w_{k|k}^{(\ell)}, \mathbf{m}_{k|k}^{(\ell)}, \mathbf{P}_{k|k}^{(\ell)}\}_{\ell=1}^{L_{k|k}}$ `)`
end for

3.4.3 Airport Tracking Example

The recursive splitting approach is demonstrated in the context of tracking a person of interest through a crowded airport. This problem was originally posed in [93] and solved using a particle filter implementation of the Bernoulli filter. The object state is defined as

$$\mathbf{x}_k^T = [x_k \quad y_k \quad \dot{x}_k \quad \dot{y}_k] = [\mathbf{s}_k^T \quad \mathbf{v}_k^T] \tag{3.56}$$

where $\mathbf{s}_k$ is the person's 2D position in the airport and $\mathbf{v}_k$ is the person's velocity, where dimensionless distance units are used throughout. Measurements of the person are composed of natural language statements describing the person's current location in the form $Z_k = \{\zeta_{k,1}, \ldots, \zeta_{k,M_k}\}$, where M_k is the number of statements received at time k and

$$\zeta = a \implies \text{the person is near the anchor } a \tag{3.57}$$

In (3.57), the integer $a \in \mathbb{A} \subset \mathbb{N}$ represents a fixed anchor, such as a taco stand or coffee shop, with corresponding known position $\mathbf{r}_a \in \mathbb{Z}$. Observers sometimes report incorrect statements (as false alarms) and sometimes fail to report true statements (as misdetections). The corresponding generalized likelihood function is

$$\tilde{g}_k(\zeta = a \,|\, \mathbf{x}_k) = \begin{cases} 1 & \text{if } \|\mathbf{s}_k - \mathbf{r}_a\| < 2d_a/3 \\ 0 & \text{otherwise} \end{cases} \tag{3.58}$$

where d_a is the distance between anchor a and its nearest neighbor. If the target is within $2d_a/3$ of anchor a, the natural language statement reports that the target is near a (unless misdetected). Defining the compact subset

$$\mathcal{A}_a = \{\mathbf{s} \,:\, \|\mathbf{s} - \mathbf{r}_a\| < 2d_a/3\} \tag{3.59}$$

the generalized likelihood function (3.58) can be written in terms of an indicator function as

$$\tilde{g}_k(\zeta = a \,|\, \mathbf{x}_k) = 1_{\mathcal{A}_a}(\mathbf{s}_k) \tag{3.60}$$

By this likelihood function, (3.52)-(3.53) simplify to

$$w_{k|k}^{(\ell)} = \frac{w_{k|k-1}^{(\ell)}}{1 - \Delta_k}\left(1 - p_D(\mathbf{m}_{k|k-1}^{(\ell)}; \mathcal{S}_k) + p_D(\mathbf{m}_{k|k-1}^{(\ell)}; \mathcal{S}_k) \sum_{\zeta \in Z_k} \frac{1_{\mathcal{A}_\zeta}(\mathbf{m}_{s,k|k-1}^{(\ell)})}{\lambda_c \tilde{c}(\zeta)}\right) \tag{3.61}$$

$$\begin{aligned} \Delta_k = &\sum_{\ell=1}^{L_{k|k-1}} w_{k|k-1}^{(\ell)} p_D(\mathbf{m}_{k|k-1}^{(\ell)}; \mathcal{S}_k) \\ &- \sum_{\zeta \in Z_k} \frac{\sum_{\ell=1}^{L_{k|k-1}} w_{k|k-1}^{(\ell)} p_D(\mathbf{m}_{k|k-1}^{(\ell)}; \mathcal{S}_k) 1_{\mathcal{A}_\zeta}(\mathbf{m}_{s,k|k-1}^{(\ell)}; \mathcal{S}_k)}{\lambda_c \tilde{c}(\zeta)} \end{aligned} \tag{3.62}$$

where the density of false alarms (clutter) $\tilde{c}(\zeta)$ is taken to be uniform over support $\mathbb{A}$ with rate λ_c.

The anchor locations and bounds $\partial\mathcal{A}_a$ are shown in Fig. 3.6. The gray shaded regions indicate exclusion regions the person cannot occupy due to physical barriers, and thus, $p_k(\mathbf{x}) = 0$ in these regions. Detections are reported every $T_k = 15\,[\mathrm{s}]$

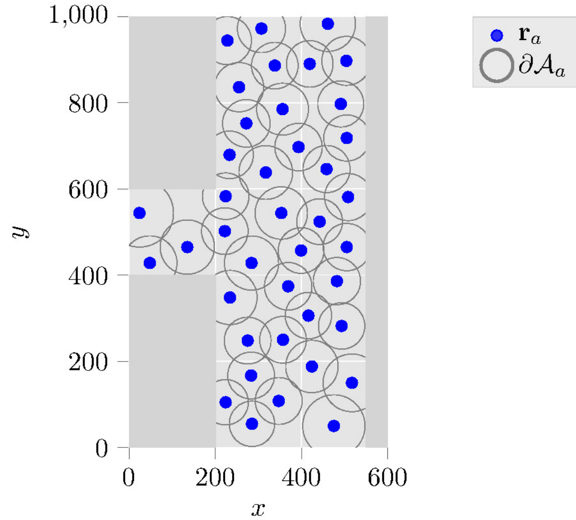

Figure 3.6: Anchor locations and association extents.

and include an average of $\lambda_c = 0.25$ false detections per reporting period. True detections are reported with a probability of detection $p_D(\mathbf{x}_k; \mathcal{S}_k)$ given by (3.46) with $p_D(\mathbf{s}_k) = 0.9$ and composite detection FoV

$$\mathcal{S}_k = \bigcup_{a \in \mathbb{A}} \mathcal{A}_a \tag{3.63}$$

The person state is governed by the linear-Gaussian transition density

$$\pi_{k|k-1}(\mathbf{x}|\mathbf{x}') = \mathcal{N}(\mathbf{x};\, \mathbf{F}_{k-1}\mathbf{x}',\, \mathbf{Q}_{k-1}) \tag{3.64}$$

where

$$\mathbf{F}_k = \begin{bmatrix} 1 & 0 & T_k & 0 \\ 0 & 1 & 0 & T_k \\ 0 & 0 & 1 & 0 \\ 0 & 0 & 0 & 1 \end{bmatrix} \quad \text{and} \quad \mathbf{Q}_k = \begin{bmatrix} \frac{\varpi T_k^3}{3} & 0 & \frac{\varpi T_k^2}{2} & 0 \\ 0 & \frac{\varpi T_k^3}{3} & 0 & \frac{\varpi T_k^2}{2} \\ \frac{\varpi T_k^2}{2} & 0 & \varpi T_k & 0 \\ 0 & \frac{\varpi T_k^2}{2} & 0 & \varpi T_k \end{bmatrix} \tag{3.65}$$

and $\varpi = 0.04$ is the intensity of process noise.

The simulated reports are processed by the GM Bernoulli filter for imprecise measurements (Alg. 3) at each time step to obtain the posterior probability of existence and state density. By splitting the density about the relevant anchor boundaries, the imprecise measurements are incorporated to refine the probabilistic belief and estimate the person's trajectory over time. The true and estimated trajectories and densities at select time steps are shown in Fig. 3.7a. As shown, the true trajectory is consistently within the spatial distribution support. For computational performance, Runnal's GM reduction algorithm [94] is employed to reduce the posterior mixture to 100 components. The posterior probability of existence is shown over time in Fig. 3.7b. The probability of existence of the object is consistently near one, falling momentarily to $r_{k|k} = 0.4$, which appropriately reflects the increased uncertainty after receiving three consecutive misdetections.

The state estimation performance is quantified using the root-sum-square (RSS) of the posterior conditional covariance and shown in Fig. 3.8. The velocity RSS quickly converges to a steady state of approximately 1.6 [dist/s], the lower bound of which is largely determined by the person's assumed maneuverability and associated process noise covariance. Similarly, the largest uncertainty is observed near $k = 21$ ($t = 315$ [s]), after three consecutive misdetections.

While this example considers single-object estimation, the expansion and splitting approach described in Section 3.4.2 is applicable to any GM RFS filter and, thus, can be used in multi-object estimation problems. In the example problem on tracking a person of interest and its multi-object extension involving multiple persons of interest, the posterior RFS density can be used to intelligently query or deploy resources to find or intercept persons of interest. In this case, one particularly useful statistic is the probability that a given number of people are present near a particular anchor. This information is fully described by the RFS FoV cardinality distribution, as presented in the following section.

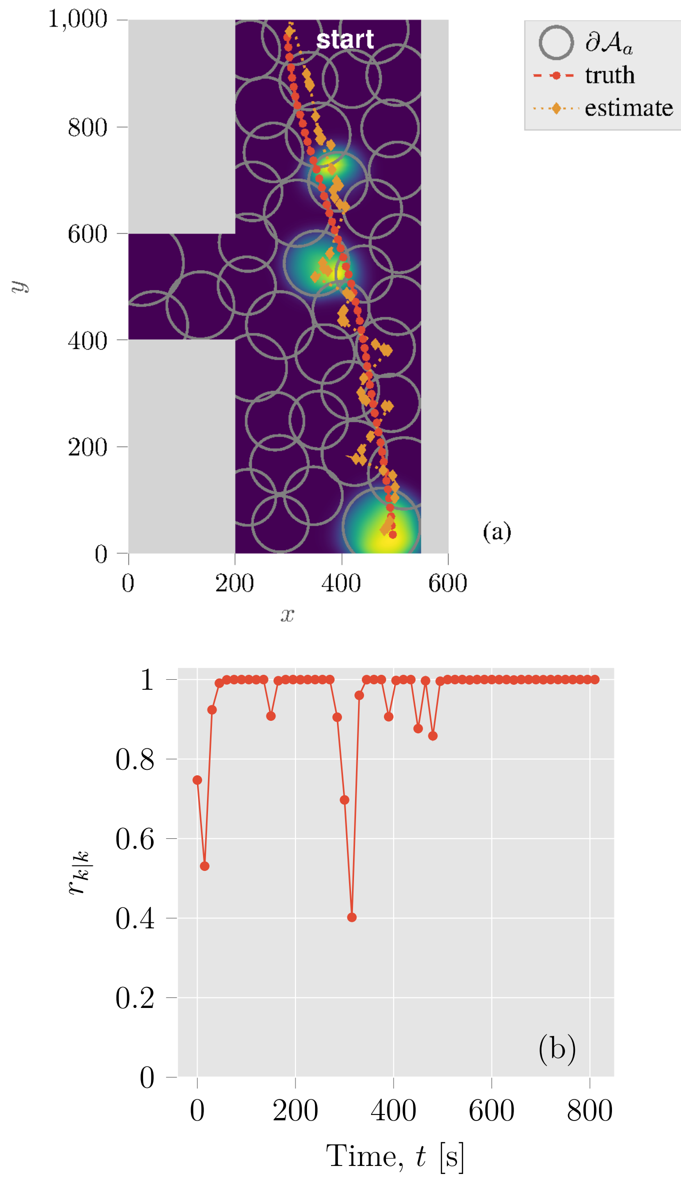

Figure 3.7: (a) True trajectory and state estimates over time, where position state densities are shown for time steps $k = 15, 25, 55$ ($t = 225, 375, 825$ [s]) and (b) posterior probability of existence over time.

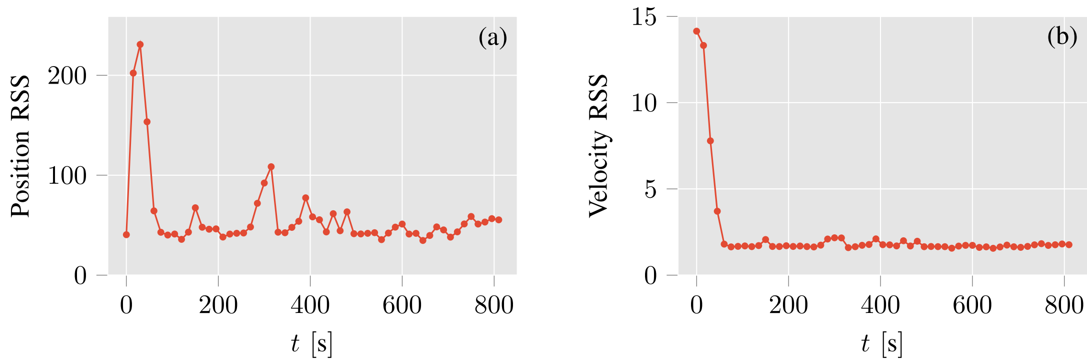

Figure 3.8: RSS of position (a) and velocity (b) conditional covariance.

3.5 FoV Cardinality Distribution

This section presents pmfs for the cardinality of objects inside a bounded FoV $\mathcal{S}$ given different multi-object workspace densities $f(\cdot)$. A similar concept is discussed in [75] in the context of "censored" RFSs, and a general expression is provided in terms of set derivatives and belief mass functions. This dissertation presents a new direct approach to obtain FoV cardinality distributions based on conditional cardinality functions and derives new simplified expressions for representative RFS distribution classes. The Poisson, i.i.d.c., MB, and GLMB distributions are considered in Subsections 3.5.1, 3.5.2, 3.5.3, and 3.5.4, respectively.

The probability of n objects existing inside FoV $\mathcal{S}$ conditioned on X can be written in terms of the indicator function as

$$\rho_{\mathcal{S}}(n \,|\, X) = \sum_{X^n \subseteq X} [1_{\mathcal{S}}(\cdot)]^{X^n} [1 - 1_{\mathcal{S}}(\cdot)]^{X \setminus X^n} \tag{3.66}$$

where the summation is taken over all subsets $X^n \subseteq X$ with cardinality n. Given the RFS density $f(X)$, the FoV cardinality distribution is obtained via the set integral as

$$\rho_{\mathcal{S}}(n) = \int \rho_{\mathcal{S}}(n \,|\, X) f(X) \delta X \tag{3.67}$$

Expanding the integral,

$$\rho_{\mathcal{S}}(n) = \quad \sum_{m=n}^{\infty} \frac{1}{m!} \int\limits_{\mathbb{X}^m} \rho_{\mathcal{S}}(n \,|\, \{\mathbf{x}_1,\ldots,\mathbf{x}_m\}) f(\{\mathbf{x}_1,\ldots,\mathbf{x}_m\}) \mathrm{d}\mathbf{x}_1 \cdots \mathrm{d}\mathbf{x}_m$$

Remark. *The results presented in this section can be extended to express the cardinality distribution of object-originated detections Z (excluding false alarms) by noting that*

$$\rho_{\mathcal{S}}(n_Z \,|\, X) = \sum_{X^n \subseteq X} [p_D(\cdot) 1_{\mathcal{S}}(\cdot)]^{X^n} [1 - p_D(\cdot) 1_{\mathcal{S}}(\cdot)]^{X \setminus X^n} \tag{3.68}$$

where $n_Z = |Z|$.

3.5.1 Poisson Distribution

The following proposition establishes the FoV cardinality distribution for the Poisson RFS prior, which is commonly used to model false alarm and object birth distributions.

Proposition 1. *Given a Poisson-distributed RFS with PHD $D(\mathbf{x})$ and global cardinality mean N_X, the cardinality of objects inside the FoV $\mathcal{S} \subseteq \mathbb{X}$ is distributed according to*

$$\rho_{\mathcal{S}}(n) = \sum_{m=n}^{\infty} \frac{e^{-N_X}}{n!(m-n)!} \langle 1_{\mathcal{S}}, D \rangle^n \langle 1 - 1_{\mathcal{S}}, D \rangle^{m-n} \tag{3.69}$$

Proof: Substituting (2.16) into (3.68),

$$\rho_{\mathcal{S}}(n) = \sum_{m=n}^{\infty} \frac{1}{m!} e^{-N_X} \int_{\mathbb{X}^m} \sum_{X^n \subseteq X} [1_{\mathcal{S}}(\cdot) D(\cdot)]^{X^n} \cdot [(1 - 1_{\mathcal{S}}(\cdot)) D(\cdot)]^{X \setminus X^n} \mathrm{d}\mathbf{x}_1 \cdots \mathrm{d}\mathbf{x}_m \tag{3.70}$$

The nested integrals of (3.70) can be distributed, rewriting the second sum over n-cardinality index sets $\mathcal{I}^n$ as

$$\rho_{\mathcal{S}}(n) = \sum_{m=n}^{\infty} \frac{1}{m!} e^{-N_X} \sum_{\mathcal{I}^n \subseteq \mathbb{N}_m} \left[\int 1_{\mathcal{S}}(\mathbf{x}_{(\cdot)}) D(\mathbf{x}_{(\cdot)}) \mathrm{d}\mathbf{x}_{(\cdot)} \right]^{\mathcal{I}^n} \cdot \left[\int (1 - 1_{\mathcal{S}}(\mathbf{x}_{(\cdot)})) D(\mathbf{x}_{(\cdot)}) \right]^{\mathbb{N}_m \backslash \mathcal{I}^n} \tag{3.71}$$

Note that the value of the integrals is independent of the variable index, and thus

$$\rho_{\mathcal{S}}(n) = \sum_{m=n}^{\infty} e^{-N_X} \frac{1}{m!} \frac{m!}{n!(m-n)!} \langle 1_{\mathcal{S}}, D \rangle^n \langle 1 - 1_{\mathcal{S}}, D \rangle^{m-n} \tag{3.72}$$

from which (3.69) trivially follows. ■

Remark. *Computation of (3.69) requires only one integral computation; namely $\left\langle 1_{\mathcal{S}}, D \right\rangle$, which can be found either by summing the weights of (3.6) or through Monte Carlo integration. Using the integral property of the PHD (2.19), the integral*

$$\left\langle 1 - 1_{\mathcal{S}}, D \right\rangle = N_X - \left\langle 1_{\mathcal{S}}, D \right\rangle \tag{3.73}$$

Furthermore, for $m \gg N_X$, the summand of (3.69) is negligible, and the infinite sum can be safely truncated at an appropriately chosen $m = m_{\max}(N_X)$.

3.5.2 Independent Identically Distributed Cluster (i.i.d.c.) Distribution

The i.i.d.c. RFS distribution is a generalization of the Poisson RFS in which the cardinality is not restricted to be Poisson but rather described by an arbitrary pmf. As such, i.i.d.c. distributions can describe false alarm and birth object processes when more specific cardinality information is available. The following proposition establishes the corresponding FoV cardinality distribution for i.i.d.c. distributions.

Proposition 2. *Given an i.i.d.c.-distributed RFS with cardinality pmf $\rho(\cdot)$ and state density $p(\cdot)$, the cardinality of objects inside the FoV $\mathcal{S}$ is distributed according to*

$$\rho_{\mathcal{S}}(n) = \sum_{m=n}^{\infty} \rho(m) \binom{m}{n} \langle 1_{\mathcal{S}}, p \rangle^{n} \langle 1 - 1_{\mathcal{S}}, p \rangle^{m-n} \tag{3.74}$$

where $\binom{m}{n}$ is the binomial coefficient.

Proof: Substituting (2.22) into (3.68),

$$\rho_{\mathcal{S}}(n) = \sum_{m=n}^{\infty} \frac{1}{m!} m! \rho(m) \int_{\mathbb{X}^m} \sum_{X^n \subseteq X} \cdot [1_s(\cdot) p(\cdot)]^{X^n} [(1 - 1_s(\cdot)) p(\cdot)]^{X \setminus X^n} \mathrm{d}\mathbf{x}_1 \cdots \mathrm{d}\mathbf{x}_m \tag{3.75}$$

The integral can be moved inside the products so that

$$\begin{aligned} \rho_{\mathcal{S}}(n) = \sum_{m=n}^{\infty} \rho(m) \sum_{\mathcal{I}^n \subseteq \mathbb{N}_m} & \left[\int 1_s(\mathbf{x}_{(\cdot)}) p(\mathbf{x}_{(\cdot)}) \mathrm{d}\mathbf{x}_{(\cdot)} \right]^{\mathcal{I}^n} \\ & \cdot \left[\int (1 - 1_s(\mathbf{x}_{(\cdot)})) p(\mathbf{x}_{(\cdot)}) \mathrm{d}\mathbf{x}_{(\cdot)} \right]^{\mathbb{N}_m \setminus \mathcal{I}^n} \end{aligned} \tag{3.76}$$

Equation (3.74) follows from (3.76) by noting that there are $\binom{m}{n}$ unique unordered n-cardinality index subsets of $\mathbb{N}_m$. ■

3.5.3 Multi-Bernoulli Distribution

Multi-object processes characterized by object existence uncertainty and spatial uncertainty can be modeled efficiently as MB RFSs. Given the MB density describing a multi-object distribution over the surveillance region, a useful statistic is the probability that a given number of objects exist within a given subregion, such as a sensor FoV. The following proposition establishes the FoV cardinality distribution for an MB distribution.

Proposition 3. *Given an MB density of the form of (2.25), the cardinality of objects inside the FoV $\mathcal{S}$ is distributed according to*

$$\rho_{\mathcal{S}}(n) = \left[\left(1 - r^{(\cdot)}\right)\right]^{\mathbb{N}_M} \cdot \sum_{\mathcal{I}_1 \uplus \mathcal{I}_2 \uplus \mathcal{I}_3} \delta_n(|\mathcal{I}_1|) \left[\frac{\left\langle 1_{\mathcal{S}}, r^{(\cdot)} p^{(\cdot)} \right\rangle}{1 - r^{(\cdot)}}\right]^{\mathcal{I}_1} \left[\frac{\left\langle 1 - 1_{\mathcal{S}}, r^{(\cdot)} p^{(\cdot)} \right\rangle}{1 - r^{(\cdot)}}\right]^{\mathcal{I}_2} \quad (3.77)$$

where the summation is taken over all mutually exclusive index partitions $\mathcal{I}_1 \uplus \mathcal{I}_2 \uplus \mathcal{I}_3 = \mathbb{N}_M$.

The proof of Proposition 3 is given in Appendix A.1. Following the same procedure, similar results for the labeled multi-Bernoulli (LMB) [89] and multi-Bernoulli mixture (MBM) [125] RFS distributions may be obtained.

Direct computation of (3.77) is only feasible for small M due to the sum over all permutations $\mathcal{I}_1 \uplus \mathcal{I}_2 \uplus \mathcal{I}_3$. For large M, an alternative formulation based on Fourier transforms allows fast numerical computation. For each MB component, the integral $\left\langle 1_{\mathcal{S}}, p^{(i)} \right\rangle$ is computed either by summing the weights of the partitioned GM or by Monte Carlo integration. Using the integral results, the probability of object i existing inside the FoV is found as

$$r_{\mathcal{S}}^{(i)} = r^{(i)} \left\langle 1_{\mathcal{S}}, p^{(i)} \right\rangle \quad (3.78)$$

Then, following the approach of [32], (3.77) can be equivalently written as

$$\rho_{\mathcal{S}}(n) = \frac{1}{M+1} \cdot \sum_{m=0}^{M} \left\{ e^{-j2\pi mn/(M+1)} \prod_{k=1}^{M} \left[r_{\mathcal{S}}^{(k)} e^{j2\pi m/(M+1)} + (1 - r_{\mathcal{S}}^{(k)}) \right] \right\} \quad (3.79)$$

and solved using the discrete Fourier transform, for which a number of efficient algorithms exist.

3.5.4 Generalized Labeled Multi-Bernoulli Distribution

The GLMB LRFS is among the most descriptive RFS distribution classes and is a conjugate prior under the GLMB filter "standard" transition and likelihood density models. The following proposition establishes the FoV cardinality distribution for GLMB distributions.

Proposition 4. *Given a GLMB density $\mathring{f}(\mathring{X})$ of the form of (2.27), the cardinality of objects inside a bounded FoV $\mathcal{S}$ is distributed according to*

$$\rho_{\mathcal{S}}(n) = \sum_{(\xi,\mathcal{I}_1 \uplus \mathcal{I}_2)\in\Xi\times\mathcal{F}(\mathbb{L})} w^{(\xi)}(I)\delta_n(|\mathcal{I}_1|)\left\langle 1_{\mathcal{S}}, p\right\rangle^{\mathcal{I}_1}\left\langle 1-1_{\mathcal{S}}, p\right\rangle^{\mathcal{I}_2} \tag{3.80}$$

Proof: Equation (3.66) can be rewritten to accommodate the labeled RFS as

$$\rho_{\mathcal{S}}(n \,|\, \mathring{X}) = \sum_{\mathring{X}^n\subseteq\mathring{X}} [1_{\mathcal{S}}(\cdot)]^{\mathring{X}^n}[1-1_{\mathcal{S}}(\cdot)]^{\mathring{X}\setminus\mathring{X}^n} \tag{3.81}$$

If $\mathring{X}$ is distributed according to the LRFS density $\mathring{f}(\mathring{X})$, the FoV cardinality distribution is obtained via the set integral

$$\rho_{\mathcal{S}}(n) = \int \rho_{\mathcal{S}}(n \,|\, \mathring{X})\mathring{f}(\mathring{X})\delta\mathring{X} \tag{3.82}$$

Expanding the integral,

$$\begin{aligned}\rho_{\mathcal{S}}(n) = \sum_{m=n}^{\infty}\frac{1}{m!}\sum_{(\ell_1,\ldots,\ell_m)\in\mathbb{L}^m}\int_{\mathbb{X}^m}&\rho_{\mathcal{S}}(n \,|\, \{(\mathbf{x}_1,\ell_1),\ldots,(\mathbf{x}_m,\ell_m)\}) \\ &\cdot\mathring{f}(\{(\mathbf{x}_1,\ell_1),\ldots,(\mathbf{x}_m,\ell_m)\})\mathrm{d}\mathbf{x}_1\cdots\mathrm{d}\mathbf{x}_m \end{aligned} \tag{3.83}$$

Defining $p^{(\xi,\ell)}(x) \triangleq p^{(\xi)}(x,\ell)$, substitution of (2.27) and (3.81) into (3.83) yields

$$\begin{aligned}\rho_{\mathcal{S}}(n) &= \sum_{m=n}^{\infty}\frac{1}{m!}m!\sum_{\{\ell_1,\ldots,\ell_m\}\in\mathbb{L}^m}\sum_{\xi\in\Xi} w^{(\xi)}(\{\ell_1,\ldots,\ell_m\}) \\ &\qquad \sum_{I^n\subseteq\{\ell_1,\ldots\ell_m\}}\left\langle 1_{\mathcal{S}}, p^{(\xi,\cdot)}\right\rangle^{I^n}\left\langle 1-1_{\mathcal{S}}, p^{(\xi,\cdot)}\right\rangle^{\{\ell_1,\ldots,\ell_m\}\setminus I^n} \\ &= \sum_{(\xi,I)\in\Xi\times\mathcal{F}(\mathbb{L})} w^{(\xi)}(I)\sum_{I^n\subseteq I}\left\langle 1_{\mathcal{S}}, p^{(\xi,\cdot)}\right\rangle^{I^n}\left\langle 1-1_{\mathcal{S}}, p^{(\xi,\cdot)}\right\rangle^{I\setminus I^n}\end{aligned} \tag{3.84}$$

from which (3.80) follows. ■

Remark. *Substitution of $n = 0$ in (3.80) gives the GLMB void probability functional [12, Eq. 22], which, while less general, has theoretical significance and practical applications in sensor management.*

3.6 Sensor Placement Example

The FoV statistics developed in this chapter are demonstrated through a sensor placement optimization problem subject to multi-object uncertainty. The multi-object state is unknown, random, and distributed according to a known MB distribution $f(X)$. Numerical simulation is performed for the case of 100 MB components, with probabilities of existence randomly chosen between 0.35 and 1. Each MB component has a Gaussian density and randomly chosen mean and covariance. To visualize the workspace distribution, the PHD is shown in Fig. 3.9.

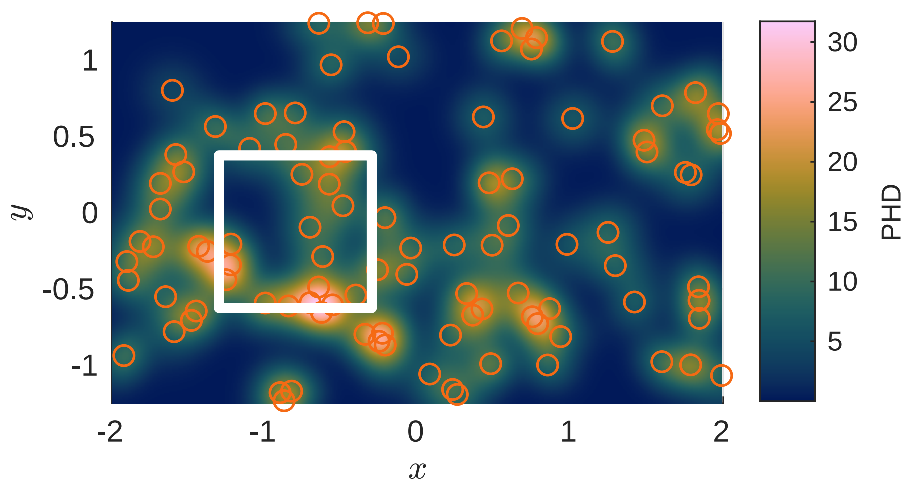

Figure 3.9: PHD of MB workspace distribution with 100 potential objects, where object means are represented by orange circles and the bounds of the FoV that maximizes the FoV cardinality variance are shown in white.

The objective of the sensor control problem is to place the FoV $\mathcal{S}(\mathbf{u})$, consisting of a square of 1×1 dimensions centered at $\mathbf{u} \in \mathbb{U} \subseteq \mathbb{R}^2$, in the ROI (Fig. 3.9) such that the variance of object cardinality inside the FoV is maximized. This objective can be interpreted as placing the FoV in a region of the workspace where the object cardinality is most uncertain. A related objective which minimizes the variance of the *global* cardinality using cardinality-balanced multi-object multi-Bernoulli (CB-MeMBer) predictions was first proposed in [51]. For each candidate FoV placement $\mathbf{u} \in \mathbb{U}$, the FoV cardinality pmf $\rho_{\mathcal{S}(\mathbf{u})}(n)$ is given by (3.77) and is efficiently computed using (3.79). The variance of the resulting pmf is shown as a function of the FoV center location in Fig. 3.10. The optimal FoV center location is found to be $\mathbf{u}^* = [-0.8 \;\; -1.25]^T$.

A compelling result is that, by virtue of the bounded FoV geometry, spatial information is encoded in the FoV cardinality pmf. It can be seen that the optimal FoV (Fig. 3.9) has boundary segments (lower half of left boundary and right half of lower boundary) that bisect clusters of MB components. These boundary segments divide the components' single-object densities such that significant mass appears inside and outside the FoV, increasing the overall FoV cardinality variance.

Note that, by the proposed FoV cardinality objective function, the only sensor parameter considered is the FoV geometry and location. In general, it may be desirable to consider other sensing parameters which may vary with $\mathbf{u}$, such as the probability of detection within the FoV, the false alarm distribution, and sensor noise. The following chapters present objective functions based on *information gain* that account for the complete probabilistic sensing model in a theoretically rigorous fashion.

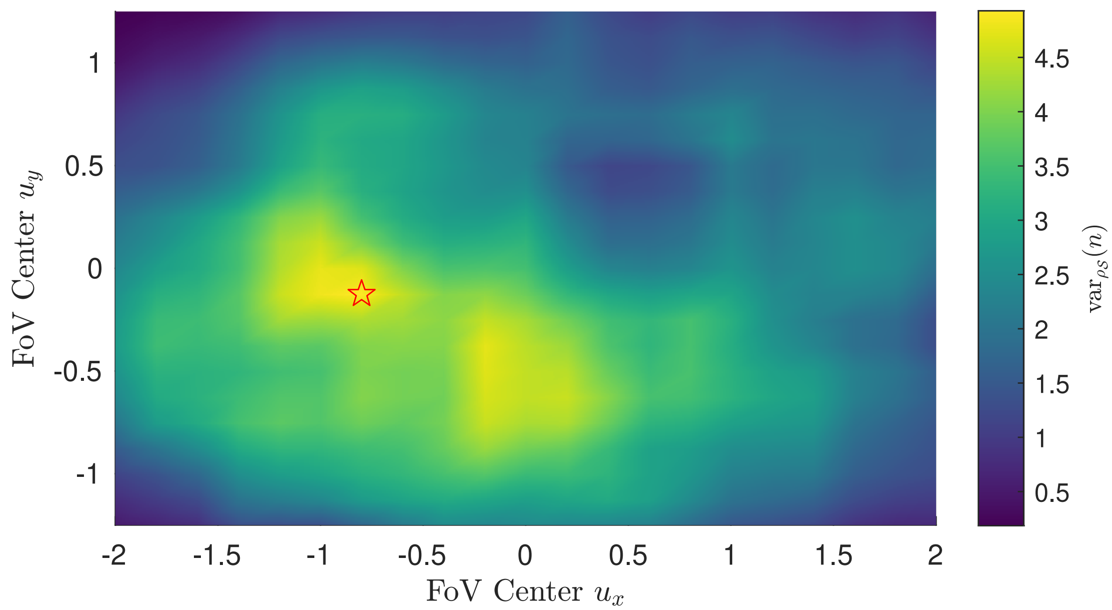

Figure 3.10: FoV cardinality variance as a function of FoV center location, where the red star denotes the maximum variance point.

3.7 Conclusions

This chapter presents an approach for incorporating bounded field-of-view (FoV) geometry into state density updates and object cardinality predictions via finite set statistics (FISST). Negative information is processed in state density updates via a novel Gaussian splitting algorithm that recursively refines a Gaussian mixture approximation near the boundaries of the discrete FoV geometry. Using FISST, cardinality probability mass functions that describe the probability that a given number of objects exist inside the FoV are derived. The approach is presented for representative labeled and unlabeled random finite set distributions and, thus, is applicable to a wide range of tracking, perception, and sensor planning problems.

CHAPTER 4

SINGLE SENSOR INFORMATION-DRIVEN CONTROL

4.1 Introduction

Many modern multi-object tracking applications involve mobile and reconfigurable sensors able to control the position and orientation of their FoV in order to expand their operational tracking capacity and improve state estimation accuracy when compared to fixed sensor systems. By incorporating active sensor control in these dynamic tracking systems, the sensor can autonomously make decisions that produce observations with the highest information content based on prior knowledge and sensor measurements [34, 122, 121]. Also, the sensor FoV is able to move and cover large regions of interest, potentially for prolonged periods of time. By expanding the autonomy and operability of sensors, however, several new challenges are introduced. As the sensor moves and reconfigures itself, the number of objects inside the FoV changes over time. Also, both the number of objects and the objects' states are unknown, time-varying, and subject to significant measurement errors. As a result, existing tracking algorithms and information gain functions (e.g., [34, 122, 121, 100]) that assume a known number of objects and known data association, are either inapplicable or significantly degrade in performance due to measurement noise, object maneuvers, missed/spurious detections, and unknown measurement origin.

Through the use of RFS theory, this chapter formulates the multi-object information-driven control problem as a partially-observed Markov decision process (POMDP). Sensor actions can then be decided to maximize the expected information gain conditioned on a probabilistic belief state. Information-theoretic functions, such as expected entropy reduction (EER) [19, 128], Cauchy-Schwarz Divergence (CSD) [50, 11, 43], KLD [41], and Rényi divergence [91, 92], have been successfully used to represent sensing objectives, such as detection, classification, identification, and tracking, circumventing exhaustive enumeration of all possible outcomes. However, RFS-based information-theoretic sensor control policies remain computationally challenging. Alternatively, they require simplifying assumptions that limit their applicability to SWT systems. Existing tractable solutions employ the so-called predicted ideal measurement set (PIMS) approximation [76], by which sensor actions are selected based on ideal measurements with no measurement noise, false alarms, or missed detections. This chapter presents a new computationally tractable higher-order approximation called the *cell multi-Bernoulli (cell-MB)* approximation for a restricted class of multi-object information gain functions satisfying cell-additivity constraints. Unlike existing approximation methods, the cell-MB approximation accounts for higher-order effects due to false alarms, missed detections, and non-Gaussian object probability distributions.

The cell-MB approximation and KLD information gain function presented in this chapter also account for both discovered and undiscovered objects by enabling the efficient computation of the RFS expectation operation. In particular, a partially piecewise homogeneous Poisson process is used to model undiscovered objects efficiently over space and time, including in challenging settings in which objects are diffusely distributed over a large geographic region. Prior work in [81] established a multi-agent PHD-based path planning algorithm aimed at maximizing the detection of relatively static objects. In [39], the exploration/exploitation problem was addressed by establishing an information-theoretic uncertainty threshold for triggering pre-planned search modalities. The occupancy grid approach in [79] was successfully implemented for tracking and discovering objects with identity-tagged observations. Task-driven approaches were considered in [42] and [17] based on LMB and Poisson multi-Bernoulli mixture (PMBM) priors, respectively. However, these existing methods all rely on the PIMS approximation and, therefore, neglect the contribution of nonideal measurements in the prediction of information gain.

The new RFS information-driven approach presented in this chapter derives a cell-MB approximation of the RFS information gain expectation that accounts for nonideal measurements. A new KLD function is shown to be cell-additive and employed to represent information gain for discovered and undiscovered objects and, subsequently, is approximated efficiently using the cell-MB decomposition. The effectiveness of this new approach is demonstrated using real video data in a challenging tracking application involving multiple closely-spaced vehicles maneuvering in a cluttered and remote environment. The proposed approach is demonstrated by tracking and maintaining discovered vehicles using an optical sensor with a bounded FoV, while simultaneously searching and discovering new vehicles as they enter the surveillance region.

4.2 Problem Formulation

This chapter considers an online SWT problem involving a single sensor with a bounded and mobile FoV that can be manipulated by an automatic controller, as illustrated in Fig. 4.1. The sensor objective is to discover and track multiple unidentified moving objects in an ROI that far exceeds the size of the FoV. The objects are characterized by partially hidden states and are subject to unknown random inputs, such as driver commands, and may leave and enter the ROI at any time. The sensor control inputs are to be optimized at every time step in order to maximize the expected reduction in track uncertainty, as well as the overall state estimation performance.

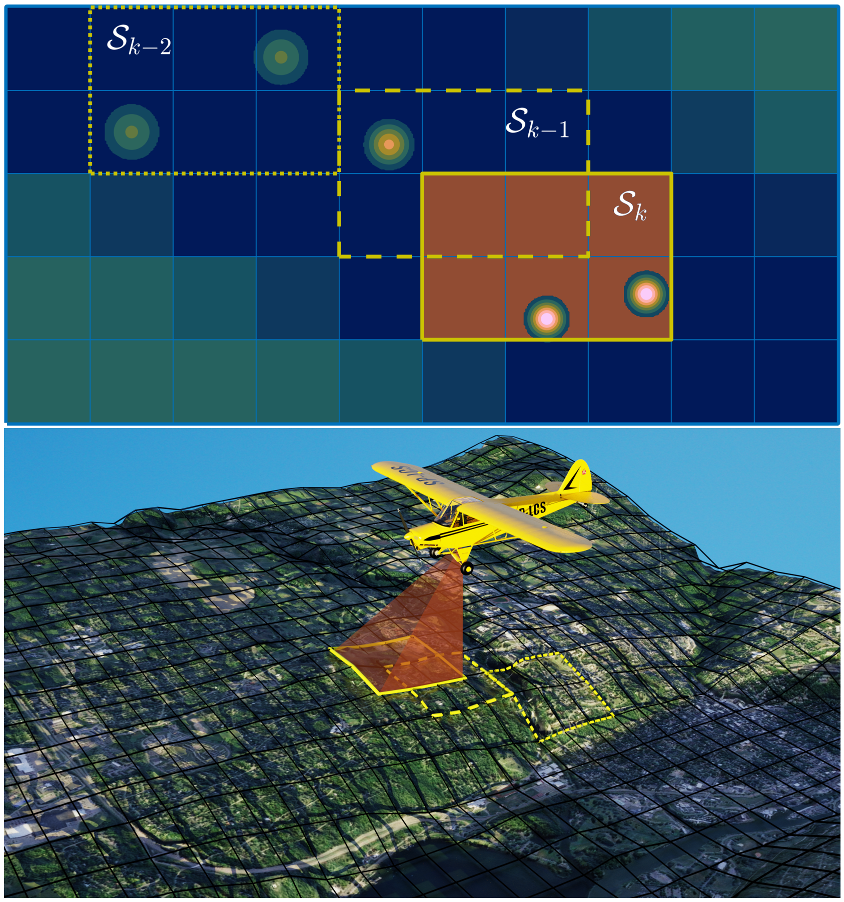

Figure 4.1: Conceptual image of multi-object search-while-tracking, wherein the sensor field-of-view $\mathcal{S}$ is controlled to maximize the cell multi-Bernoulli approximated information gain.

The number of objects is unknown *a priori* and changes over time because objects enter and exit the surveillance region as well as, potentially, the sensor FoV. Let N_k denote the number of objects present in the surveillance region $\mathcal{W}$ at time k. The multi-object state X_k is the collection of N_k single-object states at time k and is expressed as the finite set

$$X_k = \{\mathbf{x}_{k,1}, \ldots, \mathbf{x}_{k,N_k}\} \in \mathcal{F}(\mathbb{X}) \tag{4.1}$$

where $\mathbf{x}_{k,i}$ is the i^{th} element of X_k and $\mathcal{F}(\mathbb{X})$ denotes the collection of all finite subsets of the object state space $\mathbb{X}$.

The multi-object measurement is the collection of M_k single-object measurements at time k and is expressed as the set

$$Z_k = \{\mathbf{z}_{k,1}, \ldots, \mathbf{z}_{k,M_k}\} \in \mathcal{F}(\mathbb{Z}) \tag{4.2}$$

where $\mathbb{Z}$ denotes the measurement space. The sensor resolution is such that single-object detections $\mathbf{z}_{k,i}$ are represented by points, e.g., a centroidal pixel, with no additional classification-quality information. Because detections contain no identifying labels or features, the association between tracked objects and incoming measurement data is unknown.

Depending on the sensor, object detection may depend only a partial state $\mathbf{s} \in \mathbb{X}_s \subseteq \mathbb{R}^{n_s}$, where $\mathbb{X}_s \times \mathbb{X}_v = \mathbb{X} \subseteq \mathbb{R}^{n_x}$ forms the full object state space. For example, the instantaneous ability of a sensor to detect an object may depend only on the object's position. In that case, $\mathbb{X}_s$ is the position space, and $\mathbb{X}_v$ is composed of non-position states, such as object velocity. This nomenclature is adopted throughout the chapter while noting that the approach is applicable to other state definitions.

The sensor FoV is defined as a compact subset $\mathcal{S}_k \subset \mathbb{X}_s$. Then, object detection is assumed to be random and characterized by the probability function

$$p_{D,k}(\mathbf{x}_k; \mathcal{S}_k) = 1_{\mathcal{S}_k}(\mathbf{s}_k) \cdot p_{D,k}(\mathbf{s}_k) \tag{4.3}$$

where the single-argument function $p_{D,k}(\mathbf{s}_k)$ is the probability of object detection for an unbounded FoV. When an object is detected, a noisy measurement of its state $\mathbf{x}_k$ is produced according to the likelihood function

$$\mathbf{z}_k \sim g_k(\mathbf{z}_k | \mathbf{x}_k) \tag{4.4}$$

where $\mathbf{z}_k \in \mathbb{Z}$. In addition to detections originating from true objects, the sensor produces extraneous measurements due to random phenomena, which are referred to as "clutter" or "false alarms." Each resolution cell (e.g., a pixel) of the sensor image plane is equally likely to produce a false alarm, and thus, the clutter process is modeled as a Poisson RFS process with PHD $\kappa_{c,k}(\mathbf{z})$ [9]. Further discussion on Poisson RFSs and the PHD function can be found in Section 2.3.1.

Let $\mathbf{u}_k \in \mathbb{U}_k$ denote the sensor control inputs that, through actuation, determine the position of the sensor FoV at time k, $\mathcal{S}_k$, where $\mathbb{U}_k$ is the set of all admissible controls at time k. The control $\mathbf{u}_k$ influences both the FoV geometry, $\mathcal{S}_k$, and the sensor measurements, Z_k, due to varying object visibility. Because in many modern applications the surveillance region $\mathcal{W}$ is much larger than the sensor FoV, only a fraction of the total object population can be observed at any given time. Therefore, given the admissible control inputs $\mathbb{U}_k$, let the field-of-regard (FoR) be defined as

$$\mathcal{T}_k \triangleq \bigcup_{\mathbf{u}_k \in \mathbb{U}_k} \mathcal{S}_k(\mathbf{u}_k) \tag{4.5}$$

and represent the composite of regions that the sensor can potentially cover (although not simultaneously) at the next time step.

Then, the sensor control problem can be formulated as an RFS POMDP [91, 62, 21], that includes a partially- and noisily-observed state X_k, a known initial distribution of the state $f_0(X_0)$, a probabilistic transition model $f_{k|k-1}(X_k|X_{k-1})$, a set of admissible control actions $\mathbb{U}_k$, and a reward $\mathcal{R}_k$ associated with each control action. At every time k, an RFS multi-object tracker provides the prior $f_{k|k-1}(X_k|Z_{0:k-1})$ and the sensor control input is chosen so as to maximize the expected information gain, or

$$\mathbf{u}_k^* = \underset{\mathbf{u}_k \in \mathbb{U}_k}{\arg\max} \left\{ \mathrm{E}\left[\mathcal{R}_k(Z_k;\, \mathcal{S}_k,\, f_{k|k-1}(X_k|Z_{0:k-1}),\, \mathbf{u}_{0:k-1}) \right] \right\} \tag{4.6}$$

where the functional dependence of Z_k and $\mathcal{S}_k$ on $\mathbf{u}_k$ is omitted for brevity here but is described in [75]. Upon applying the sensor control input, the multi-object observation Z_k is received and processed by the RFS multi-object tracker to produce the posterior belief state $f_k(X_k|Z_{0:k})$. In this dissertation, $\mathcal{R}_k$ is taken to be an information gain function, while noting that the presented results are more broadly applicable to any integrable reward function satisfying the cell-additivity constraint defined in Section 4.3.

A computationally tractable approximation of the expected information gain in (4.6) is derived using the new cell-MB approximation presented in Section 4.3. Based on this approximation, a new sensor control policy for SWT applications is obtained in Section 4.4 using a joint information gain function. The joint information gain formulation treats discovered and undiscovered objects as separate processes, modeling undiscovered objects as a partially piecewise homogeneous Poisson process. By this approach, a computationally efficient sensor controller is developed for SWT over potentially large geographic regions.

4.3 Information-Driven Control

The objective of information-driven control is to maximize the value of the information gained by future measurements before they are known to the sensor. The expected information gain, therefore, can be obtained by marginalizing over the set Z_k, using an available measurement model. Then, the expected information gain obtained at the *next* time step can be obtained from the set integral

$$\mathrm{E}[\mathcal{R}_k] = \int \mathcal{R}_k(Z_k; \cdot) f(Z_k) \delta Z_k \tag{4.7}$$

where $f(Z_k)$ is the predicted measurement density conditioned on past measurements. In general, direct evaluation of (4.7) is computationally intractable due to the infinite summation of nested single-object integrals (see (2.21)). Furthermore, each integrand evaluation encompasses a multi-object filter update and subsequent divergence computation. As such, principled approximations are needed for tractable computation of the expected information gain.

4.3.1 The Cell-MB Distribution

A new approximation of RFS density functions is presented in this section and, then, used to obtain the information gain expectation. This approach, referred to hereon as the cell-MB approach, approximates an arbitrary measurement density as an MB density with existence probabilities and single-object densities derived from a cell decomposition of the measurement space.

Definition 1. *Consider the decomposition of the space $\mathbb{Y}$ into P disjoint subspaces, or cells, as*

$$\mathbb{Y} = \overset{1}{\mathbb{Y}} \uplus \cdots \uplus \overset{P}{\mathbb{Y}} \tag{4.8}$$

Given the cell-decomposition (4.8), the RFS

$$Y = \{\mathbf{y}_1, \ldots, \mathbf{y}_n\}$$

is considered to be cell-MB if it is distributed according to the density

$$f(Y) = \Delta(Y, \mathbb{Y}) \left[1 - r^{(\cdot)}\right]^{\mathbb{N}_P} \cdot \sum_{1 \leq j_1 \neq \cdots \neq j_n \leq P} \left[\frac{r^{j_{(\cdot)}} p^{j_{(\cdot)}}(\mathbf{y}_{(\cdot)})}{1 - r^{j_{(\cdot)}}}\right]^{\mathbb{N}_n} \tag{4.9}$$

where

$$\Delta(Y, \mathbb{Y}) \triangleq \begin{cases} 1 & |Y \cap \overset{j}{\mathbb{Y}}| \leq 1 \, \forall \, j \in \{1, \ldots, P\} \\ 0 & \textit{otherwise} \end{cases} \tag{4.10}$$

and

$$\int_{\overset{j}{\mathbb{Y}}} p^j(\mathbf{y})\mathrm{d}\mathbf{y} = 1, \qquad j = 1, \ldots, P \tag{4.11}$$

The cell-MB distribution is a special case of the MB distribution in which the probability of more than one object occupying the same cell is zero.

In [80], a collection of Bernoulli distributions was defined over an occupancy grid by integration of the PHD for dynamic map estimation applications. Inspired by [80], in this chapter, a general cell-MB approximation is developed for an arbitrary density and appropriate cell-decomposition. The following proposition shows that the best cell-MB approximation, as defined by KLD minimization, has a matching PHD and cell weights equal to the expected number of objects in each cell.

Proposition 5. *Let $f(Y)$ be an arbitrary set density with PHD $D(\mathbf{y})$ and $\overset{1}{\mathbb{Y}} \uplus \cdots \uplus \overset{P}{\mathbb{Y}}$ be a cell decomposition of space $\mathbb{Y}$ such that*

$$\int_{\overset{j}{\mathbb{Y}}} D(\mathbf{y})\mathrm{d}\mathbf{y} \le 1, \quad j = 1, \ldots, P \tag{4.12}$$

If $\bar{f}(Y)$ is a cell-MB distribution over the same cell-decomposition with parameters $\{r^j, p^j\}_{j=1}^{P}$, the KLD between $f(Y)$ and $\bar{f}(Y)$ is minimized by parameters

$$r^j = \int 1_{\overset{j}{\mathbb{Y}}}(\mathbf{y}) D(\mathbf{y})\mathrm{d}\mathbf{y} \tag{4.13}$$

$$p^j(\mathbf{y}) = \frac{1}{r^j} 1_{\overset{j}{\mathbb{Y}}}(\mathbf{y}) D(\mathbf{y}) \tag{4.14}$$

The proof is provided in Appendix A.2. When applied to the predicted measurement density, the cell-MB approximation results in a simplified multi-object expectation for a restricted class of information gain functions, as described in the following subsection.

4.3.2 Information Gain Expectation: Cell-MB

In order to reduce the computational complexity associated with the set integral in (4.7), this subsection shows that the multi-object information gain expectation simplifies to a finite sum involving only single-object integrals, assuming the measurement is cell-MB distributed and the information gain function in (4.7) is cell-additive, as defined in this subsection.

Given the FoV $\mathcal{S} \subset \mathbb{X}_s$, let the abbreviation $\overset{j}{\mathcal{S}}$ denote the intersection function

$$\overset{j}{\mathcal{S}} \triangleq \mu(\mathcal{S}, j) \triangleq \mathcal{S} \cap \overset{j}{\mathbb{X}}_s \tag{4.15}$$

Furthermore, assume that position state cells do not overlap at the FoV bounds, such that each position state cell $\overset{j}{\mathbb{X}}_s$ is either wholly included in or wholly excluded by $\mathcal{S}$:

$$\overset{j}{\mathbb{X}}_s \setminus \overset{j}{\mathcal{S}} = \emptyset \quad \forall \overset{j}{\mathcal{S}} \neq \emptyset \tag{4.16}$$

The FoV alignment constraint of (4.16) is assumed to hold throughout the dissertation. This is without loss of generality, as a cell $\overset{j}{\mathbb{X}}_s$ can be trivially subdivided in the event (4.16) does not hold such that, under the new decomposition, the condition holds. Then, the cell-additivity condition can be defined as follows.

Definition 2. *Given a decomposition* $\overset{1}{\mathbb{Z}} \uplus \cdots \uplus \overset{P}{\mathbb{Z}}$ *of space* $\mathbb{Z}$*, the information gain function* $\mathcal{R}_k(\cdot)$ *is cell-additive if*

$$\mathcal{R}_k(Z_k; \mathcal{S}_k) = \sum_{j=1}^{P} \mathcal{R}_k(Z_k \cap \overset{j}{\mathbb{Z}}; \overset{j}{\mathcal{S}}_k) \tag{4.17}$$

Theorem 1. *Let* Z_k *be distributed according to the cell-MB density* $f(Z_k)$ *with parameters* $\{r^j, p^j\}_{j=1}^{P}$ *and the cell decomposition*

$$\mathbb{Z} = \overset{1}{\mathbb{Z}} \uplus \cdots \uplus \overset{P}{\mathbb{Z}} \tag{4.18}$$

If the information gain function $\mathcal{R}_k(\cdot)$ is integrable and cell-additive (Def. 2), then the expected information gain is

$$\mathrm{E}[\mathcal{R}_k] = \sum_{j=1}^{P} \mathcal{R}_k(\emptyset; \overset{j}{\mathcal{S}}_k)\left(1 - r^j\right) + \hat{\mathcal{R}}^j_{\mathrm{z},k} \cdot r^j \tag{4.19}$$

where

$$\hat{\mathcal{R}}^j_{\mathrm{z},k} \triangleq \int_{\overset{j}{\mathbb{Z}}} \mathcal{R}_k(\{\mathbf{z}\}; \overset{j}{\mathcal{S}}_k) p^j(\mathbf{z}) \mathrm{d}\mathbf{z} \tag{4.20}$$

Proof of Theorem 1 is given in Appendix A.3.

Remark. *In (4.17), (4.19), and (4.20), the auxiliary information gain arguments are suppressed for brevity and to highlight the structure of the cell-MB approximation.*

The remainder of this chapter considers information gain functions satisfying the cell-additivity constraint of (4.17), such as the PHD filter based KLD information gain. Note that adopting the PHD filter for estimating the information gain does not require using it for multi-object tracking. Given an arbitrary RFS prior density $f_{k|k-1}(X)$ and its PHD $D_{k|k-1}(\mathbf{x})$, the PHD-based KLD information gain is

$$\mathcal{R}_k(Z; \mathcal{S}, D_{k|k-1}) = \int_{\mathbb{X}} D_{k|k-1}(\mathbf{x}) \cdot \{1 - L_Z(\mathbf{x}; \mathcal{S}) + L_Z(\mathbf{x}; \mathcal{S}) \log[L_Z(\mathbf{x}; \mathcal{S})]\} \mathrm{d}\mathbf{x} \tag{4.21}$$

where the pseudo-likelihood function

$$L_Z(\mathbf{x}; \mathcal{S}) = 1 - p_D(\mathbf{x}; \mathcal{S}) + \sum_{\mathbf{z} \in Z} \frac{p_D(\mathbf{x}; \mathcal{S}) \cdot g(\mathbf{z}|\mathbf{x})}{\kappa_c(\mathbf{z}) + \int p_D(\mathbf{x}; \mathcal{S}) g(\mathbf{z}|\mathbf{x}) D_{k|k-1}(\mathbf{x}) \mathrm{d}\mathbf{x}} \tag{4.22}$$

is adopted from [75, p. 193]. Note that, in (4.21), the information gain is written explicitly as a function of $D_{k|k-1}$ in place of the full RFS density $f_{k|k-1}$ to emphasize that the reward depends only on the prior PHD. The following proposition establishes that (4.21) is cell-additive for appropriate cell decompositions.

Proposition 6. *Assume there exists a decomposition*

$$\mathbb{Z} = \overset{1}{\mathbb{Z}} \uplus \cdots \uplus \overset{P}{\mathbb{Z}}, \qquad \mathbb{X} = \overset{1}{\mathbb{X}} \uplus \cdots \uplus \overset{P}{\mathbb{X}} \tag{4.23}$$

such that (4.16) is satisfied, and assume that an object in a given cell can only generate measurements within its corresponding measurement cell; i.e.:

$$D_{k|k-1}(\mathbf{x})g_k(\mathbf{z}|\mathbf{x}) = 0 \qquad \forall\, \mathbf{x} \in \overset{j}{\mathbb{X}},\, \mathbf{z} \in \overset{j'}{\mathbb{Z}}, j \neq j' \tag{4.24}$$

Then, the PHD-based KLD is cell-additive:

$$\mathcal{R}_k(Z; \mathcal{S}, D_{k|k-1}) = \sum_{j=1}^{P} \mathcal{R}_k(Z \cap \overset{j}{\mathbb{Z}}; \overset{j}{\mathcal{S}}, D_{k|k-1}) \tag{4.25}$$

Proof of Proposition 6 is provided in Appendix A.4. Proposition 6 establishes that for appropriate cell decompositions, the PHD-based KLD for a given FoV is equivalent to the sum of PHD-based KLD information gains for smaller "virtual" FoVs. Perfect cell-additivity requires satisfying (4.24), which, in turn, implies that an object in cell $\overset{i}{\mathbb{X}}$ does not generate a measurement in $\overset{j}{\mathbb{Z}}$ for $i \neq j$. In general, violations of (4.24) are tolerable and result in approximation errors that are negligible in comparison to the stochastic variations in the actual information gain. Furthermore, these simplifying assumptions need not be satisfied by the multi-object tracker.

The cell-MB approximation accounts for the potential information gain of non-ideal measurements, which may include missed detections, clutter, and measurements originating from new objects. The latter case is particularly important for the search of undiscovered objects, as is shown in the following section.

4.4 Search-While-Tracking (SWT) Sensor Control

This section presents a joint information gain function and associated sensor control policy that takes into account both discovered and undiscovered objects. The information gain function proposed in Section 4.4.1 balances the competing objectives of object search and tracking by means of a unified information-theoretic framework. Sections 4.4.2 and 4.4.3 derive the expected information gain functions for discovered and undiscovered objects, respectively, the combination of which is maximized by the sensor control policy in Section 4.4.4. Sections 4.4.5 and 4.4.6 describe multi-object filters for recursive estimation of the undiscovered and discovered object densities, respectively, and the overall SWT algorithm is summarized in Section 4.4.7.

4.4.1 Joint Information Gain Function

Separate density parameterizations for discovered and undiscovered objects are employed such that their unique characteristics may be leveraged for computational efficiency. Let $X_{u,k} \in \mathcal{F}(\mathbb{X})$ be the state of objects that were not detected during steps $0, \ldots, k-1$ and $X_{d,k} \in \mathcal{F}(\mathbb{X})$ be the state of objects detected prior to k. Denote by $Z_{u,k}$, $Z_{d,k}$, and $Z_{c,k}$ the detections generated by $X_{u,k}$, $X_{d,k}$, and clutter, respectively. Let $V_k \triangleq Z_{d,k} \cup Z_{c,k}$ and $W_k \triangleq Z_{u,k} \cup Z_{c,k}$. Then, the sensor control policy is defined in terms of the joint information gain as

$$\mathbf{u}_k^* = \underset{\mathbf{u}_k \in \mathbb{U}_k}{\arg\max} \left\{ \mathrm{E}[\mathcal{R}_k^d(V_k; \mathcal{S}_k(\mathbf{u}_k))] + \mathrm{E}[\mathcal{R}_k^u(W_k; \mathcal{S}_k(\mathbf{u}_k))] \right\} \tag{4.26}$$

where

$$\mathcal{R}_k^d(\cdot;\cdot) = \mathcal{R}_k(\cdot;\cdot, D_{d,k|k-1}) \tag{4.27}$$

$$\mathcal{R}_k^u(\cdot;\cdot) = \mathcal{R}_k(\cdot;\cdot, D_{u,k|k-1}) \tag{4.28}$$

are used for brevity, and $D_{d,k|k-1}$ and $D_{u,k|k-1}$ are the prior PHDs of discovered and undiscovered objects, respectively. The individual information gain expectations for discovered and undiscovered objects are derived in the following subsections.

4.4.2 Expected Information Gain of Discovered Objects

If $f_{k|k-1}(V_k)$ is cell-MB with parameters $\{r_{\mathrm{v}}^j, p_{\mathrm{v}}^j\}_{j=1}^P$, then from Theorem 1 it follows that

$$\mathrm{E}[\mathcal{R}_k^d] = \sum_{j=1}^{P} \mathcal{R}_k^d(\emptyset; \overset{j}{\mathcal{S}}_k)\left(1 - r_{\mathrm{v}}^j\right) + \hat{\mathcal{R}}_{\mathrm{v},k}^{d,j}(\overset{j}{\mathcal{S}}_k) \cdot r_{\mathrm{v}}^j \tag{4.29}$$

where

$$\hat{\mathcal{R}}_{\mathrm{v},k}^{d,j}(\overset{j}{\mathcal{S}}) \triangleq \int_{\overset{j}{\mathbb{Z}}} \mathcal{R}_k^d(\{\mathbf{z}\}; \overset{j}{\mathcal{S}}) p_{\mathrm{v}}^j(\mathbf{z}) \mathrm{d}\mathbf{z} \tag{4.30}$$

$$r_{\mathrm{v}}^j(\mathcal{S}) = \int 1_{\overset{j}{\mathbb{Z}}}(\mathbf{z}) D_{\mathrm{v},k|k-1}(\mathbf{z}; \mathcal{S}) \mathrm{d}\mathbf{z} \tag{4.31}$$

$$p_{\mathrm{v}}^j(\mathbf{z}; \mathcal{S}) = \frac{1}{r_{\mathrm{v}}^j} 1_{\overset{j}{\mathbb{Z}}}(\mathbf{z}) D_{\mathrm{v},k|k-1}(\mathbf{z}; \mathcal{S}) \tag{4.32}$$

The multi-object tracker provides the prior GLMB density $\mathring{f}_{\mathrm{p},k|k-1}(\mathring{X}_{\mathrm{p},k}|Z_{0:k-1})$, from which the discovered object PHD is obtained as

$$D_{d,k|k-1}(\mathbf{x}) = \sum_{(I,\xi)\in\mathcal{F}(\mathbb{L})\times\Xi} \sum_{\ell\in I} w^{(\xi)}(I) p^{(\xi)}(\mathbf{x}, \ell) \tag{4.33}$$

The PHD $D_{\mathrm{v},k|k-1}$ can be obtained from the predicted measurement density $f_{k|k-1}(V_k)$ through application of (2.20). From the prior GLMB density,

$$f_{k|k-1}(V_k) = \int g_k(V_k|\mathring{X}) \mathring{f}_{k|k-1}(\mathring{X}) \delta\mathring{X} \tag{4.34}$$

Given a GLMB prior, explicit computation of the predicted measurement density is computationally challenging. Thus, $D_{\mathrm{v},k|k-1}$ is directly computed from the discovered object PHD using the approximation

$$D_{\mathrm{v},k|k-1}(\mathbf{z};\mathcal{S}) \approx \int D_{d,k|k-1}(\mathbf{x}) p_{D,k}(\mathbf{x};\mathcal{S}) g_k(\mathbf{z}|\mathbf{x}) \mathrm{d}\mathbf{x} + \kappa_{c,k}(\mathbf{z}) \tag{4.35}$$

Because an analytic solution of the integral in (4.30) is not available, a numerical quadrature rule is employed. In the proposed approach, a measurement cell is further tessellated into regions $\{\overset{j}{\Omega}_i\}_{i=1}^{R_j} \subset \overset{j}{\mathbb{Z}}$ based on the anticipated information value of measurements within each region, as illustrated in Fig. 4.2. Then, given a representative measurement $\mathbf{z}_{j,i}$ for each region, the conditional information gain expectation is approximated as

$$\hat{\mathcal{R}}^{d,j}_{\mathrm{v},k}(\overset{j}{\mathcal{S}}) \approx \sum_{i=1}^{R_j} \mathcal{R}^d_k(\{\mathbf{z}_{j,i}\};\overset{j}{\mathcal{S}}) p^j_{\mathrm{v}}(\mathbf{z}_{j,i}) A_{j,i} \tag{4.36}$$

where $A_{j,i}$ is the volume of region $\overset{j}{\Omega}_i$. By this approach, the PHD-based KLD information gain function is only evaluated R_j times. Further details regarding the computation of the quadrature regions and representative measurement points are provided in Appendix A.5.

4.4.3 Expected Information Gain of Undiscovered Objects

This subsection presents a new approach to efficiently model the undiscovered object distribution, which may be diffuse over a large region. Although GMs and particle representations can be used to model undiscovered objects, they are highly inefficient at representing diffuse distributions. Thus, in this chapter, the position-marginal density of undiscovered objects is taken to be piecewise homogeneous

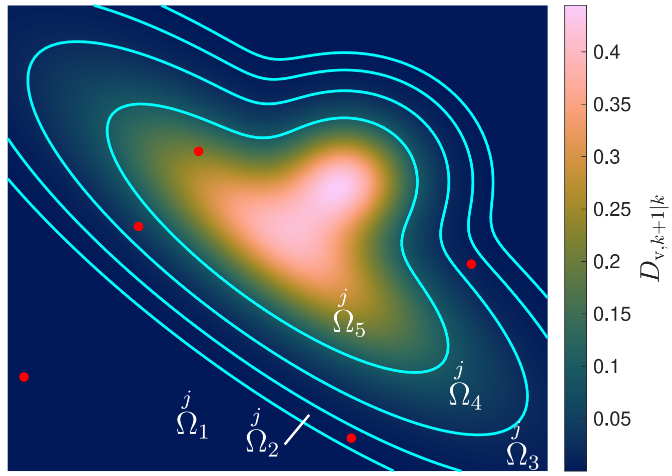

Figure 4.2: Example quadrature of the single-measurement conditional expected information gain, where representative measurements $\mathbf{z}_{j,i}$ are denoted by red dots and quadrature regions are outlined in cyan.

with PHD

$$D_{u,k|k-1}(\mathbf{s}) = \sum_{j=1}^{P} \frac{1_{\overset{j}{\mathbb{X}}_s}(\mathbf{s})}{A(\overset{j}{\mathbb{X}}_s)} \cdot \lambda_{j,k|k-1} \tag{4.37}$$

where $\lambda_{j,k|k-1}$ is the expected number of undiscovered objects in $\overset{j}{\mathbb{X}}_s$ at time step k and $A(\overset{j}{\mathbb{X}}_s)$ is the volume of cell $\overset{j}{\mathbb{X}}_s$. For ease of exposition, the undiscovered object PHD is modeled using the same cell decomposition employed in the cell-MB approximation.

If $f_{k|k-1}(W_k)$ is cell-MB with parameters $\{r_{\mathrm{w}}^j, p_{\mathrm{w}}^j\}_{j=1}^P$, then by Theorem 1,

$$\mathrm{E}[\mathcal{R}_k^u] = \sum_{j=1}^{P} \mathcal{R}_k^u(\emptyset; \overset{j}{\mathcal{S}}_k)\left(1 - r_{\mathrm{w}}^j\right) + \hat{\mathcal{R}}_{\mathrm{w},k}^{u,j}(\overset{j}{\mathcal{S}}_k) \cdot r_{\mathrm{w}}^j \tag{4.38}$$

where

$$\hat{\mathcal{R}}^{u,j}_{\mathrm{w},k}(\overset{j}{\mathcal{S}}) \triangleq \int_{\overset{j}{\mathbb{Z}}} \mathcal{R}^u_k(\{\mathbf{z}\}; \overset{j}{\mathcal{S}}) p^j_{\mathrm{w}}(\mathbf{z}) \mathrm{d}\mathbf{z} \tag{4.39}$$

$$r^j_{\mathrm{w}}(\mathcal{S}) = \int 1_{\overset{j}{\mathbb{Z}}}(\mathbf{z}) D_{\mathrm{w},k|k-1}(\mathbf{z}; \mathcal{S}) \mathrm{d}\mathbf{z} \tag{4.40}$$

$$\approx \frac{\lambda_{j,k|k-1}}{A(\overset{j}{\mathbb{X}}_s)} \int_{\overset{j}{\mathbb{X}}_s} p_D(\mathbf{s}; \mathcal{S}) \mathrm{d}\mathbf{s} \tag{4.41}$$

$$p^j_{\mathrm{w}}(\mathbf{z}; \mathcal{S}) = \frac{1}{r^j_{\mathrm{w}}} 1_{\overset{j}{\mathbb{Z}}}(\mathbf{z}) D_{\mathrm{w},k|k-1}(\mathbf{z}; \mathcal{S}) \tag{4.42}$$

$$D_{\mathrm{w},k|k-1}(\mathbf{z}; \mathcal{S}) = \int D_{u,k|k-1}(\mathbf{x}) p_{D,k}(\mathbf{x}; \mathcal{S}) g_k(\mathbf{z}|\mathbf{x}) \mathrm{d}\mathbf{x} + \kappa_{c,k}(\mathbf{z}) \tag{4.43}$$

Under a piecewise homogeneous PHD, the undiscovered object information gain simplifies drastically if the measurement likelihood is independent of non-position states: i.e. $g_k(\cdot|\mathbf{x}) = g_k(\cdot|\mathbf{s})$. Following (4.21),

$$\mathcal{R}^u_k(W_k; \mathcal{S}_k) = \int_{\mathbb{X}_s} D_{u,k|k-1}(\mathbf{s}) \{1 - L_{W_k}(\mathbf{s}; \mathcal{S}_k) + L_{W_k}(\mathbf{s}; \mathcal{S}_k) \log[L_{W_k}(\mathbf{s}; \mathcal{S}_k)]\} \mathrm{d}\mathbf{s} \tag{4.44}$$

Given that at most one measurement may exist per cell, two cases need to be considered: the null (empty) measurement case and the singleton measurement case. Letting $W_k = \emptyset$, and after some algebraic manipulation, the undiscovered object information gain for a null measurement can be written as

$$\mathcal{R}^u_k(\emptyset; \mathcal{S}_k) = \sum_{j=1}^{P} \mathcal{R}^u_k(\emptyset; \overset{j}{\mathcal{S}}_k) \tag{4.45}$$

$$\mathcal{R}^u_k(\emptyset; \overset{j}{\mathcal{S}}_k) = \lambda_{j,k|k-1} \cdot d_j \cdot (1 - \delta_{\emptyset}(\overset{j}{\mathcal{S}}_k)) \tag{4.46}$$

$$d_j \triangleq \frac{1}{A(\overset{j}{\mathbb{X}}_s)} \int_{\overset{j}{\mathbb{X}}_s} p_D(\mathbf{s}) + (1 - p_D(\mathbf{s})) \log[1 - p_D(\mathbf{s})] \mathrm{d}\mathbf{s} \tag{4.47}$$

Furthermore, if the probability of detection is homogeneous within cells such that

$$p_D(\mathbf{s}) = p_{D,j} \quad \forall\, \mathbf{s} \in \overset{j}{\mathbb{X}}_s \tag{4.48}$$

then (4.47) simplifies to

$$d_j = p_{D,j} + (1 - p_{D,j}) \log(1 - p_{D,j}) \tag{4.49}$$

For the singleton measurement case, similar analytic simplifications of the conditional information gain (4.39) are limited. However, within a cell, the uniform position density of undiscovered objects is known *a priori* up to an unknown factor $\lambda_{j,k|k-1}$. Thus, the undiscovered object information gain can be pre-computed for efficiency and

$$\hat{\mathcal{R}}^{u,j}_{\mathrm{w},k}(\overset{j}{\mathcal{S}}_k) \approx \bar{\mathcal{R}}^{u,j}_{\mathrm{w}}(\lambda_{j,k|k-1}) \tag{4.50}$$

where the function $\bar{\mathcal{R}}^{u,j}_{\mathrm{w}}(\lambda_{j,k|k-1})$ returns interpolated information gain values over $\lambda_{j,k|k-1} \in [0, 1]$.

4.4.4 Field-of-View (FoV) Optimization and Sensor Control

Prior to optimization of the FoV, the information gain associated with each cell in the FoR is computed, as described in Algorithm 4. The FoR cell information gains for discovered and undiscovered objects are stored as arrays $\{\mathcal{R}^d_k[j]\}_{j=1}^P$ and $\{\mathcal{R}^u_k[j]\}_{j=1}^P$, respectively. Then, the optimal FoV is found as the one composed of the cells with the highest composite information gain, without reevaluating the information gain. With this, the sensor control that produces the desired optimal FoV can be written as

$$\mathbf{u}^*_k = \arg\max_{\mathbf{u}\in\mathbb{U}_k} \left\{ \sum_{j\in\mathbb{N}_P,\, \overset{j}{\mathbb{X}}_s\subseteq\mathcal{S}_k(\mathbf{u})} \left(\mathcal{R}^u_k[j] + \mathcal{R}^d_k[j]\right) \right\} \tag{4.51}$$

Algorithm 4 FoR Information Gain Pseudocode

Input: $\mathcal{T}_k$, $\mathring{f}_{k|k-1}(\mathring{X})$, $D_{u,k|k-1}(\mathbf{x})$

Compute $D_{d,k|k-1}(\mathbf{x})$ from $\mathring{f}_{k|k-1}(\mathring{X})$ (4.33)
Compute $D_{\mathrm{v},k|k-1}(\mathbf{z};\mathcal{T}_k)$ (4.35)
for $j = 1, \ldots, P$ for j such that $\overset{j}{\mathbb{X}}_s \in \mathcal{T}_k$ **do**
  $r^j_{\mathrm{v}} \leftarrow \int 1_{\overset{j}{\mathbb{Z}}}(\mathbf{z}) D_{\mathrm{v},k|k-1}(\mathbf{z};\mathcal{T}_k)\mathrm{d}\mathbf{z}$
  $r^j_{\mathrm{w}} \leftarrow \int 1_{\overset{j}{\mathbb{Z}}}(\mathbf{z}) D_{\mathrm{w},k|k-1}(\mathbf{z};\mathcal{T}_k)\mathrm{d}\mathbf{z}$
  Compute $\hat{\mathcal{R}}^{d,j}_{\mathrm{v},k}(\overset{j}{\mathcal{T}})$ (4.36)
  Compute $\hat{\mathcal{R}}^{u,j}_{\mathrm{w},k}(\overset{j}{\mathcal{T}})$ (4.50)
  $\mathcal{R}^d_k[j] \leftarrow \mathcal{R}^d_k(\emptyset;\overset{j}{\mathcal{T}}_k)(1-r^j_{\mathrm{v}}) + \hat{\mathcal{R}}^{d,j}_{\mathrm{v},k}(\overset{j}{\mathcal{T}}_k)\cdot r^j_{\mathrm{v}}$
  $\mathcal{R}^u_k[j] \leftarrow \mathcal{R}^u_k(\emptyset;\overset{j}{\mathcal{T}}_k)(1-r^j_{\mathrm{w}}) + \hat{\mathcal{R}}^{u,j}_{\mathrm{w},k}(\overset{j}{\mathcal{T}}_k)\cdot r^j_{\mathrm{w}}$
end for
return $(\mathcal{R}^d_k[j])^P_{j=1}$, $(\mathcal{R}^u_k[j])^P_{j=1}$

Remark. *Explicit computation of the cell-MB single-object densities* p^j_{v} *and* p^j_{w} *is not required. Instead, these densities are implicitly computed when evaluating the conditional information gain expectations* $\hat{\mathcal{R}}^{d,j}_{\mathrm{v},k}$ *and* $\hat{\mathcal{R}}^{u,j}_{\mathrm{w},k}$.

4.4.5 Undiscovered Object Prediction and Update

The prediction and update of the undiscovered object PHD is accomplished using the cell-discretized PHD filter. The prediction step incorporates undiscovered object motion, birth, and death. The undiscovered object distribution parameters are predicted and updated as

$$\lambda_{j,k|k-1} = \lambda_{B,j,k} + \sum_{i=1}^{P} p_{S,i,k} \cdot P_{j|i} \cdot \lambda_{i,k-1} \tag{4.52}$$

$$\lambda_{j,k} = \left[1 - p_{D,j} \cdot (1 - \delta_{\emptyset}(\overset{j}{\mathcal{S}}_k))\right] \cdot \lambda_{j,k|k-1} \tag{4.53}$$

where $\lambda_{B,j,k}$ is the expected number of newborn objects in cell j, $p_{S,i,k}$ is the probability that an object in cell i not detected before k survives, and $P_{j|i}$ is the probability that an undiscovered object moves to cell j given that it exists in cell i.

4.4.6 Discovered Object Tracking

Discovered object tracking is performed using the data-driven GLMB filter. While a detailed description of the data-driven GLMB filter is beyond the scope of this chapter, one important consideration is highlighted involving the FoV-dependent nonlinear probability of detection. The data-driven GLMB is implemented in GM form, such that single-object densities are

$$p^{(\xi)}(\mathbf{x},\ell) = \sum_{i=1}^{J^{(\xi)}(\ell)} w_i^{(\xi)}(\ell)\mathcal{N}(\mathbf{x};\boldsymbol{m}_i^{(\xi)}(\ell),\boldsymbol{P}_i^{(\xi)}(\ell)) \tag{4.54}$$

It is through the FoV-dependent p_D that the filter probabilistically incorporates the knowledge of where objects were not observed.

In the filter, products of the form $p_D(\mathbf{x};\mathcal{S})p^{(\xi)}(\mathbf{x})$ are expanded about the GM component means. The accuracy of this expansion is dependent on the GM resolution near the FoV boundaries. Thus, the recursive splitting algorithm (Algorithm 1) is employed to identify and split Gaussian components that overlap the FoV boundaries into several "smaller" Gaussians. The resulting $J'^{(\xi)}(\ell)$ component mixture replaces the original density, enabling the accurate zeroth-order expansion approximation

$$p_D(\mathbf{x};\mathcal{S})p^{(\xi)}(\mathbf{x},\ell) \approx \sum_{i=1}^{J'^{(\xi,\ell)}} w_i^{(\xi,\ell)} p_D(\boldsymbol{m}_i^{(\xi,\ell)};\mathcal{S})\mathcal{N}(\mathbf{x};\boldsymbol{m}_i^{(\xi,\ell)},\boldsymbol{P}_i^{(\xi,\ell)}) \tag{4.55}$$

An example is provided in Fig. 4.3, wherein the prior density is split prior to a Bayes update, allowing for the accurate incorporation of negative information from a non-detection.

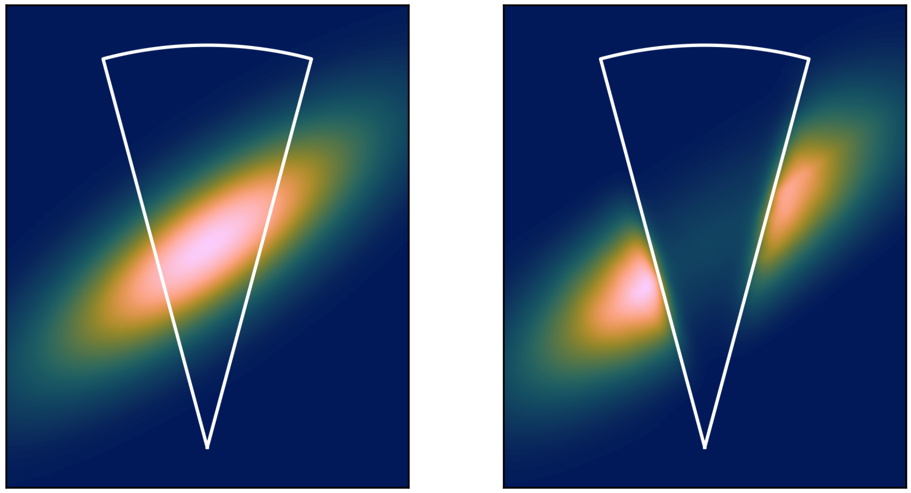

(a) (b)

Figure 4.3: Prior object density and FoV (a), and posterior object density after recursive split and non-detection (b).

4.4.7 Numerical Implementation

This subsection summarizes the SWT algorithmic implementation. At each step k, a time-update (2.32), (4.52) of the previous posterior densities yields predicted prior densities for the time of the next decision. The FoR is constructed from admissible control actions as shown in (4.5), and the expected information gain for each cell within the FoR is computed. The candidate FoV that contains the maximizing sum of cell information gains is found, and the corresponding control (4.51) which yields that FoV is applied. The sensor collects a new multi-object measurement which is processed in the data-driven GLMB filter to update the multi-object density, giving the posterior density in (2.33). The algorithm is summarized in Algorithm 5.

Algorithm 5 SWT Sensor Control Pseudocode

Input: $\mathring{f}_0(\mathring{X})$, $D_{u,0}(\mathbf{x})$

for $k = 1, \ldots, K$ **do**
  $\mathring{f}_{k|k-1}(\mathring{X})$, $D_{u,k|k-1}(\mathbf{x}) \leftarrow$ `filter_prediction(`$\mathring{f}_{k-1}(\mathring{X})$, $D_{u,k-1}(\mathbf{x})$`)` (2.32), (4.52)
  $(\mathcal{R}^d_k[j])^P_{j=1}$, $(\mathcal{R}^u_k[j])^P_{j=1} \leftarrow$ `FoR_information_gain(`$\mathcal{T}_k, \mathring{f}_{k|k-1}(\mathring{X}), D_{u,k|k-1}(\mathbf{x})$`)` Alg. 4
  $\mathbf{u}^*_k \leftarrow$ `maximize_expected_reward(`$(\mathcal{R}^d_k[j])^P_{j=1}$, $(\mathcal{R}^u_k[j])^P_{j=1}$`)` (4.51)
  $\mathcal{S}_k(\mathbf{u}^*_k) \leftarrow$ apply sensor control
  $Z_k \leftarrow$ obtain measurement
  $\mathring{f}_{k|k-1}(\mathring{X}) \leftarrow$ `split_for_FoV(`$\mathring{f}_{k|k-1}(\mathring{X})$, $\mathcal{S}_k$`)` [67]
  $\mathring{f}_k(\mathring{X})$, $D_{u,k} \leftarrow$ `filter_update(`$\mathring{f}_{k|k-1}(\mathring{X}), D_{u,k|k-1}(\mathbf{x})$, Z_k, $\mathcal{S}_k$`)` (2.33), (4.53)
end for

4.5 Application to Remote Multi-Vehicle SWT

The cell-MB SWT framework is demonstrated in a vehicle tracking problem using real video data. The video was recorded using a fixed camera with a large FoV (Fig. 4.4.a), and real-time FoV controlled motion was simulated by windowing the data over a small fraction of the image, as illustrated in Fig. 4.4.b. This dataset presents significant tracking challenges, including jitter-induced noise and clutter, unknown measurement origin, merged detections from closely-spaced vehicles, and most significantly, temporal sparsity of detections.

4.5.1 Ground Vehicle Dynamics

Vehicle dynamics are modeled directly in the image frame. While vehicle dynamics are more naturally expressed in the terrestrial frame, the camera's precise location and orientation are unknown. Thus, transformation between image and terrestrial coordinates could not be readily established.

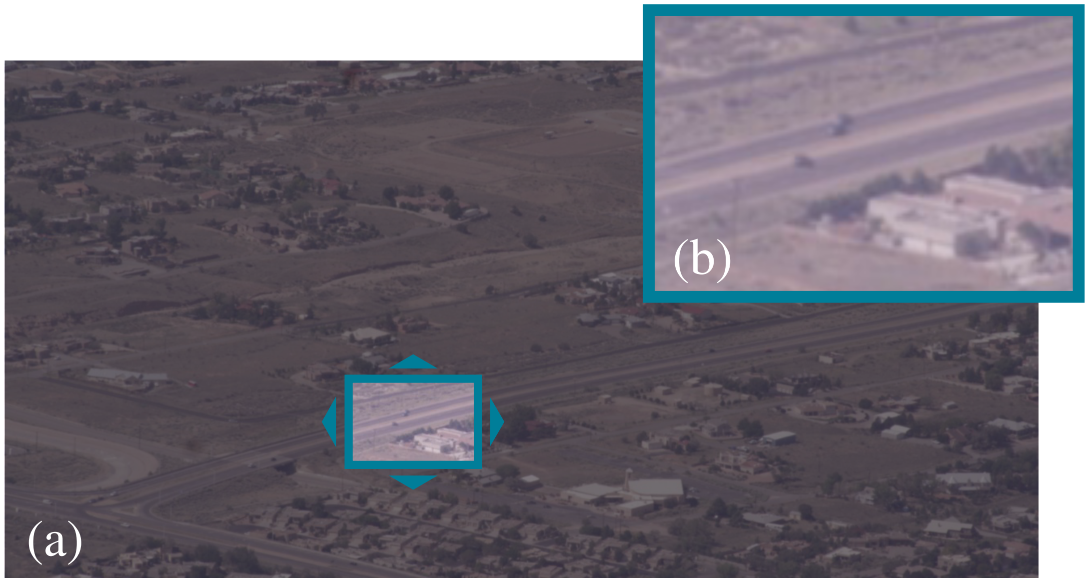

Figure 4.4: Example video frame (a), artificially windowed to emulate smaller, movable FoV, which is enlarged in (b) to show detail.

The object state is modeled as

$$\mathbf{x}_k = [\mathbf{s}_k^T \quad \boldsymbol{\zeta}_k^T]^T \tag{4.56}$$

$$\mathbf{s}_k = [\xi_k \quad \eta_k]^T , \qquad \boldsymbol{\zeta}_k = [\dot{\xi}_k \quad \dot{\eta}_k \quad \Omega_k]^T \tag{4.57}$$

where ξ_k and η_k are the horizontal and vertical coordinates, respectively, of the vehicle position with respect to the full-frame origin, $\dot{\xi}_k$ and $\dot{\eta}_k$ are the corresponding rates, and Ω_k is the vehicle turn rate.

Vehicle motion is modeled using the nearly coordinated turn model with directional process noise [9, 127] as

$$\mathbf{x}_{k+1} = \mathbf{f}_k(\mathbf{x}_k) + \boldsymbol{\Gamma}_k \boldsymbol{\nu}_k(\mathbf{s}_k) \tag{4.58}$$

where

$$\mathbf{f}_k(\mathbf{x}_k) = \begin{bmatrix} 1 & 0 & \frac{\sin(\Omega_k \Delta t)}{\Omega_k} & -\frac{1-\cos(\Omega_k \Delta t)}{\Omega_k} & 0 \\ 0 & 1 & \frac{1-\cos(\Omega_k \Delta t)}{\Omega_k} & \frac{\sin(\Omega_k \Delta t)}{\Omega_k} & 0 \\ 0 & 0 & \cos(\Omega_k \Delta t) & -\sin(\Omega_k \Delta t) & 0 \\ 0 & 0 & \sin(\Omega_k \Delta t) & \cos(\Omega_k \Delta t) & 0 \\ 0 & 0 & 0 & 0 & 1 \end{bmatrix} \mathbf{x}_k \tag{4.59}$$

$$\mathbf{\Gamma}_k = \begin{bmatrix} \frac{1}{2}(\Delta t)^2 \mathbf{I}_{2\times 2} & \mathbf{0}_{2\times 1} \\ (\Delta t)\mathbf{I}_{2\times 2} & \mathbf{0}_{2\times 1} \\ \mathbf{0}_{1\times 2} & \Delta t \end{bmatrix} \tag{4.60}$$

where $\Delta t = 1\,[\text{sec}]$ is the discrete time step interval, $\mathbf{I}_{n\times n}$ denotes the $n \times n$ identity matrix, and $\mathbf{0}_{m\times n}$ denotes the $m \times n$ matrix whose elements are zero. The covariance of the process noise is

$$\mathrm{E}[\boldsymbol{\nu}_k \boldsymbol{\nu}_k^T] = \mathbf{Q}_k(\mathbf{s}) = \begin{bmatrix} \mathbf{D}^T(\mathbf{s})\mathbf{Q}_d\mathbf{D}(\mathbf{s}) & 0 \\ \mathbf{0}_{1\times 2} & \sigma_\Omega^2 \end{bmatrix} \tag{4.61}$$

$$\mathbf{Q}_d = \begin{bmatrix} \sigma_t^2 & 0 \\ 0 & \sigma_n^2 \end{bmatrix}, \quad \mathbf{D}(\mathbf{s}) = \begin{bmatrix} \cos\Psi(\mathbf{s}) & \sin\Psi(\mathbf{s}) \\ -\sin\Psi(\mathbf{s}) & \cos\Psi(\mathbf{s}) \end{bmatrix} \tag{4.62}$$

where $\sigma_\Omega = 180\,[\text{arcmin/sec}]$ is the turn rate process noise standard deviation, $\sigma_t = 5\,[\text{pixel/sec}^2]$ and $\sigma_n = 0.01\,[\text{pixel/sec}^2]$ are the standard deviation of process noise tangential and normal to the road, respectively, and $\Psi(\mathbf{s})$ is the angle of the road segment nearest $\mathbf{s}$, measured from the horizontal axis to the tangent direction. The true trajectories of all moving objects are shown in Fig. 4.5.

4.5.2 Sensor and Scene Model

Object detections are generated from raw frame data using normalized difference change detection [99] and fast approximate power iteration subspace tracking [6]

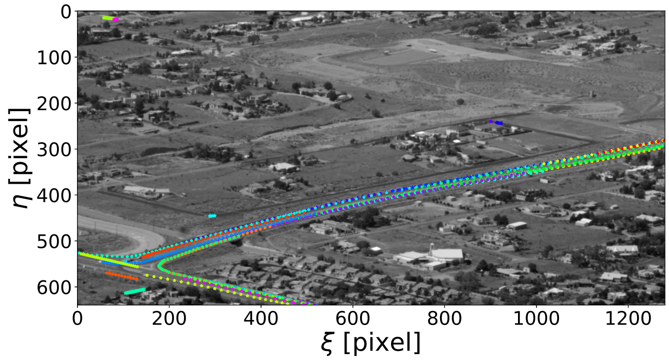

Figure 4.5: True trajectories of moving objects with an example image as frame as background.

for temporal background estimation. The single-object measurement function is linear-Gaussian with corresponding likelihood

$$g(\mathbf{z}|\mathbf{x}) = \mathcal{N}(\mathbf{z};\, \mathbf{H}\mathbf{x},\, \mathbf{R})\,, \tag{4.63}$$

$$\mathbf{H} = \begin{bmatrix} \mathbf{I}_{2\times2} & \mathbf{0}_{2\times3} \end{bmatrix}, \qquad \mathbf{R} = 9 \cdot \mathbf{I}_{2\times2}\,[\text{pixel}^2] \tag{4.64}$$

The sensor FoV is a rectangular region that is 240 pixels wide and 160 pixels tall. Moving objects within the FoV are assumed to be detectable with probability $p_{D,k}(\mathbf{s}_k) = 0.9$.

The scene is tessellated by a 16×32 grid of uniformly sized rectangular cells as shown in Fig. 4.6. Within the scene, an ROI is specified which contains the scene's two primary roads and is denoted by $\mathcal{T}$ due to its equivalence to the FoR for this problem. Within the ROI, cells containing road pixels comprise the set $\mathcal{B}$, which is used to establish an initial uniform distribution of undiscovered objects. Thus, following the assumptions established in Section 4.4.3, the initial undiscovered object position marginal PHD is characterized by (4.37) with

$$\lambda_{j,0} = \begin{cases} 0.137 & \overset{j}{\mathbb{X}} \subseteq \mathcal{B} \\ 0 & \text{otherwise} \end{cases} \tag{4.65}$$

which corresponds to an initial estimate of ten undiscovered objects in the scene.

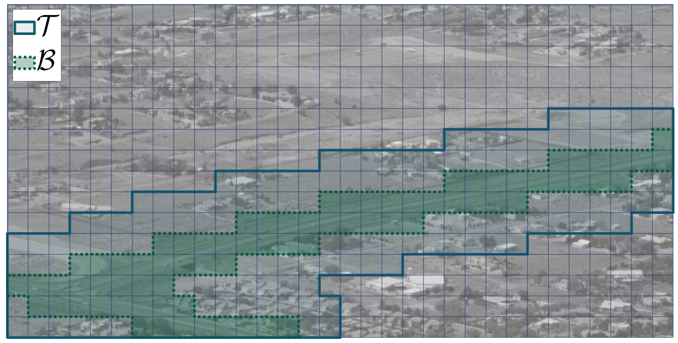

Figure 4.6: Field-of-regard, $\mathcal{T}$, and primary road region $\mathcal{B}$, with example image frame as background.

4.5.3 Experiment Results

An experiment consisting of sixty time steps is performed. To emulate a pan/tilt camera from the wider available frame data, the FoV is assumed to be able to be moved to any location within the scene in a single time step. This is a reasonable assumption as these adjustments would be less than a degree. While not considered in this experiment, kinematic constraints can be easily imposed on sensor motion. However, because the sensor control policy is solved myopically (one stage at a time), some motion constraints may result in the sensor becoming "trapped" in local maxima. Multi-stage information-driven control will be considered in future work.

Some key frames of the experiment are shown in Fig. 4.7. In the early time steps, the FoV motion is dominated by the undiscovered object component of the information gain. As more objects are discovered and tracked, the observed actions demonstrate a balance of revisiting established tracks to reduce state uncertainty and exploring new areas where undiscovered objects may exist.

The performance of the SWT sensor control is evaluated by the multi-object tracking accuracy, as measured using the generalized optimal sub-pattern assignment (GOSPA) metric [85]. The GOSPA metric, the number of missed objects, and the number of false tracks over time are shown in Fig 4.8. The cell-MB SWT sensor control effectively balances the competing objectives of new object discovery and maintenance of established tracks, as illustrated by the decline in missed objects and consistently low number of false tracks. An increase in GOSPA is observed in the final time steps of the experiment, which is caused by a sharp uptick in new object appearances.

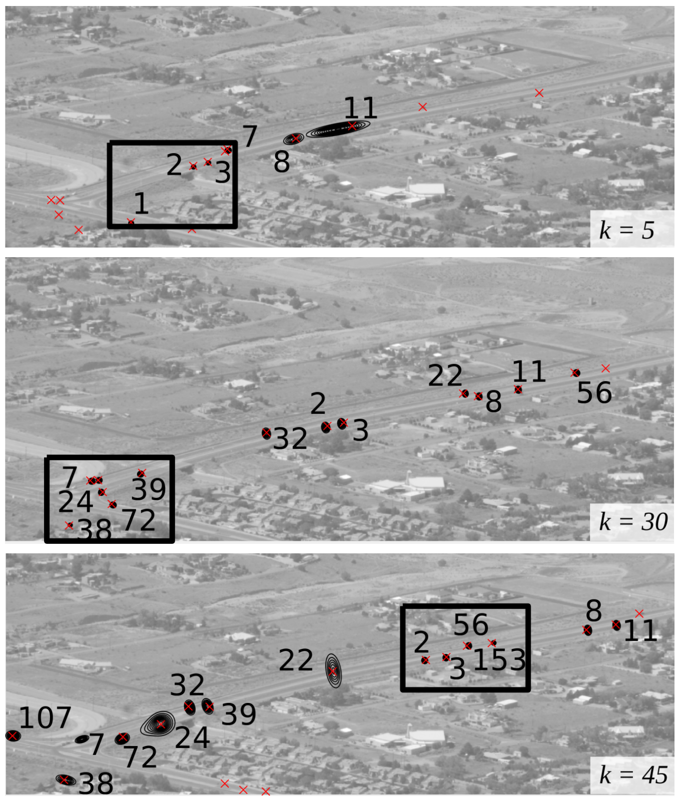

Figure 4.7: FoV position and tracker estimates in the form of single-object density contours for objects with probabilities of existence greater than 0.5, shown at select time steps.

The average GOSPA over the experiment is compared with the PIMS-based information driven control and random FoV motion in Table 4.1. The cell-MB sensor control achieves significant improvement with respect to other methods in the number of missed and false tracks, as well as the overall GOSPA metric, which

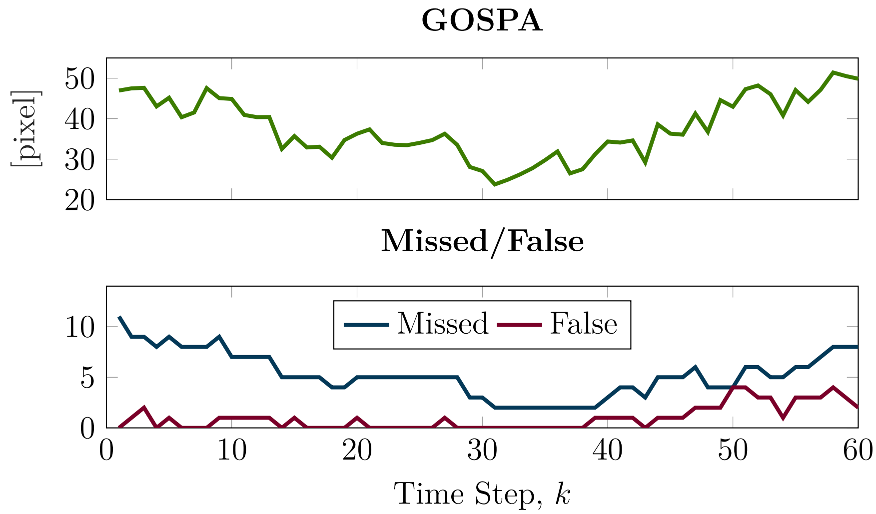

Figure 4.8: GOSPA metric and component errors over time using cutoff distance $c = 20$ [pixel], order $p = 2$, and $\alpha = 2$.

encompasses cardinality errors and localization errors. While the PIMS approach

Table 4.1: GOSPA performance, averaged over experiment duration, with percentage improvement over baseline random control shown parenthetically.

Algorithm	GOSPA [pixel]	Missed	False
Cell-MB	37.84 (56%)	5.27 (168%)	0.97 (158%)
PIMS	47.46 (24%)	9.95 (42%)	0.90 (178%)
Random	59.07 (N/A)	14.10 (N/A)	2.50 (N/A)

performs poorly in this application, it should still be considered as a viable method when using an information gain function that is non-additive.

4.6 Conclusion

This chapter presents a novel cell multi-Bernoulli (cell-MB) approximation that enables the tractable higher-order approximation of the expectation of set functions that are additive over disjoint measurable subsets. The cell-MB approximation is useful for approximating the expectation of computationally-expensive set functions, such as information-theoretic reward functions employed in sensor control applications. The approach is developed in the context of information-driven sensor control in which the objective is to discover and track an unknown time-varying number of non-cooperative objects with minimal estimation error. The problem is formulated as a partially-observed Markov decision process with a new Kullback-Leibler divergence-based information gain that incorporates both discovered and undiscovered object information gain. In a demonstration using real sensor data, the search-while-tracking sensor control is used to manipulate the sensor field-of-view to discover and track multiple moving ground objects from an aerial vantage point.

CHAPTER 5

MULTIPLE SENSOR INFORMATION DRIVEN CONTROL

5.1 Introduction

Many modern robotic and aerospace systems employ multiple sensors for navigation, perception and surveillance. Sensors may be collocated on a single platform or distributed across many agents or vehicles. Such systems, referred to as multi-sensor systems, offer distinct advantages over single-sensor systems. Multi-sensor systems are inherently more robust to individual sensor failures and, when distributed, can cover larger ROIs. Through the exchange of data over a connected network of sensors, information from separate sources can be fused to provide more refined classification assessments or state estimates. Examples of multi-sensor systems include terrestrial wireless sensor networks [84, 103, 3], underwater sensor networks [109], SSA sensor networks [46, 45, 38, 39, 71, 98, 20], unmanned aerial systems (UASs) [123], climate measurement systems [120], satellite systems [18], and multi-static radar systems [27, 129, 105].

Dynamic and configurable sensor networks can offer even greater sensing capability, but require sophisticated coordination to maximize the collective performance and avoid unwanted redundancy. While human-centric operation of multi-sensor networks is feasible for small numbers of sensors, efficient orchestration of large sensor networks ultimately requires machine-driven autonomy.

Multi-sensor control objective functions generally fall into one of two categories: task-driven and information-driven [61]. Task-driven objective functions are typically heuristic and designed to encode some tangible goal, such as regional coverage, detection of objects, or object classification. Task-driven approaches are often amenable to dynamic programming-based solutions and perform well in applications where the desired system behavior is well-described by a single goal or figure of merit. Information-driven objective functions, on the other hand, are theoretically rigorous and elegantly encapsulate multiple complex and competing objectives. It is for these reasons that information-theoretic policies have been described as “a near-universal proxy” to convey their ability to achieve similar performance to tailored task-driven policies for a wide range of tasks [48, 61].

This chapter considers the problem of information-driven autonomous multi-sensor SWT with an unknown and time-varying number of objects using noisy measurements with unknown origin. In such scenarios, approaches that assume prior knowledge of the number of objects [47, 104] are either inapplicable or exhibit significant performance degradation. Recent work [57, 20, 83, 129, 117] has shown that such problems can be formulated as an RFS POMDP, wherein the belief state is described by a set density formed from the recursive assimilation of multi-sensor measurement data. A key challenge of the RFS approach to multi-sensor control is in evaluating the *expected* information gain which is generally intractable. For this reason, all existing RFS multi-sensor control approaches [57, 20, 83, 129, 117] employ a computationally-inexpensive yet severe single-sample approximation of the expected information gain known as the PIMS approximation. This chapter presents the first RFS multi-sensor control approach based on higher-order approximations of the expected information gain which capture the contributions of non-ideal measurements. In particular, this chapter treats the general and nontrivial case in which sensor FoVs may fully or partially overlap, in which the information gain is nonadditive across sensors.

The remainder of the chapter is organized as follows: Section 5.2 describes the problem formulation. Section 5.3 derives a cell-MB approximation of the expected multi-sensor information gain for information gain functions satisfying cell-additivity constraints. An information-theoretic reward based on iterated-corrector updates is proposed and proven to satisfy the cell-additivity property under appropriate cell-decompositions. Section 5.4 derives the information gain for joint SWT by use of a joint representation of discovered and undiscovered objects and presents a computationally efficient suboptimal solution to multi-FoV optimization. Section 5.5 includes a demonstration of the approach in a challenging SWT problem involving multiple remote sensors and ground vehicles, with tracking performance analyzed and compared across different numbers of sensors.

5.2 Problem Formulation

This chapter considers an online SWT problem involving multiple homogeneous sensors with bounded and mobile FoVs that can be manipulated by an automatic controller, as illustrated in Fig. 5.1. The sensing objective is to discover and track multiple unidentified moving objects in an ROI that far exceeds the size of the FoV of an individual sensor. The objects are characterized by partially hidden states and are subject to unknown random inputs, such as driver commands, and may leave and enter the ROI at any time. The sensor control inputs are to be optimized at every time step in order to maximize the expected reduction in track uncertainty, as well as the overall state estimation performance.

The number of objects is unknown *a priori* and changes over time because objects enter and exit the surveillance region as well as, potentially, the sensor

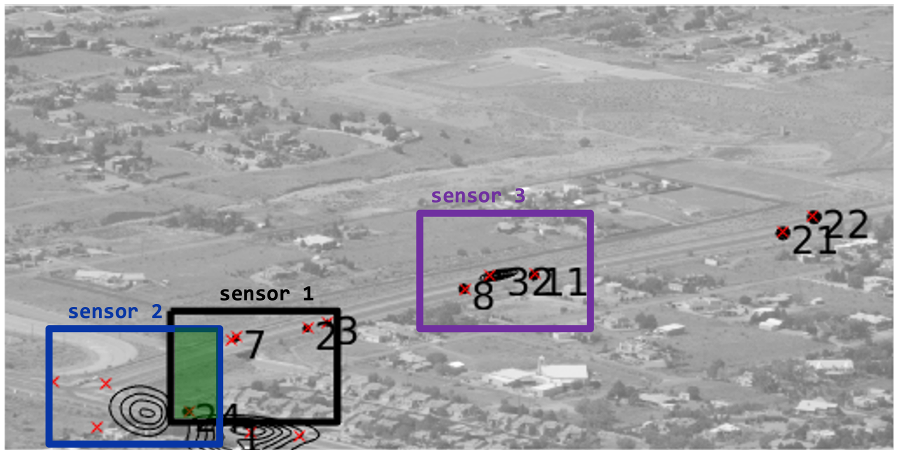

Figure 5.1: Multi-sensor multi-object search-while-tracking with M = 3 sensors, where due to sensor FoV overlap (green region), the information gain is nonadditive over sensors.

FoVs. Let N_k denote the number of objects present in the surveillance region $\mathcal{W}$ at time k. The multi-object state X_k is the collection of N_k single-object states at time k and is expressed as the finite set

$$X_k = \{\mathbf{x}_{k,1}, \ldots, \mathbf{x}_{k,N_k}\} \in \mathcal{F}(\mathbb{X}) \tag{5.1}$$

where $\mathbf{x}_{k,i}$ is the i^{th} element of X_k and $\mathcal{F}(\mathbb{X})$ denotes the collection of all finite subsets of the object state space $\mathbb{X}$.

The multi-object measurement produced by sensor i is the collection of $M_k^{(i)}$ single-object measurements at time k and is expressed as the set

$$Z_k^{(i)} = \{\mathbf{z}_{k,1}, \ldots, \mathbf{z}_{k,M_k^{(i)}}\}^{(i)} \in \mathcal{F}(\mathbb{Z}^{(i)}) \tag{5.2}$$

where $\mathbb{Z}^{(i)}$ denotes the measurement space of sensor i. The sensor resolution is such that single-object detections $\mathbf{z}_{k,j}$ are represented by points, e.g., a centroidal pixel, with no additional classification-quality information. Because detections contain no identifying labels or features, the association between tracked objects and incoming measurement data is unknown.

The FoV of sensor i is defined as a compact subset $\mathcal{S}_k^{(i)} \in \mathbb{S}$, where $\mathbb{S}$ denotes the space of compact subsets on $\mathbb{X}_s$. Then, object detection is assumed to be random and characterized by the probability function,

$$p_{D,k}^{(i)}(\mathbf{x}_k; \mathcal{S}_k^{(i)}) = 1_{\mathcal{S}_k^{(i)}}(\mathbf{s}_k) \cdot p_{D,k}(\mathbf{s}_k) \tag{5.3}$$

where the single-argument function $p_{D,k}^{(i)}(\mathbf{s}_k)$ is the probability of object detection for an unbounded FoV. In general, sensor FoVs may overlap, in which case multiple simultaneous detections may be made of the same object. When an object is detected, a noisy measurement of its state $\mathbf{x}_k$ is produced according to the likelihood function

$$\mathbf{z}_k \sim g_k^{(i)}(\mathbf{z}_k|\mathbf{x}_k) \tag{5.4}$$

where $\mathbf{z}_k \in \mathbb{Z}$. In addition to detections originating from true objects, sensors produce spurious measurements due to random phenomena, which are referred to as clutter or false alarms. Each resolution cell (e.g., a pixel) of the sensor image plane is equally likely to produce a false alarm, and thus, the clutter process is modeled as a Poisson RFS process with PHD $\kappa_{c,k}^{(i)}(\mathbf{z})$ [9]. For simplicity, it is assumed that sensors are homogeneous such that $p_{D,k}^{(i)}(\cdot) = p_{D,k}(\cdot)$, $g_k^{(i)}(\cdot) = g_k(\cdot)$, and $\kappa_{c,k}^{(i)}(\cdot) = \kappa_{c,k}(\cdot)$ for all sensors i.

Let $\mathbf{u}_k^{(i)} \in \mathbb{U}_k^{(i)}$ denote the sensor control inputs that, through actuation, determine the position of the sensor FoV at time k, $\mathcal{S}_k^{(i)}$, where $\mathbb{U}_k^{(i)}$ is the set of all admissible controls for sensor i. The control $\mathbf{u}_k^{(i)}$ influences both the FoV geometry, $\mathcal{S}_k^{(i)}$, and the sensor measurements, $Z_k^{(i)}$, due to varying object visibility. Because in many modern applications the surveillance region $\mathcal{W}$ is much larger than the sensor FoV, only a fraction of the total object population can be observed at any given time. Therefore, given the admissible control inputs $\mathbb{U}_k^{(i)}$, let the FoR be defined as

$$\mathcal{T}_k^{(i)} \triangleq \bigcup_{\mathbf{u}_k^{(i)} \in \mathbb{U}_k^{(i)}} \mathcal{S}_k^{(i)}(\mathbf{u}_k^{(i)}) \tag{5.5}$$

and represent the composite of regions that the sensor can potentially cover (although not simultaneously) at the next time step.

Then, the sensor control problem can be formulated as an RFS POMDP [91, 62, 21], that includes a partially- and noisily-observed state X_k, a known initial distribution of the state $f_0(X_0)$, a probabilistic transition model $f_{k|k-1}(X_k|X_{k-1})$, a set of admissible control actions $\mathbb{U}_k^{(1:\mathrm{M})}$, and a reward $\mathcal{R}_k$ associated with each control action. At every time step k, an RFS multi-sensor multi-object tracker processes incoming measurements to produce the posterior information state $f_k(X_k|Z_{0:k}^{(1)}, \ldots, Z_{0:k}^{(\mathrm{M})})$, where M denotes the total number of sensors. Then, the sensor control input is chosen so as to maximize the expected information gain, or,

$$\mathbf{u}_k^{*(1:\mathrm{M})} = \boldsymbol{\mu}^*(f_{k|k-1}(X_k|Z_{0:k-1}^{(1:\mathrm{M})})) \tag{5.6}$$

$$\boldsymbol{\mu}^*(f_{k|k-1}(X_k|Z_{0:k-1}^{(1:\mathrm{M})})) \triangleq \operatorname*{arg\,max}_{\mathbf{u}_k^{(1:\mathrm{M})} \in \mathbb{U}_k^{(1:\mathrm{M})}} \Big\{ \mathrm{E}\Big[\mathcal{R}_k(Z_k^{(1:\mathrm{M})}; \mathcal{S}_k^{(1:\mathrm{M})}, f_{k|k-1}(X_k|Z_{0:k-1}^{(1:\mathrm{M})}), \mathbf{u}_{0:k-1}^{(1:\mathrm{M})}) \Big] \Big\} \tag{5.7}$$

$$\mathcal{S}_k^{(1:\mathrm{M})} \triangleq (\mathcal{S}_k^{(1)}, \ldots, \mathcal{S}_k^{(\mathrm{M})}) \in \mathbb{S}^{(1:\mathrm{M})} \tag{5.8}$$

$$\mathbf{u}_{0:k-1}^{(1:\mathrm{M})} \triangleq (\mathbf{u}_{0:k-1}^{(1)}, \ldots, \mathbf{u}_{0:k-1}^{(\mathrm{M})}) \in \mathbb{U}_{0:k-1}^{(1:\mathrm{M})} \tag{5.9}$$

$$\mathbb{U}_k^{(1:\mathrm{M})} \triangleq \mathbb{U}_k^{(1)} \times \cdots \times \mathbb{U}_k^{(\mathrm{M})} \tag{5.10}$$

where the functional dependence of $Z_k^{(1:\mathrm{M})}$ and $\mathcal{S}_k^{(1:\mathrm{M})}$ on $\mathbf{u}_k^{(1:\mathrm{M})}$ is omitted for brevity. In this chapter, $\mathcal{R}_k : \mathbb{Z}^{(1:\mathrm{M})} \times \mathbb{S}^{(1:\mathrm{M})} \times \mathbb{F} \times \mathbb{U}_k^{(1:\mathrm{M})} \mapsto \mathbb{R}$ is taken to be a multi-sensor information gain function, where $\mathbb{F}$ represents the space of valid RFS densities, while noting that the presented results are more broadly applicable to any integrable reward function satisfying the cell-additivity constraint defined in Section 4.3. In general, the optimal decision may result in sensor FoVs that partially or fully overlap, in which case the information value is not additive over sensors.

Policies of the form of (5.7) are sometimes referred to as *myopic*, as they only consider the reward or information gain for the single next time step, thereby reducing the computational complexity compared to longer-horizon planning policies. However, even in the reduced complexity myopic setting, direct evaluation of the optimal policy $\boldsymbol{\mu}^*$ is intractable due to the RFS expectation, which involves an infinite summation of multivariate integrals. Optimization of sensor decisions is further complicated by the high-dimensional admissible control space, which grows exponentially with the number of sensors. Thus, principled approximations of the optimal policy are required for tractability. Three forms of approximation are considered in this chapter:

1. Approximation of the multi-sensor information gain using the PHD iterated-corrector recursion (Section 5.3.1)
2. Approximation of the RFS expectation using the cell-MB approximation (Section 5.3.1)
3. Constraints on admissible multi-sensor control actions (Sections 5.3.2 and 5.4.4)

5.3 Multi-Sensor Multi-Object Expected Information Gain

At every time step k, the multi-sensor decision $\mathbf{u}_k^{(1:M)}$ must be determined on the basis of its resulting information value. However, because the future multi-sensor measurement is unknown and random, so too is the actual information gain. Thus, a "risk neutral" strategy is to control sensors according to the *expected* information gain. Given the known multi-sensor measurement distribution $f(Z^{(1:\mathrm{M})})$, the information gain is averaged over all possible multi-sensor measurements via the RFS expectation

$$\mathrm{E}[\mathcal{R}] = \int \mathcal{R}(Z^{(1:\mathrm{M})}; \mathcal{S}^{(1:\mathrm{M})}) f(Z^{(1:\mathrm{M})}) \delta Z^{(1)} \delta Z^{(2)} \cdots \delta Z^{(\mathrm{M})} \tag{5.11}$$

Direct computation of (5.11), which involves multiple set integrals, is clearly intractable. This section shows, however, that for certain classes of information gain functionals, the multi-sensor multi-object information gain expectation can be approximated through nested cell-MB expectations. For clarity of presentation, the approximation is first developed for the specific case of two sensors before proceeding to the general case of M sensors.

5.3.1 Information Gain for Two Sensors with Common FoV

This subsection establishes the cell-MB approximation of the multi-sensor multi-object information gain expectation for the case of two sensors. For conceptual clarity and ease of exposition, it is assumed that the sensors have identical FoVs $\mathcal{S}^{(1)} = \mathcal{S}^{(2)} = \mathcal{S}$. This is without loss of generally, as the result holds when applied over regions of partial FoV overlap, as is shown in Section 5.3.2.

The cell-MB approach to multi-sensor information driven control is based on cell-MB approximations of the "last" sensor's measurement distribution $f(Z^{(\mathrm{M})})$ and of the conditional measurement distributions $f(Z^{(i)}|Z^{(i+1:\mathrm{M})}; \mathcal{S})$ for $i = 1, ..., \mathrm{M} - 1$. In the case of two sensors, this corresponds to the approximation of $f(Z^{(2)})$ and $f(Z^{(1)}|Z^{(2)};\mathcal{S})$ as cell-MB. By this approach, the expected multi-sensor multi-object information gain reduces to a finite sum, as established more formally in the following theorem.

Theorem 2. *Let $f(Z^{(2)})$ be cell-MB with parameters $\{r^j, p^j\}_{j=1}^P$. Let the conditional measurement density $f(Z^{(1)}|Z^{(2)};\mathcal{S})$ be cell-MB with conditional parameters $\{\check{r}^j(Z^{(2)} \cap \overset{j}{\mathbb{Z}}), \check{p}^j(\mathbf{z}|Z^{(2)} \cap \overset{j}{\mathbb{Z}})\}_{j=1}^P$. If $\mathcal{R}(Z^{(1)}, Z^{(2)};\mathcal{S})$ is integrable and cell-additive, then*

$$
\begin{aligned}
&\mathrm{E}_{Z^{(1)},Z^{(2)}}[\mathcal{R}(Z^{(1)}, Z^{(2)};\mathcal{S})] \\
&\quad= \sum_{j=1}^{P}(1-r^j)(1-\check{r}^j(\emptyset))\mathcal{R}(\emptyset,\emptyset;\overset{j}{\mathcal{S}}) \\
&\quad\quad+ \sum_{j=1}^{P}(1-r^j)\check{r}^j(\emptyset)\left[\int_{\overset{j}{\mathbb{Z}}}\mathcal{R}(\{\mathbf{z}'\},\emptyset;\overset{j}{\mathcal{S}})\check{p}^j(\mathbf{z}'|\emptyset)\mathrm{d}\mathbf{z}'\right] \\
&\quad\quad+ \sum_{j=1}^{P} r^j\left[\int_{\overset{j}{\mathbb{Z}}}\mathcal{R}(\emptyset,\{\mathbf{z}\};\overset{j}{\mathcal{S}})(1-\check{r}^j(\{\mathbf{z}\}))p^j(\mathbf{z})\mathrm{d}\mathbf{z}\right] \\
&\quad\quad+ \sum_{j=1}^{P} r^j\left\{\int_{\overset{j}{\mathbb{Z}}}\check{r}^j(\{\mathbf{z}\})\left[\int_{\overset{j}{\mathbb{Z}}}\mathcal{R}(\{\mathbf{z}'\},\{\mathbf{z}\};\overset{j}{\mathcal{S}})\check{p}^j(\mathbf{z}'|\{\mathbf{z}\})\mathrm{d}\mathbf{z}'\right]p^j(\mathbf{z})\mathrm{d}\mathbf{z}\right\}
\end{aligned}
\tag{5.12}
$$

The proof is provided in Appendix A.6. Equation (5.12) is the two-sensor cell-MB expected multi-sensor reward. The right-hand-side (RHS) of (5.12) is organized intentionally to reveal that the expectation considers four possible outcomes for each cell. From top to bottom, the four groups of terms correspond to the cases of "miss/miss," "detect/miss," "miss/detect," and "detect/detect," respectively. That is, the first line of the RHS corresponds to the information gain achieved when both sensors produce no measurements in a given cell. The second (third) line, then, corresponds to the information gain for sensor one (two) producing a singleton measurement and sensor two (one) producing no measurement in a given cell. Lastly, the fourth line corresponds to both sensors producing singleton measurements. Unlike the previous terms, this "detect/detect" case involves integration over $\overset{j}{\mathbb{Z}} \times \overset{j}{\mathbb{Z}}$ and thus is the most computationally burdensome term.

In Theorem 2, the conditional density $f(Z^{(1)}|Z^{(2)};\mathcal{S})$ is taken to be cell-MB. Recall that, given a suitable cell-decomposition, a cell-MB density approximation can be obtained for an arbitrary density, as shown in Section 4.3.1. Specifically, by Proposition 5, given the conditional density $f(Z^{(1)}|Z^{(2)};\mathcal{S})$ and its corresponding conditional PHD $\check{D}(\mathbf{z}|Z^{(2)};\mathcal{S})$, the best cell-MB approximation is specified by the parameters

$$\check{r}^j(Z^{(2)} \cap \overset{j}{\mathbb{Z}}) = \int 1_{\overset{j}{\mathbb{Z}}}(\mathbf{z})\check{D}(\mathbf{z}|Z^{(2)} \cap \overset{j}{\mathbb{Z}}; \overset{j}{\mathcal{S}})\mathrm{d}\mathbf{z} \tag{5.13}$$

$$\check{p}^j(\mathbf{z}|Z^{(2)} \cap \overset{j}{\mathbb{Z}}) = \frac{1}{\check{r}^j(Z^{(2)} \cap \overset{j}{\mathbb{Z}})} 1_{\overset{j}{\mathbb{Z}}}(\mathbf{z})\check{D}(\mathbf{z}|Z^{(2)} \cap \overset{j}{\mathbb{Z}}; \overset{j}{\mathcal{S}}) \tag{5.14}$$

In general, direct computation of $f(Z^{(1)}|Z^{(2)};\mathcal{S})$ may be impractical. Instead, the conditional PHD can be approximated directly from the prior PHD as

$$\check{D}(\mathbf{z}|Z;\mathcal{S}_k) \approx \int_{\mathbb{X}} D_{k|k-1}(\mathbf{x})L_Z(\mathbf{x};\mathcal{S},D_{k|k-1})p_{D,k}(\mathbf{x};\mathcal{S}_k)g_k(\mathbf{z}|\mathbf{x})\mathrm{d}\mathbf{x} + \kappa_{c,k}(\mathbf{z}) \tag{5.15}$$

The remainder of this subsection establishes a multi-sensor information gain approximation that satisfies cell-additivity constraints and thus can be applied in concert with Theorem 2. Consider the KLD multi-sensor information gain for the case when the prior and posterior distributions are Poisson, where by (2.38),

$$I_{\mathrm{KL,Pois}}(f(X_k|Z_{0:k}^{(1:\mathrm{M})}); f(X_k|Z_{0:k-1}^{(1:\mathrm{M})})) = N_0 - N_1 + \int D_{k|k}(\mathbf{x}) \log\left(\frac{D_{k|k}(\mathbf{x})}{D_{k|k-1}(\mathbf{x})}\right) \mathrm{d}\mathbf{x} \tag{5.16}$$

where $N_0 = \int D_{k|k-1}(\mathbf{x})\mathrm{d}\mathbf{x}$ and $N_1 = \int D_{k|k}(\mathbf{x})\mathrm{d}\mathbf{x}$. Recall that a Poisson RFS distribution is completely described by its PHD. Thus, the multi-sensor posterior can be approximated by the *multi-sensor iterated corrector PHD update* [72]:

$$D_{k|k}(\mathbf{x}) \approx L_{Z^{(2)}}(\mathbf{x};\mathcal{S},D_k^{(1)}(\cdot|Z^{(1)};\mathcal{S})) \cdot L_{Z^{(1)}}(\mathbf{x};\mathcal{S},D_{k|k-1}) \cdot D_{k|k-1}(\mathbf{x}) \tag{5.17}$$

where $D_{k|k}$ is the posterior PHD, $D_{k|k-1}(\mathbf{x})$ is the prior PHD, and

$$D_k^{(1)}(\mathbf{x}|Z^{(1)};\mathcal{S}) = L_{Z^{(1)}}(\mathbf{x};\mathcal{S},D_{k|k-1}) \cdot D_{k|k-1}(\mathbf{x}) \tag{5.18}$$

is the intermediate result of updating applying the first PHD update with $Z^{(1)}$.

By the iterated-corrector update (5.17), the KLD information gain is

$$\begin{aligned}\mathcal{R}_k(Z^{(1)},Z^{(2)};\mathcal{S},D_{k|k-1}) = \int_{\mathbb{X}} & D_{k|k-1}(\mathbf{x}) \cdot \\ & \Big[1 - L_{Z^{(2)}}(\mathbf{x};\mathcal{S},D_k^{(1)}(\cdot|Z^{(1)};\mathcal{S})) \cdot L_{Z^{(1)}}(\mathbf{x};\mathcal{S},D_{k|k-1}) \\ & + L_{Z^{(2)}}(\mathbf{x};\mathcal{S},D_k^{(1)}(\cdot|Z^{(1)};\mathcal{S})) \cdot L_{Z^{(1)}}(\mathbf{x};\mathcal{S},D_{k|k-1}) \\ & \cdot \log\big(L_{Z^{(2)}}(\mathbf{x};\mathcal{S},D_k^{(1)}(\cdot|Z^{(1)};\mathcal{S})) \cdot L_{Z^{(1)}}(\mathbf{x};\mathcal{S},D_{k|k-1})\big)\Big] \mathrm{d}\mathbf{x}\end{aligned} \tag{5.19}$$

The following theorem establishes that (5.19) is cell-additive.

Theorem 3. *Let the joint decomposition*

$$\mathbb{Z} = \overset{1}{\mathbb{Z}} \uplus \cdots \uplus \overset{P}{\mathbb{Z}}, \qquad \mathbb{X} = \overset{1}{\mathbb{X}} \uplus \cdots \uplus \overset{P}{\mathbb{X}} \tag{5.20}$$

be such that (4.16) and (4.24) hold. Let both sensors share a common $\mathcal{S}_k$, $g_k(\mathbf{z}|\mathbf{x})$, $p_{D,k}(\mathbf{x};\mathcal{S}_k)$, and $\kappa_{c,k}(\mathbf{z})$. Then, the multi-sensor iterated-corrector PHD KLD information gain (5.19) is cell-additive. That is

$$\mathcal{R}_k(Z^{(1)},Z^{(2)};\mathcal{S}_k,D_{k|k-1}) = \sum_{j=1}^{P} \mathcal{R}_k(Z^{(1)} \cap \overset{j}{\mathbb{Z}}, Z^{(2)} \cap \overset{j}{\mathbb{Z}}; \overset{j}{\mathcal{S}}_k, D_{k|k-1}) \tag{5.21}$$

The proof is provided in Appendix A.7.

Thus, given the conditional cell-MB parameters (5.13)-(5.14), and cell-additivity satisfaction by Theorem 3, the expected multi-sensor multi-object information gain is obtained via Theorem 2. The significance of this result is that the expectation, which is generally intractable due to the infinite summation of multivariate integrals (see (5.11) and (2.21)), is given by a finite sum. Note that the terms corresponding to the “detect/detect” case in (5.12) require integration on $\overset{j}{\mathbb{Z}} \times \overset{j}{\mathbb{Z}}$, and thus is more computationally demanding than the single-sensor cell-MB expectation.

Fortunately, by the nature of the cell decomposition, the information gain expectation can be computed cell-wise, where the two-sensor cell-MB expectation is computed for cells covered by two sensors, and the less expensive single-sensor cell-MB expectation is computed for cells covered by one sensor, as shown in Section 5.3.2. While, in principle, nested cell-MB approximations can be applied to express the expected information gain for regions covered by three or more sensors, the resulting expressions are increasingly cumbersome to compute due to the increased dimensionality of the integral in the “all detect” case. Thus, the remainder of this chapter considers information gain functions and corresponding control policies that restrict a given cell’s coverage to at most two sensors, without restricting the number of sensors in general, which may be greater than two.

5.3.2 Information Gain for M Sensors with Partial FoV Overlap

This section establishes the expected multi-sensor information gain for the general case of M homogeneous sensors under the restriction that no region is covered by more than two sensors simultaneously. This assumption is illustrated in Fig. 5.2 and formalized in the following assumption:

Assumption 1. *No cell is covered by more than two sensors simultaneously.*

Equivalently,

$$\mathcal{S}_k^{(i)} \cap \mathcal{S}_k^{(j)} \cap \mathcal{S}_k^{(\ell)} = \emptyset \quad \forall i \neq j \neq \ell,\ i, j, \ell \in \mathbb{N}_{\mathrm{M}} \tag{5.22}$$

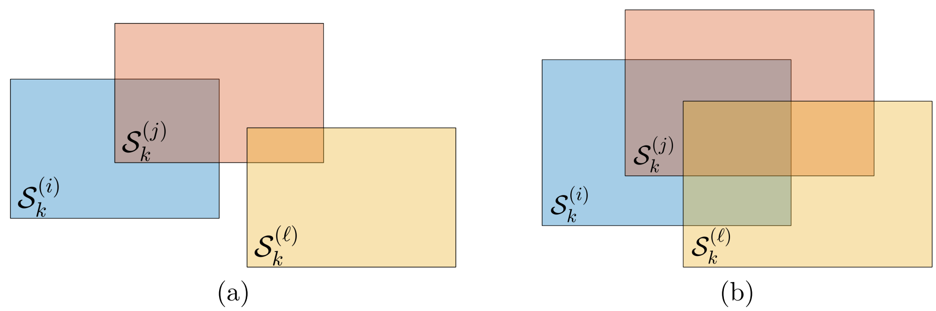

Figure 5.2: Examples of (a) allowable FoV overlap where $\mathcal{S}_k^{(i)} \cap \mathcal{S}_k^{(j)} \cap \mathcal{S}_k^{(\ell)} = \emptyset$, and (b) unallowable FoV overlap where $\mathcal{S}_k^{(i)} \cap \mathcal{S}_k^{(j)} \cap \mathcal{S}_k^{(\ell)} \neq \emptyset$.

Theorem 4. *Let Assumption 1 hold. Let $f(Z^{(\mathrm{M})})$ be cell-MB and $f(Z^{(i)}|Z^{(i+1:\mathrm{M})})$ be conditionally cell-MB for $1 \leq i < \mathrm{M}$. Then, the multi-sensor multi-object expected information gain is*

$$\mathrm{E}_{Z^{(1:\mathrm{M})}}[\mathcal{R}(Z^{(1:\mathrm{M})}; \mathcal{S}^{(1:\mathrm{M})})] = \sum_{j=1}^{P} \mathcal{E}(j, Z^{(1:\mathrm{M})}, \mathcal{S}^{(1:\mathrm{M})}) \tag{5.23}$$

where, for $b \in \mathbb{N}_{\mathrm{M}}$,

$$\begin{aligned} &\mathcal{E}(j, Z^{(b:\mathrm{M})}, \mathcal{S}^{(b:\mathrm{M})}) \\ &= \begin{cases} \mathrm{E}[\mathcal{R}(Z^{(i)} \cap \overset{j}{\mathbb{Z}}; \overset{j}{\mathcal{S}})] & \overset{j}{\mathbb{X}} \subseteq \mathcal{S}^{(i)},\ \overset{j}{\mathbb{X}} \nsubseteq \mathcal{S}^{(t)}\ \forall b \leq t \leq \mathrm{M},\ t \neq i \\ \mathrm{E}[\mathcal{R}(Z^{(i)} \cap \overset{j}{\mathbb{Z}}, Z^{(t)} \cap \overset{j}{\mathbb{Z}}; \overset{j}{\mathcal{S}})] & \overset{j}{\mathbb{X}} \subseteq \mathcal{S}^{(i)} \cap \mathcal{S}^{(t)}, b \leq i < t \leq \mathrm{M} \\ 0 & \textit{otherwise} \end{cases} \end{aligned} \tag{5.24}$$

A proof by induction is provided in Appendix A.8.

5.4 Search-While-Tracking (SWT) Multi-Sensor Control

This section presents a joint multi-sensor multi-object information gain function and multi-sensor control policy that accounts for both discovered and undiscovered objects. The information gain function proposed in Section 5.4.1 balances the competing objects of maintaining existing track estimates and discovering new objects without introducing heuristics. The discovered object and undiscovered object components of the joint multi-sensor information gain function are derived in Sections 5.4.2 and 5.4.3. Section 5.4.4 presents a greedy approach to multi-sensor FoV optimization under the joint information-theoretic control objective.

5.4.1 Joint Information Gain Function

As shown in Section 4.4.1, separate density parameterizations for discovered and undiscovered objects enable efficient computation of the joint information gain. This section lifts the joint information gain approach to the multi-sensor setting. Denote by $X_{u,k} \in \mathcal{F}(\mathbb{X})$ the *undiscovered* multi-object state, defined here as the state of objects that were not detected during steps $0, \ldots, k-1$. Let $X_{d,k} \in \mathcal{F}(\mathbb{X})$ be the *discovered* state, defined as the state of objects detected prior to k. Then, sensor i's measurement is composed by $Z^{(i)}_{u,k}$, $Z^{(i)}_{d,k}$, and $Z^{(i)}_{c,k}$, which denote the detections generated by $X_{u,k}$, $X_{d,k}$, and clutter, respectively. Let $V^{(i)}_k \triangleq Z^{(i)}_{d,k} \cup Z^{(i)}_{c,k}$ and $W^{(i)}_k \triangleq Z^{(i)}_{u,k} \cup Z^{(i)}_{c,k}$. Then, the multi-sensor control policy is defined in terms of the joint information gain as

$$\begin{aligned}
&\boldsymbol{\mu}(\mathring{f}_{\mathrm{p},k|k-1}(\mathring{X}_{\mathrm{p},k}|Z^{(1:\mathrm{M})}_{0:k-1}), f_{u,k|k-1}(X_{u,k})) \\
&\quad = \underset{\mathbf{u}^{(1:\mathrm{M})}_k \in \mathbb{U}^{(1:\mathrm{M})}_k}{\arg\max} \left\{ \mathrm{E}[\mathcal{R}^d_k(V^{(1:\mathrm{M})}_k; \mathcal{S}^{(1:\mathrm{M})}_k)] + \mathrm{E}[\mathcal{R}^u_k(W^{(1:\mathrm{M})}_k; \mathcal{S}^{(1:\mathrm{M})}_k)] \right\}
\end{aligned} \tag{5.25}$$

where

$$\mathcal{R}_k^d(\cdot;\cdot) = \mathcal{R}_k(\cdot;\cdot, D_{d,k|k-1}) \tag{5.26}$$

$$\mathcal{R}_k^u(\cdot;\cdot) = \mathcal{R}_k(\cdot;\cdot, D_{u,k|k-1}) \tag{5.27}$$

are used for brevity, and $D_{d,k|k-1}$ and $D_{u,k|k-1}$ are the prior PHDs of discovered and undiscovered objects, respectively. The multi-sensor control policy is a function of the predicted distribution of discovered objects and the predicted distribution of undiscovered objects. Furthermore, the proposed iterated-corrector based KLD information gain functions are described completely in terms of the PHDs of the underlying distributions, and thus are written explicitly as functions of $D_{d,k|k-1}$ and $D_{u,k|k-1}$. The individual information gain expectations for discovered and undiscovered objects are derived in the following subsections.

5.4.2 Expected Information Gain of Discovered Objects

If $f(V_k^{(\mathrm{M})})$ is cell-MB with parameters $\{r_{\mathrm{v}}^j, p_{\mathrm{v}}^j\}_{j=1}^P$, $f(V_k^{(i)}|V_k^{(i+1:\mathrm{M})})$ is conditionally cell-MB with parameters $\{r_{\mathrm{v}}^j(V_k^{(i+1:\mathrm{M})} \cap \overset{j}{\mathbb{Z}}), p_{\mathrm{v}}^j(\mathbf{z}|V_k^{(i+1:\mathrm{M})} \cap \overset{j}{\mathbb{Z}})\}_{j=1}^P$, and no cell is covered by more than two sensors, then it follows from Theorem 4 that

$$\mathrm{E}_{V^{(1:\mathrm{M})}}[\mathcal{R}^d(V^{(1:\mathrm{M})};\mathcal{S}^{(1:\mathrm{M})})] = \sum_{j=1}^{P} \mathcal{E}^d(j, V^{(1:\mathrm{M})}, \mathcal{S}^{(1:\mathrm{M})}) \tag{5.28}$$

where the time subscripts have been omitted for brevity and, as a slight abuse of notation,

$$V_k^{(i+1:\mathrm{M})} \cap \overset{j}{\mathbb{Z}} \triangleq V_k^{(i+1)} \cap \overset{j}{\mathbb{Z}}, \ldots, V_k^{(\mathrm{M})} \cap \overset{j}{\mathbb{Z}} \tag{5.29}$$

and

$$
\mathcal{E}^d(j, V^{(1:\mathrm{M})}, \mathcal{S}^{(1:\mathrm{M})}) \tag{5.30}
$$

$$
= \begin{cases} \mathrm{E}[\mathcal{R}^d(V^{(i)} \cap \overset{j}{\mathbb{Z}}; \overset{j}{\mathcal{S}})] & \overset{j}{\mathbb{X}} \subseteq \mathcal{S}^{(i)},\ \overset{j}{\mathbb{X}} \nsubseteq \mathcal{S}^{(t)}\ \forall\, 1 \leq t \leq \mathrm{M},\ t \neq i \\ \mathrm{E}[\mathcal{R}^d(V^{(i)} \cap \overset{j}{\mathbb{Z}}, V^{(t)} \cap \overset{j}{\mathbb{Z}}; \overset{j}{\mathcal{S}})] & \overset{j}{\mathbb{X}} \subseteq \mathcal{S}^{(i)} \cap \mathcal{S}^{(t)}, 1 \leq i < t \leq \mathrm{M} \\ 0 & \text{otherwise} \end{cases}
$$

The first case of (5.30) is given by (4.29). The second case corresponds to two sensors overlapping a given cell and is given by

$$
\begin{aligned}
&\mathrm{E}[\mathcal{R}^d(V^{(i)} \cap \overset{j}{\mathbb{Z}}, V^{(t)} \cap \overset{j}{\mathbb{Z}}; \overset{j}{\mathcal{S}})] \\
&\quad = (1 - r_{\mathrm{v}}^j)(1 - \check{r}_{\mathrm{v}}^j(\emptyset))\mathcal{R}^d(\emptyset, \emptyset; \overset{j}{\mathcal{S}}) \\
&\quad\quad + (1 - r_{\mathrm{v}}^j)\check{r}_{\mathrm{v}}^j(\emptyset)\left[\int_{\overset{j}{\mathbb{Z}}} \mathcal{R}^d(\{\mathbf{z}'\}, \emptyset; \overset{j}{\mathcal{S}})\check{p}_{\mathrm{v}}^j(\mathbf{z}'|\emptyset)\mathrm{d}\mathbf{z}'\right] \\
&\quad\quad + r^j\left[\int_{\overset{j}{\mathbb{Z}}} \mathcal{R}^d(\emptyset, \{\mathbf{z}\}; \overset{j}{\mathcal{S}})(1 - \check{r}_{\mathrm{v}}^j(\{\mathbf{z}\}))p_{\mathrm{v}}^j(\mathbf{z})\mathrm{d}\mathbf{z}\right] \\
&\quad\quad + r^j\left\{\int_{\overset{j}{\mathbb{Z}}} \check{r}_{\mathrm{v}}^j(\{\mathbf{z}\})\left[\int_{\overset{j}{\mathbb{Z}}} \mathcal{R}^d(\{\mathbf{z}'\}, \{\mathbf{z}\}; \overset{j}{\mathcal{S}})\check{p}_{\mathrm{v}}^j(\mathbf{z}'|\{\mathbf{z}\})\mathrm{d}\mathbf{z}'\right]p_{\mathrm{v}}^j(\mathbf{z})\mathrm{d}\mathbf{z}\right\}
\end{aligned} \tag{5.31}
$$

5.4.3 Expected Information Gain of Undiscovered Objects

If $f(W_k^{(\mathrm{M})})$ is cell-MB with parameters $\{r_{\mathrm{w}}^j, p_{\mathrm{w}}^j\}_{j=1}^P$, $f(W_k^{(i)}|W_k^{(i+1:\mathrm{M})})$ is conditionally cell-MB with parameters $\{r_{\mathrm{w}}^j(W_k^{(i+1:\mathrm{M})} \cap \overset{j}{\mathbb{Z}}), p_{\mathrm{w}}^j(\mathbf{z}|W_k^{(i+1:\mathrm{M})} \cap \overset{j}{\mathbb{Z}})\}_{j=1}^P$, and no cell is covered by more than two sensors, then it follows from Theorem 4 that

$$
\mathrm{E}_{W^{(1:\mathrm{M})}}[\mathcal{R}^u(W^{(1:\mathrm{M})}; \mathcal{S}^{(1:\mathrm{M})})] = \sum_{j=1}^{P} \mathcal{E}^d(j, W^{(1:\mathrm{M})}, \mathcal{S}^{(1:\mathrm{M})}) \tag{5.32}
$$

where the time subscripts have been omitted for brevity, and

$$
\begin{aligned}
&\mathcal{E}^u(j, W^{(1:\mathrm{M})}, \mathcal{S}^{(1:\mathrm{M})}) \\
&= \begin{cases}
\mathrm{E}[\mathcal{R}^u(W^{(i)} \cap \overset{j}{\mathbb{Z}}; \overset{j}{\mathcal{S}})] & \overset{j}{\mathbb{X}} \subseteq \mathcal{S}^{(i)},\, \overset{j}{\mathbb{X}} \nsubseteq \mathcal{S}^{(t)}\, \forall\, 1 \le t \le \mathrm{M},\, t \neq i \\
\mathrm{E}[\mathcal{R}^u(W^{(i)} \cap \overset{j}{\mathbb{Z}}, W^{(t)} \cap \overset{j}{\mathbb{Z}}; \overset{j}{\mathcal{S}})] & \overset{j}{\mathbb{X}} \subseteq \mathcal{S}^{(i)} \cap \mathcal{S}^{(t)}, 1 \le i < t \le \mathrm{M} \\
0 & \text{otherwise}
\end{cases}
\end{aligned}
\tag{5.33}
$$

The first case of (5.33) is given by (4.44). The second case corresponds to two sensors overlapping a given cell and is given by

$$
\begin{aligned}
&\mathrm{E}[\mathcal{R}^u(W^{(i)} \cap \overset{j}{\mathbb{Z}}, W^{(t)} \cap \overset{j}{\mathbb{Z}}; \overset{j}{\mathcal{S}})] \\
&\quad = (1 - r^j_{\mathrm{w}})(1 - \check{r}^j_{\mathrm{w}}(\emptyset))\mathcal{R}^u(\emptyset, \emptyset; \overset{j}{\mathcal{S}}) \\
&\qquad + (1 - r^j_{\mathrm{w}})\check{r}^j_{\mathrm{w}}(\emptyset) \left[\int_{\overset{j}{\mathbb{Z}}} \mathcal{R}^u(\{\mathbf{z}'\}, \emptyset; \overset{j}{\mathcal{S}}) \check{p}^j_{\mathrm{w}}(\mathbf{z}'|\emptyset) \mathrm{d}\mathbf{z}' \right] \\
&\qquad + r^j \left[\int_{\overset{j}{\mathbb{Z}}} \mathcal{R}^u(\emptyset, \{\mathbf{z}\}; \overset{j}{\mathcal{S}})(1 - \check{r}^j_{\mathrm{w}}(\{\mathbf{z}\})) p^j_{\mathrm{w}}(\mathbf{z}) \mathrm{d}\mathbf{z} \right] \\
&\qquad + r^j \left\{ \int_{\overset{j}{\mathbb{Z}}} \check{r}^j_{\mathrm{w}}(\{\mathbf{z}\}) \left[\int_{\overset{j}{\mathbb{Z}}} \mathcal{R}^u(\{\mathbf{z}'\}, \{\mathbf{z}\}; \overset{j}{\mathcal{S}}) \check{p}^j_{\mathrm{w}}(\mathbf{z}'|\{\mathbf{z}\}) \mathrm{d}\mathbf{z}' \right] p^j_{\mathrm{w}}(\mathbf{z}) \mathrm{d}\mathbf{z} \right\}
\end{aligned}
\tag{5.34}
$$

As discussed in Section 4.4.3, if the prior PHD of undiscovered objects is taken to be partially piecewise homogeneous with a position-marginal PHD given by (4.37), then it can be shown that (5.34) is a function only of the prior expected number of undiscovered objects in each cell, $\lambda_{j,k|k-1}$. Thus, for a one-time computational cost, (5.34) can be computed at the outset for a range of values $\lambda_{j,k|k-1} \in [0, 1]$, and then simply interpolated at each time k.

5.4.4 Field-of-View Optimization and Multi-Sensor Control

Because exhaustive search over the complete space of multi-sensor actions $\mathbb{U}^{(1:\mathrm{M})}$ is NP-hard [104, 126], suboptimal solutions of (5.7) are needed. The constraint on the maximum cell overlap reduces the search space considerably. The computational burden can be further reduced by considering a greedy optimization algorithm [58]. To avoid computing the expected two-sensor reward for every cell, a greedy optimization strategy can be applied as follows:

$$\mathbf{u}^{(\mathrm{M})*} \leftarrow \underset{\mathbf{u}\in\mathbb{U}^{(\mathrm{M})}}{\arg\min}\left\{\mathrm{E}_{Z^{(\mathrm{M})}}[\mathcal{R}(Z^{(\mathrm{M})};(\mathcal{S}^{(\mathrm{M})}(\mathbf{u})))]\right\} \tag{5.35}$$

$$\mathbf{u}^{(\mathrm{M}-1)*} \leftarrow \underset{\mathbf{u}\in\mathbb{U}^{(\mathrm{M}-1)}}{\arg\min}\left\{\mathrm{E}_{Z^{(\mathrm{M}-1)},Z^{(\mathrm{M})}}[\mathcal{R}(Z^{(\mathrm{M}-1)},Z^{(\mathrm{M})};(\mathcal{S}^{(\mathrm{M}-1)}(\mathbf{u}),\mathcal{S}^{(\mathrm{M})*}))]\right\} \tag{5.36}$$

$$\mathbf{u}^{(\mathrm{M}-2)*} \leftarrow \underset{\mathbf{u}\in\bar{\mathbb{U}}^{(\mathrm{M}-2)}}{\arg\min}\left\{\mathrm{E}_{Z^{(\mathrm{M}-2:\mathrm{M})}}[\mathcal{R}(Z^{(\mathrm{M}-2)},Z^{(\mathrm{M}-1)},Z^{(\mathrm{M})};(\mathcal{S}^{(\mathrm{M}-2)}(\mathbf{u}),\mathcal{S}^{(\mathrm{M}-1)*},\mathcal{S}^{(\mathrm{M})*}))]\right\} \tag{5.37}$$

$$\vdots$$

$$\mathbf{u}^{(1)*} \leftarrow \underset{\mathbf{u}\in\bar{\mathbb{U}}^{(1)}}{\arg\min}\left\{\mathrm{E}_{Z^{(1:\mathrm{M})}}[\mathcal{R}(Z^{(1)},\ldots,Z^{(\mathrm{M})};(\mathcal{S}^{(1)}(\mathbf{u}),\mathcal{S}^{(2)*},\ldots,\mathcal{S}^{(\mathrm{M})*}))]\right\} \tag{5.38}$$

where $\mathcal{S}^{(i)*} \triangleq \mathcal{S}^{(i)}(\mathbf{u}^{(i)*})$ and, for sensors $i = 1,\ldots,\mathrm{M}-2$, the restricted space of admissible control actions

$$\bar{\mathbb{U}}^{(i)} \triangleq \{\mathbf{u} : \mathbf{u}\in\mathbb{U}^{(i)}, \mathcal{S}^{(i)}(\mathbf{u})\cap\mathcal{S}^{(j)}\cap\mathcal{S}^{(h)} = \emptyset\,\forall\, i<j<h\le \mathrm{M}\} \tag{5.39}$$

ensures that no cell is covered by more than two sensors simultaneously. The greedy strategy begins by determining the sensor input $\mathbf{u}^{(\mathrm{M})*}$ according to (4.51). Then, for sensor $\mathrm{M}-1$, evaluation of the more computationally expensive two-sensor information gain expectation is required only for the subset of cells within $\mathcal{S}^{(\mathrm{M})*}\cap\mathcal{T}^{(\mathrm{M}-1)}$, and so forth for the remaining sensors.

5.5 Application to Remote Multi-Vehicle SWT

In this section, the efficacy of the cell-MB multi-sensor information driven control is demonstrated on an SWT problem involving multiple ground vehicles and real video data. A detailed description of the experiment can be found in Section 4.5, which is summarized here for convenience. The experiment consists of discovering and tracking an unknown and time-varying number of vehicles which are observed by a camera system approximately five kilometers away. Vehicle motion is modeled using the nonlinear nearly coordinated turn model. Each sensor's single-object measurement likelihood is linear-Gaussian as described in Section 4.5.2. One key difference in the multi-sensor experiment is that synthetic noisy measurements are generated from the ground truth in place of the image processing-based measurements. This ensures that the measurement noise is independent across the simulated sensors since the dataset was collected from a single physical sensor.

At each time step, sensor decisions are determined by the greedy optimization program (5.38). The noisy measurements are incorporated to update the information state using the multi-sensor data-driven GLMB filter [65]. State estimates are computed from the posterior multi-object distribution. The GOSPA metric measures the error between the ground truth and the state estimates and is used to assess the overall SWT performance. GOSPA values for simulations involving $\mathrm{M} = 2, 3$, and 4 sensors are shown in Fig. 5.3.

Unsurprisingly, the best SWT performance is achieved by the four-sensor system. The most significant performance differences occur at the early time steps due to the larger networks' ability to more quickly discover all objects in the scene. These differences are less pronounced at the later time steps, when control decisions are less influenced by discovering objects and more driven by the information

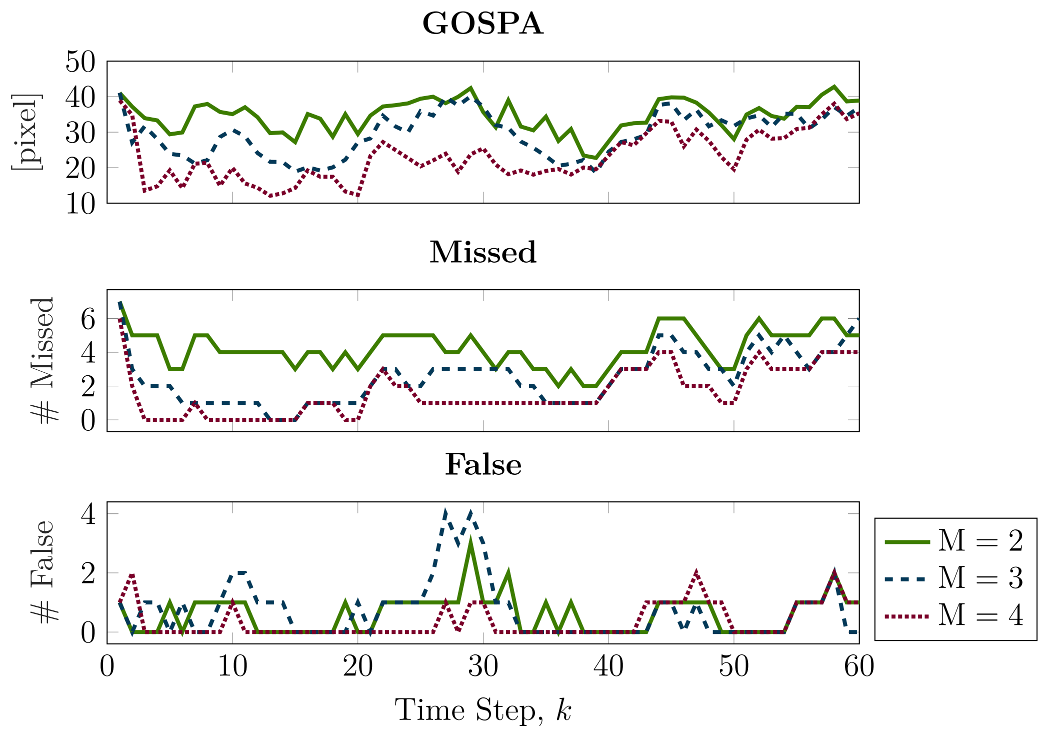

Figure 5.3: GOSPA metric and component errors over time using cutoff distance $c = 20$ [pixel], order $p = 2$, and $\alpha = 2$.

gain associated with maintaining tracks of discovered objects.

Snapshots of the sensor FoV positions and the multi-object state uncertainty are shown at three time steps for each of the experiments in Fig. 5.4. When considering the added complexity associated with allowing sensor FoV overlap, a natural question that arises is “Is it worth it?”. A related question is “Given the opportunity to overlap, how often does an overlapping FoV configuration correspond to a higher expected information gain?”. If overlapping configurations are rarely optimal, it is then reasonable to consider constraining FoV geometries to be disjoint to lessen the computational complexity of the control objective. The snapshots in Fig. 5.4 alone, however, suggest that the optimal sensor configurations often involve overlapping FoVs and that the extent of overlap increases with larger numbers of sensors. These trends are explored more thoroughly by computing the

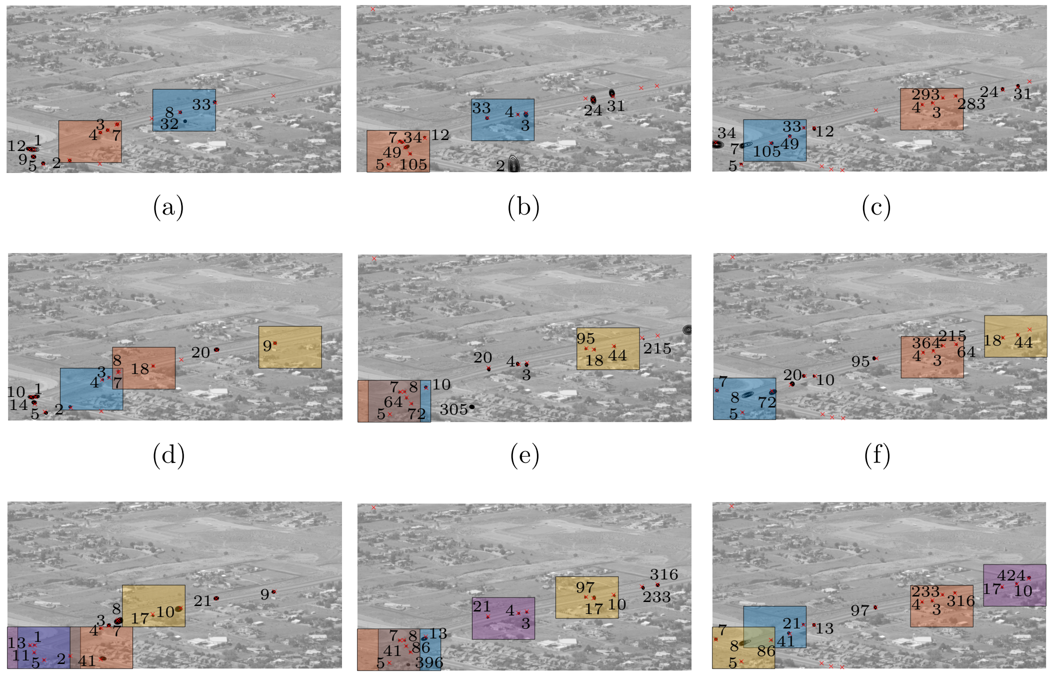

(a) (b) (c)

(d) (e) (f)

(g) (h) (i)

Figure 5.4: FoV positions and tracker estimates for M = 2 (a)-(c), M = 3 (d)-(f), and M = 4 (g)-(i), where the columns correspond to $k = 5, 30, 45$ from left to right.

ratio of unique coverage area to total FoV area, as shown over time in Fig. 5.5. In Fig. 5.5, values of 100% correspond to disjoint FoVs, and lower values correspond to increased overlap region areas. The results shown in Fig. 5.5 confirm that, in all three experiments, the optimal configuration frequently involved overlapping FoVs. The FoV overlap extent also appears to increase with the number of sensors considered. This observation suggests that, even if enough sensors are available to simultaneously cover the entire ROI, it is often better, from an information-theoretic perspective, to allow regions to go briefly uncovered in favor of doubling coverage in an area characterized by high concentrations of objects of interest.

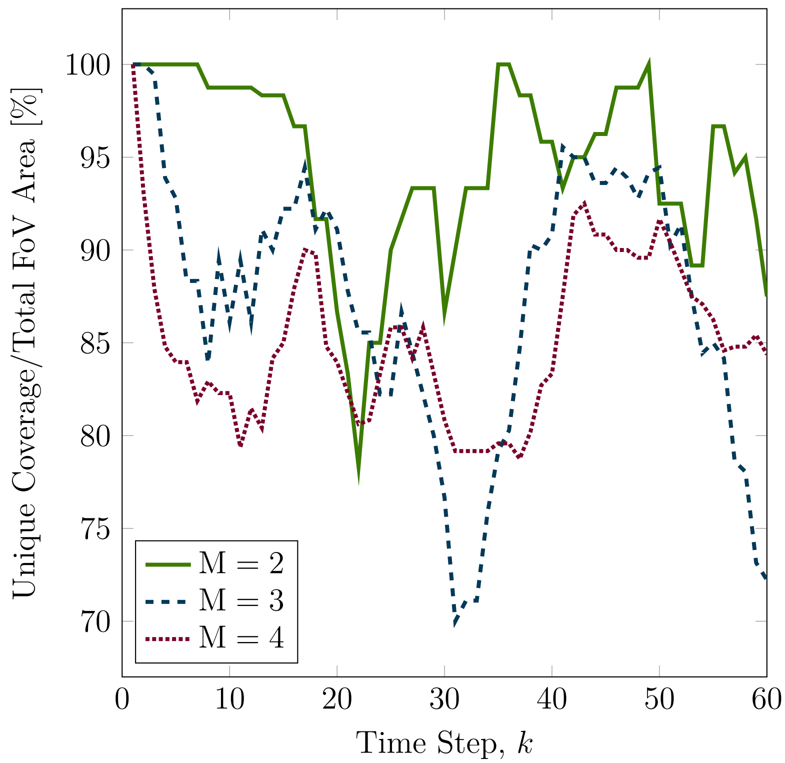

Figure 5.5: The ratio of unique area coverage to total FoV area, expressed as a percentage and smoothed by a five step rolling average filter for legibility.

5.6 Conclusion

This chapter presents an information-theoretic control policy for multi-sensor multi-object search-while-tracking (SWT) that is demonstrated in a multi-vehicle tracking problem using real video data from a remote sensor. The proposed policy is made tractable by a novel approximation of the expected information gain using cell multi-Bernoulli (cell-MB) distribution approximations, while accounting for a variety of sensing outcomes, including spurious detections, missed detections, and overlapping sensor fields-of-view (FoVs). An analysis of the experimental results reveals that optimal sensing configurations often involve overlapping sensor FoV, suggesting that other policies that require disjoint sensor coverage are suboptimal in an information-theoretic sense. Finally, the information-theoretic approach presented in this chapter is not restricted to the chosen sensor phenomenology or object dynamics and has been developed to be extensible to a wide variety of multi-sensor multi-object sensing applications.

APPENDIX A

APPENDIX

A.1 Proof of Proposition 3

Equation (2.25) can be rewritten as

$$f(X) = \left[\left(1 - r^{(\cdot)}\right)\right]^{\mathbb{N}_M} \sum_{(\mathcal{I}_\sigma)\uplus\mathcal{I}_3} \left[\frac{r^{i_{(\cdot)}} p^{i_{(\cdot)}}(x_{(\cdot)})}{1 - r^{i_{(\cdot)}}}\right]^{\mathbb{N}_n} \tag{A.1}$$

where $(\mathcal{I}_\sigma)$ denotes the (ordered) sequence $(i_1, \ldots, i_n) = (\alpha_{\sigma(1)}, \ldots, \alpha_{\sigma(n)})$, where the n-tuple index set $\{\alpha_1, \ldots, \alpha_n\} \uplus \mathcal{I}_3 = \mathbb{N}_M$ and σ is a permutation of $\mathbb{N}_n$.

Substituting (A.1) into (3.68),

$$\begin{aligned}\rho_{\mathcal{S}}(n) = {} & \left[\left(1 - r^{(\cdot)}\right)\right]^{\mathbb{N}_M} \\ & \cdot \sum_{m=n}^{M} \frac{1}{m!} \int_{\mathbb{X}^m} \sum_{(\mathcal{I}_\sigma)\uplus\mathcal{I}_3} \delta_m(|\mathcal{I}_\sigma|) \left[\frac{r^{i_{(\cdot)}} p^{i_{(\cdot)}}(\mathbf{x}_{(\cdot)})}{1 - r^{i_{(\cdot)}}}\right]^{\mathbb{N}_m} \\ & \sum_{X^n \subseteq X} [1_{\mathcal{S}}(\cdot)]^{X^n} [1 - 1_{\mathcal{S}}(\cdot)]^{X \setminus X^n} \mathrm{d}\mathbf{x}_1 \cdots \mathrm{d}\mathbf{x}_m\end{aligned} \tag{A.2}$$

The last sum can be written in terms of label index sets $\mathcal{I}_1 \uplus \mathcal{I}_2 = \mathcal{I}_\sigma$ as

$$\begin{aligned}\rho_{\mathcal{S}}(n) = {} & \left[\left(1 - r^{(\cdot)}\right)\right]^{\mathbb{N}_M} \\ & \cdot \sum_{m=n}^{M} \frac{1}{m!} \int_{\mathbb{X}^m} \sum_{(\mathcal{I}_\sigma)\uplus\mathcal{I}_3} \delta_m(|\mathcal{I}_\sigma|) \left[\frac{r^{i_{(\cdot)}} p^{i_{(\cdot)}}(\mathbf{x}_{(\cdot)})}{1 - r^{i_{(\cdot)}}}\right]^{\mathbb{N}_m} \\ & \cdot \sum_{\mathcal{I}_1\uplus\mathcal{I}_2=\mathcal{I}_\sigma} \delta_n(|\mathcal{I}_1|) [1_{\mathcal{S}}(\mathbf{x}_{(\cdot)})]^{\{j: i_j \in \mathcal{I}_1\}} [1 - 1_{\mathcal{S}}(\mathbf{x}_{(\cdot)})]^{\{j: i_j \in \mathcal{I}_2\}} \mathrm{d}\mathbf{x}_1 \cdots \mathrm{d}\mathbf{x}_m\end{aligned} \tag{A.3}$$

Distributing terms from the second summation,

$$
\begin{aligned}
\rho_{\mathcal{S}}(n) = {} & \left[\left(1 - r^{(\cdot)}\right)\right]^{\mathbb{N}_M} \\
& \cdot \sum_{m=n}^{M} \frac{1}{m!} \int_{\mathbb{X}^m} \sum_{(\mathcal{I}_\sigma)\uplus\mathcal{I}_3} \delta_m(|\mathcal{I}_\sigma|) \sum_{\mathcal{I}_1\uplus\mathcal{I}_2=\mathcal{I}_\sigma} \delta_n(|\mathcal{I}_1|) \\
& \cdot \left[\frac{1_{\mathcal{S}}(\mathbf{x}_{(\cdot)}) r^{i_{(\cdot)}} p^{i_{(\cdot)}}(\mathbf{x}_{(\cdot)})}{1 - r^{i_{(\cdot)}}}\right]^{\{j:i_j\in\mathcal{I}_1\}} \\
& \cdot \left[\frac{[1 - 1_{\mathcal{S}}(\mathbf{x}_{(\cdot)})] r^{i_{(\cdot)}} p^{i_{(\cdot)}}(\mathbf{x}_{(\cdot)})}{1 - r^{i_{(\cdot)}}}\right]^{\{j:i_j\in\mathcal{I}_2\}} \mathrm{d}\mathbf{x}_1 \cdots \mathrm{d}\mathbf{x}_m
\end{aligned}
\tag{A.4}
$$

Because $\mathcal{I}_1 \cap \mathcal{I}_2 = \emptyset$, then $\{\mathbf{x}_j : i_j \in \mathcal{I}_1\} \cap \{\mathbf{x}_j : i_j \in \mathcal{I}_2\} = \emptyset$ and the integral on $\mathbb{X}^m$ becomes a product of integrals on $\mathbb{X}$, such that

$$
\begin{aligned}
\rho_{\mathcal{S}}(n) = {} & \left[\left(1 - r^{(\cdot)}\right)\right]^{\mathbb{N}_M} \\
& \cdot \sum_{m=n}^{M} \frac{1}{m!} \sum_{(\mathcal{I}_\sigma)\uplus\mathcal{I}_3} \delta_m(|\mathcal{I}_\sigma|) \sum_{\mathcal{I}_1\uplus\mathcal{I}_2=\mathcal{I}_\sigma} \delta_n(|\mathcal{I}_1|) \\
& \cdot \left[\frac{\left\langle 1_{\mathcal{S}}, r^{i_{(\cdot)}} p^{i_{(\cdot)}}\right\rangle}{1 - r^{i_{(\cdot)}}}\right]^{\{j:i_j\in\mathcal{I}_1\}} \left[\frac{\left\langle 1 - 1_{\mathcal{S}}, r^{i_{(\cdot)}} p^{i_{(\cdot)}}\right\rangle}{1 - r^{i_{(\cdot)}}}\right]^{\{j:i_j\in\mathcal{I}_2\}}
\end{aligned}
\tag{A.5}
$$

Now note that the result of the innermost sum does not depend on the permutation order of $(\mathcal{I}_\sigma)$. Thus the property [113, Lemma 12] that for an arbitrary symmetric function h

$$
\sum_{(i_1,\ldots,i_m)} h(\{i_1,\ldots,i_m\}) = m! \sum_{\{i_1,\ldots,i_m\}} h(\{i_1,\ldots,i_m\}) \tag{A.6}
$$

is applied, yielding

$$
\begin{aligned}
\rho_{\mathcal{S}}(n) = {} & \left[\left(1 - r^{(\cdot)}\right)\right]^{\mathbb{N}_M} \cdot \sum_{m=n}^{M} \sum_{\mathcal{I}_1\uplus\mathcal{I}_2\uplus\mathcal{I}_3} \delta_m(|\mathcal{I}_1 \uplus \mathcal{I}_2|)\delta_n(|\mathcal{I}_1|) \\
& \cdot \left[\frac{\left\langle 1_{\mathcal{S}}, r^{(\cdot)} p^{(\cdot)}\right\rangle}{1 - r^{(\cdot)}}\right]^{\mathcal{I}_1} \left[\frac{\left\langle 1 - 1_{\mathcal{S}}, r^{(\cdot)} p^{(\cdot)}\right\rangle}{1 - r^{(\cdot)}}\right]^{\mathcal{I}_2}
\end{aligned}
$$

The term $\delta_m(|\mathcal{I}_1 \uplus \mathcal{I}_2|)$ is non-zero only when the combined cardinality of $\mathcal{I}_1$ and $\mathcal{I}_2$ is equal to m—the index of the outermost sum. Thus, the outermost sum is absorbed by the second sum to give (3.77). ■

A.2 Cell-MB Parameter Optimization

The minimization of the KLD between f and $\bar{f}$ can be equivalently expressed as the maximization problem

$$\max_{\{r^j,p^j\}_{j=1}^P} \left[\int f(Y) \log(\bar{f}(Y)) \delta Y \right] \tag{A.7}$$

Equation (4.9) can be equivalently written as

$$\bar{f}(Y) = \Delta(Y, \mathbb{Y}) \prod_{j=1}^{P} \left(1 - r^j\right) \left(\prod_{i=1}^{n} \sum_{j=1}^{P} \frac{r^j p^j(\mathbf{y}_i)}{1 - r^j} \right) \tag{A.8}$$

where it is noted that for each i in the rightmost product, the sum has only one nonzero term at $j = j'$ where $\overset{j'}{\mathbb{Y}} \ni \mathbf{y}_i$. Thus, (A.8) can be factored as

$$\bar{f}(Y) = \Delta(Y, \mathbb{Y}) \prod_{j=1}^{P} \left(1 - r^j\right) \left(\prod_{i=1}^{n} \sum_{j=1}^{P} \frac{1_{\overset{j}{\mathbb{Y}}}(\mathbf{y}_i)}{1 - r^j} \right) \left(\prod_{i=1}^{n} \sum_{j=1}^{P} r^j p^{j_n}(\mathbf{y}_i) \right) \tag{A.9}$$

According to (2.26), the rightmost sum of (A.9) is equal to the PHD of $\bar{f}(Y)$, such that

$$\bar{f}(Y) = \Delta(Y, \mathbb{Y}) \prod_{j=1}^{P} \left(1 - r^j\right) \left(\prod_{i=1}^{n} \sum_{j=1}^{P} \frac{1_{\overset{j}{\mathbb{Y}}}(\mathbf{y}_i)}{1 - r^j} \right) \left(\prod_{i=1}^{n} \bar{D}(\mathbf{y}_i) \right) \tag{A.10}$$

Now, taking the logarithm of (A.10),

$$\begin{aligned} \log(\bar{f}(Y)) &= \log(\Delta(Y, \mathbb{Y})) + \log \prod_{j=1}^{P} \left(1 - r^j\right) && \text{(A.11)} \\ &\quad + \log \left(\prod_{i=1}^{n} \sum_{j=1}^{P} \frac{1_{\overset{j}{\mathbb{Y}}}(\mathbf{y}_i)}{1 - r^j} \right) + \log \left(\prod_{i=1}^{n} \bar{D}(\mathbf{y}_i) \right) \\ &= \log(\Delta(Y, \mathbb{Y})) + \sum_{j=1}^{P} \log \left(1 - r^j\right) && \text{(A.12)} \\ &\quad + \sum_{i=1}^{n} \log \left(\sum_{j=1}^{P} \frac{1_{\overset{j}{\mathbb{Y}}}(\mathbf{y}_i)}{1 - r^j} \right) + \sum_{i=1}^{n} \log \left(\bar{D}(\mathbf{y}_i) \right) \end{aligned}$$

The third term in (A.13) can be modified by recognizing that the inner sum has only one nonzero term, and thus

$$\sum_{i=1}^{n} \log\left(\sum_{j=1}^{P} \frac{1_{\mathbb{Y}^j}(\mathbf{y}_i)}{1-r^j}\right) = \sum_{i=1}^{n} \log\left(\frac{1}{1-\sum_{j=1}^{P} 1_{\mathbb{Y}^j}(\mathbf{y}_i) r^j}\right) \tag{A.13}$$

$$= -\sum_{i=1}^{n} \log\left(1-\sum_{j=1}^{P} 1_{\mathbb{Y}^j}(\mathbf{y}_i) r^j\right) \tag{A.14}$$

which, by substitution of into (A.13), yields

$$\begin{aligned}\log(\bar{f}(Y)) = \log(\Delta(Y,\mathbb{Y})) + \sum_{j=1}^{P} \log\left(1-r^j\right) \\ - \sum_{i=1}^{n} \log\left(1-\sum_{j=1}^{P} 1_{\mathbb{Y}^j}(\mathbf{y}_i) r^j\right) + \sum_{i=1}^{n} \log\left(\bar{D}(\mathbf{y}_i)\right)\end{aligned} \tag{A.15}$$

Now taking the set integral of the product

$$\begin{aligned}&\int f(Y)\log(\bar{f}(Y))\delta Y \\ &= \int f(Y)\log(\Delta(Y,\mathbb{Y}))\delta Y + \int \sum_{j=1}^{P} f(Y)\log\left(1-r^j\right)\delta Y \\ &\quad - \int \sum_{i=1}^{n} f(Y)\log\left(1-\sum_{j=1}^{P} 1_{\mathbb{Y}^j}(\mathbf{y}_i) r^j\right)\delta Y \\ &\quad + \int \sum_{i=1}^{n} f(Y)\log\left(\bar{D}(\mathbf{y}_i)\right)\delta Y\end{aligned} \tag{A.16}$$

$$\begin{aligned}&= \int \sum_{j=1}^{P} f(Y)\log\left(1-r^j\right)\delta Y \\ &\quad - \int \sum_{i=1}^{n} f(Y)\log\left(1-\sum_{j=1}^{P} 1_{\mathbb{Y}^j}(\mathbf{y}_i) r^j\right)\delta Y \\ &\quad + \int \sum_{i=1}^{n} f(Y)\log\left(\bar{D}(\mathbf{y}_i)\right)\delta Y\end{aligned} \tag{A.17}$$

where in the last equation, the first term vanished due to the observation that $f(Y) = 0$ everywhere that $\Delta(Y,\mathbb{Y}) = 0$ and by application of the identity

$\lim_{x\to 0} x \log x = 0$. By applying Proposition 2a of [72], which states that

$$\int f(Y) \sum_{i=1}^{n} h(\mathbf{y}_i)\delta Y = \int D(\mathbf{y})h(\mathbf{y})\mathrm{d}\mathbf{y} \tag{A.18}$$

equation (A.17) can be rewritten in terms of the PHD as

$$\begin{aligned}
&\int f(Y)\log(\bar{f}(Y))\delta Y \\
&\quad = \sum_{j=1}^{P} \log\left(1 - r^j\right) - \int D(\mathbf{y}) \log\left(1 - \sum_{j=1}^{P} 1_{\mathbb{Y}}^{j}(\mathbf{y}) r^j\right) \mathrm{d}\mathbf{y} \\
&\qquad + \int D(\mathbf{y}) \log\left(\bar{D}(\mathbf{y})\right) \mathrm{d}\mathbf{y} \qquad (A.19)
\end{aligned}$$

$$\begin{aligned}
&\quad = \sum_{j=1}^{P} \log\left(1 - r^j\right) - \sum_{j=1}^{P} \int 1_{\mathbb{Y}}^{j}(\mathbf{y}) D(\mathbf{y}) \log\left(1 - r^j\right) \mathrm{d}\mathbf{y} \\
&\qquad + \int D(\mathbf{y}) \log\left(\bar{D}(\mathbf{y})\right) \mathrm{d}\mathbf{y} \qquad (A.20)
\end{aligned}$$

$$\begin{aligned}
&\quad = \sum_{j=1}^{P} \log\left(1 - r^j\right) \left(1 - \int 1_{\mathbb{Y}}^{j}(\mathbf{y}) D(\mathbf{y})\right) \\
&\qquad + \int D(\mathbf{y}) \log\left(\bar{D}(\mathbf{y})\right) \mathrm{d}\mathbf{y} \qquad (A.21)
\end{aligned}$$

Equation (A.21) consists of the sum of two terms and is maximized when both terms are simultaneously maximized. The first term is maximized by

$$r^j = \int 1_{\mathbb{Y}}^{j}(\mathbf{y}) D(\mathbf{y}) \mathrm{d}\mathbf{y}$$

and the second term is maximized when $\bar{D}(\mathbf{y}) = D(\mathbf{y})$. By (2.26),

$$\bar{D}(\mathbf{y}) = \sum_{j=1}^{P} r^j p^j(\mathbf{y}) = \sum_{j=1}^{P} 1_{\mathbb{Y}}^{j}(\mathbf{y}) D(\mathbf{y}) \tag{A.22}$$

By equating like-terms,

$$p^j(\mathbf{y}) = \frac{1}{r^j} 1_{\mathbb{Y}}^{j}(\mathbf{y}) D(\mathbf{y}) \tag{A.23}$$

completing the proof. ■

A.3 Cell-MB Expectation

Let $\mathbf{z}_{1:n} \triangleq \mathbf{z}_1, \ldots, \mathbf{z}_n$ and $\mathrm{d}\mathbf{z}_{1:n} \triangleq \mathrm{d}\mathbf{z}_1 \cdots \mathrm{d}\mathbf{z}_n$. Substitution of the cell-MB density (4.9) and cell-additive information gain (4.17) into (4.7) gives

$$\mathrm{E}[\mathcal{R}] = \left[\frac{r^{(\cdot)}}{1 - r^{(\cdot)}}\right]^{\mathbb{N}_P} \left(\mathcal{R}(\emptyset; \mathcal{S}) + \sum_{n=1}^{P} \frac{1}{n!}\psi(n; \mathcal{S})\right) \tag{A.24}$$

where

$$\psi(n; \mathcal{S}) \triangleq \int \Delta(\{\mathbf{z}_{1:n}\}, \mathbb{Z}) \cdot \left[\sum_{j=1}^{P} \mathcal{R}(\{\mathbf{z}_{1:n}\} \cap \overset{j}{\mathbb{Z}}; \overset{j}{\mathcal{S}})\right] \left[\sum_{j=1}^{P} \frac{r^j p^j(\mathbf{z}_{(\cdot)})}{1 - r^j}\right]^{\mathbb{N}_n} \mathrm{d}\mathbf{z}_{1:n} \tag{A.25}$$

We wish to simplify the set integral into combinations of vector integrals $\int \cdot \mathrm{d}\mathbf{z}$ such that the expected information gain is computationally feasible. Integrals on $\mathbb{Z}$ are equivalent to

$$\int h(\mathbf{z})\mathrm{d}\mathbf{z} = \int_{\overset{1}{\mathbb{Z}}} h\big(\overset{1}{\mathbf{z}}\big)\mathrm{d}\overset{1}{\mathbf{z}} + \cdots + \int_{\overset{P}{\mathbb{Z}}} h\big(\overset{P}{\mathbf{z}}\big)\mathrm{d}\overset{P}{\mathbf{z}} \tag{A.26}$$

where $\overset{j}{\mathbf{z}} \in \overset{j}{\mathbb{Z}}$, as shown in [75, Eqn. 3.50]. First, note that the rightmost sum

$$\sum_{j=1}^{P} \frac{r^j p^j(\mathbf{z}_i)}{1 - r^j} \tag{A.27}$$

has only one nonzero term: namely, when $j = j'$ where $\mathbf{z}_i \in \overset{j'}{\mathbb{Z}}$. Then, the integral can be written as a sum of integrals, each wherein $\mathbf{z}_1$ is integrated over a different subset $\overset{i_1}{\mathbb{Z}} \subseteq \mathbb{Z}, \quad i_1 \in \mathbb{N}_P$ as follows:

$$\begin{aligned}\psi(n; \mathcal{S}) = \sum_{i_1=1}^{P} \int & \Delta(\{\mathbf{z}_{2:n}\}, \overline{\mathbb{Z}}(i_1)) \\ & \cdot \left[\mathcal{R}(\{\overset{i_1}{\mathbf{z}}\}; \overset{i_1}{\mathcal{S}}) + \sum_{j=1, j\neq i_1}^{P} \mathcal{R}(\{\mathbf{z}_{2:n}\} \cap \overset{j}{\mathbb{Z}}; \overset{j}{\mathcal{S}})\right] \\ & \cdot \left(\frac{r^{i_1} p^{i_1}(\overset{i_1}{\mathbf{z}})}{1 - r^{i_1}}\right) \left[\sum_{j=1, j\neq i_1}^{P} \frac{r^j p^j(\mathbf{z}_{(\cdot)})}{1 - r^j}\right]^{\mathbb{N}_n \setminus \mathbb{N}_1} \mathrm{d}\overset{i_1}{\mathbf{z}}\, \mathrm{d}\mathbf{z}_{2:n}\end{aligned} \tag{A.28}$$

where

$$\overline{\mathbb{Z}}(i_1, ..., i_n) \triangleq \mathbb{Z} \setminus (\overset{i_1}{\mathbb{Z}} \uplus \cdots \uplus \overset{i_n}{\mathbb{Z}}) \tag{A.29}$$

Repeating the same procedure for $\mathbf{z}_2, ..., \mathbf{z}_n$

$$\begin{aligned}\psi(n; \mathcal{S}) = \sum_{i_1=1}^{P} \sum_{i_2=1, i_2 \neq i_1}^{P} \int \Delta(\{\mathbf{z}_{3:n}\}, \overline{\mathbb{Z}}(i_1, i_2)) \\ \cdot \left[\mathcal{R}(\{\overset{i_1}{\mathbf{z}}\}; \overset{i_1}{\mathcal{S}}) + \mathcal{R}(\{\overset{i_2}{\mathbf{z}}\}; \overset{i_2}{\mathcal{S}}) + \sum_{j=1, j \notin \{i_1, i_2\}}^{P} \mathcal{R}(\{\mathbf{z}_{3:n}\} \cap \overset{j}{\mathbb{Z}}; \overset{j}{\mathcal{S}})\right] \\ \cdot \left(\frac{r^{i_{(\cdot)}} p^{i_{(\cdot)}}(\overset{i_{(\cdot)}}{\mathbf{z}})}{1 - r^{i_{(\cdot)}}}\right)^{\mathbb{N}_2} \left[\sum_{j=1, j \notin \{i_1, i_2\}}^{P} \frac{r^j p^j(\mathbf{z}_{(\cdot)})}{1 - r^j}\right]^{\mathbb{N}_n \setminus \mathbb{N}_2} \mathrm{d}\overset{i_1}{\mathbf{z}}\, \mathrm{d}\overset{i_2}{\mathbf{z}}\, \mathrm{d}\mathbf{z}_{3:n}\end{aligned} \tag{A.30}$$

$$\begin{aligned}= \sum_{1 \leq i_1 \neq \cdots \neq i_n \leq P} \int \Big[\mathcal{R}(\{\overset{i_1}{\mathbf{z}}\}; \overset{i_1}{\mathcal{S}}) + \cdots + \mathcal{R}(\{\overset{i_n}{\mathbf{z}}\}; \overset{i_n}{\mathcal{S}}) + \\ \mathcal{R}(\emptyset; \overline{\mathcal{S}}(i_1, \ldots i_n))\Big] \left[\frac{r^{i_{(\cdot)}} p^{i_{(\cdot)}}(\overset{i_{(\cdot)}}{\mathbf{z}})}{1 - r^{i_{(\cdot)}}}\right]^{\mathbb{N}_n} \mathrm{d}\overset{i_1}{\mathbf{z}} \cdots \mathrm{d}\overset{i_n}{\mathbf{z}}\end{aligned} \tag{A.31}$$

where

$$\overline{\mathcal{S}}(i_1, \ldots i_n) \triangleq \mathcal{S} \setminus (\overset{i_1}{\mathcal{S}} \uplus \cdots \uplus \overset{i_n}{\mathcal{S}}) \tag{A.32}$$

Moving the existence probability terms outside the integral and exploiting symmetry over order permutations of $(i_1, \ldots, i_n)$ gives

$$\begin{aligned}\psi(n; \mathcal{S}) = n! \sum_{1 \leq i_1 < \cdots < \neq i_n \leq P} \left[\frac{r^{i_{(\cdot)}}}{1 - r^{i_{(\cdot)}}}\right]^{\mathbb{N}_n} \\ \int \left[\mathcal{R}(\{\overset{i_1}{\mathbf{z}}\}; \overset{i_1}{\mathcal{S}}) + \cdots + \mathcal{R}(\{\overset{i_n}{\mathbf{z}}\}; \overset{i_n}{\mathcal{S}}) + \mathcal{R}(\emptyset; \overline{\mathcal{S}}(i_1, \ldots i_n))\right] \\ \cdot \left[p^{i_{(\cdot)}}(\overset{i_{(\cdot)}}{\mathbf{z}})\right]^{\mathbb{N}_n} \mathrm{d}\overset{i_1}{\mathbf{z}} \cdots \mathrm{d}\overset{i_n}{\mathbf{z}}\end{aligned} \tag{A.33}$$

$$\begin{aligned}= n! \sum_{1 \leq i_1 < \cdots < \neq i_n \leq P} \left[\frac{r^{i_{(\cdot)}}}{1 - r^{i_{(\cdot)}}}\right]^{\mathbb{N}_n} \\ \cdot \left[\mathcal{R}(\emptyset; \overline{\mathcal{S}}(i_1, \ldots i_n)) + \sum_{\ell=1}^{n} \int \mathcal{R}(\{\overset{i_\ell}{\mathbf{z}}\}; \overset{i_\ell}{\mathcal{S}}) p^{i_\ell}(\overset{i_\ell}{\mathbf{z}}) \mathrm{d}\overset{i_\ell}{\mathbf{z}}\right]\end{aligned} \tag{A.34}$$

where the last line is obtained by using the pdf property $\int p^{i_\ell}(\overset{i_\ell}{\mathbf{z}})\mathrm{d}\overset{i_\ell}{\mathbf{z}} = 1$. Substitution of (A.34) into (A.24) gives

$$\begin{aligned}\mathrm{E}[\mathcal{R}] = \left[1 - r^{(\cdot)}\right]^{\mathbb{N}_P} \mathcal{R}(\emptyset; \mathcal{S}) + \Bigg[\sum_{n=1}^{P} \sum_{1 \leq i_1 < \cdots < i_n \leq P} \left[r^{i_{(\cdot)}}\right]^{\mathbb{N}_n} \\ \cdot \left[1 - r^{(\cdot)}\right]^{\mathbb{N}_P \setminus \{i_1, \ldots, i_n\}} \\ \cdot \left(\mathcal{R}(\emptyset; \overline{\mathcal{S}}(i_1, \ldots i_n)) + \sum_{\ell=1}^{n} \hat{\mathcal{R}}_{\mathrm{z}}^{i_\ell} \right) \Bigg]\end{aligned} \tag{A.35}$$

The above equation can be expressed in a more convenient form using disjoint index sets as

$$\mathrm{E}[\mathcal{R}] = \sum_{\mathcal{I}_0 \uplus \mathcal{I}_1 = \mathbb{N}_P} \left[r^{(\cdot)}\right]^{\mathcal{I}_1} \left[1 - r^{(\cdot)}\right]^{\mathcal{I}_0} \left[\sum_{i \in \mathcal{I}_0} \mathcal{R}(\emptyset; \overset{i}{\mathcal{S}}) + \sum_{\ell \in \mathcal{I}_1} \hat{\mathcal{R}}_{\mathbf{z}}^{\ell} \right] \tag{A.36}$$

Through the introduction of indicator functions, the summation hierarchy can be changed as follows:

$$\begin{aligned}\mathrm{E}[\mathcal{R}] = \sum_{j=1}^{P} \mathcal{R}(\emptyset; \overset{j}{\mathcal{S}}) \sum_{\mathcal{I}_0 \uplus \mathcal{I}_1 = \mathbb{N}_P} \left[r^{(\cdot)}\right]^{\mathcal{I}_1} \left[1 - r^{(\cdot)}\right]^{\mathcal{I}_0} \cdot 1_{\mathcal{I}_0}(j) \\ + \sum_{j=1}^{P} \hat{\mathcal{R}}_{\mathrm{z}}^{j} \sum_{\mathcal{I}_0 \uplus \mathcal{I}_1 = \mathbb{N}_P} \left[r^{(\cdot)}\right]^{\mathcal{I}_1} \left[1 - r^{(\cdot)}\right]^{\mathcal{I}_0} \cdot 1_{\mathcal{I}_1}(j)\end{aligned} \tag{A.37}$$

Consider the first line of (A.37). The inner summand is only nonzero when $j \in \mathcal{I}_0$, so all nonzero terms share the common factor $(1 - r^j)$. Similarly, in the second line, all nonzero terms in the inner summation share a common factor of r^j. Thus these terms are factored out, reducing the inner summation to one over disjoint subsets of $\mathbb{N}_P \setminus j$ as

$$\begin{aligned}\mathrm{E}[\mathcal{R}] = \sum_{j=1}^{P} \mathcal{R}(\emptyset; \overset{j}{\mathcal{S}}) \left(1 - r^j\right) \sum_{\mathcal{I}_0 \uplus \mathcal{I}_1 = \mathbb{N}_P \setminus j} \left[r^{(\cdot)}\right]^{\mathcal{I}_1} \left[1 - r^{(\cdot)}\right]^{\mathcal{I}_0} \\ + \sum_{j=1}^{P} \hat{\mathcal{R}}_{\mathrm{z}}^{j} \cdot r^j \sum_{\mathcal{I}_0 \uplus \mathcal{I}_1 = \mathbb{N}_P \setminus j} \left[r^{(\cdot)}\right]^{\mathcal{I}_1} \left[1 - r^{(\cdot)}\right]^{\mathcal{I}_0}\end{aligned} \tag{A.38}$$

A manipulation of the inner sum yields

$$\sum_{\mathcal{I}_0 \uplus \mathcal{I}_1 = \mathbb{N}_P \setminus j} \left[r^{(\cdot)}\right]^{\mathcal{I}_1} \left[1 - r^{(\cdot)}\right]^{\mathcal{I}_0} = \left[1 - r^{(\cdot)}\right]^{\mathbb{N}_P \setminus j} \sum_{\mathcal{I}_0 \uplus \mathcal{I}_1 = \mathbb{N}_P \setminus j} \left[\frac{r^{(\cdot)}}{1 - r^{(\cdot)}} \right]^{\mathcal{I}_1} \tag{A.39}$$

By the binomial theorem [74, p. 369],

$$\sum_{\mathcal{I}_0 \uplus \mathcal{I}_1 = \mathbb{N}_P \setminus j} \left[\frac{r^{(\cdot)}}{1-r^{(\cdot)}}\right]^{\mathcal{I}_1} = \left[1 + \frac{r^{(\cdot)}}{1-r^{(\cdot)}}\right]^{\mathbb{N}_P \setminus j} \tag{A.40}$$

Thus,

$$\sum_{\mathcal{I}_0 \uplus \mathcal{I}_1 = \mathbb{N}_P \setminus j} \left[r^{(\cdot)}\right]^{\mathcal{I}_1} \left[1-r^{(\cdot)}\right]^{\mathcal{I}_0} = \left[\left(1-r^{(\cdot)}\right)\left(1 + \frac{r^{(\cdot)}}{1-r^{(\cdot)}}\right)\right]^{\mathbb{N}_P \setminus j} \tag{A.41}$$

$$= \left[1 - r^{(\cdot)} + r^{(\cdot)}\right]^{\mathbb{N}_P \setminus j} = 1 \tag{A.42}$$

With this, (A.38) simplifies to

$$\mathrm{E}[\mathcal{R}] = \sum_{j=1}^{P} \mathcal{R}(\emptyset; \overset{j}{\mathcal{S}}) \left(1 - r^j\right) + \sum_{j=1}^{P} \hat{\mathcal{R}}_{\mathrm{z}}^{j} \cdot r^j \tag{A.43}$$

from which (4.19) follows, completing the proof. ■

A.4 Cell-Additivity of PHD-Based KLD Information Gain

By (4.24), the pseudo-likelihood can be written in terms of a sum of cell pseudo-likelihood functions

$$L_Z(\mathbf{x}; \mathcal{S}) = \begin{cases} \sum_{j=1}^{P} 1_{\overset{j}{\mathcal{S}}}(\mathbf{s}) L_Z^{(j)}(\mathbf{x}; \overset{j}{\mathcal{S}}) & \mathbf{s} \in \mathcal{S} \\ 1 & \mathbf{s} \notin \mathcal{S} \end{cases} \tag{A.44}$$

where

$$L_Z^{(j)}(\mathbf{x}; \overset{j}{\mathcal{S}}) = \begin{cases} 1 - p_{D,k}(\mathbf{x}; \overset{j}{\mathcal{S}}) + p_{D,k}(\mathbf{x}; \overset{j}{\mathcal{S}}) \Phi_k^{(j)}(Z|\mathbf{x}) & \mathbf{s} \in \overset{j}{\mathcal{S}} \\ 1 & \mathbf{s} \notin \overset{j}{\mathcal{S}} \end{cases} \tag{A.45}$$

$$\Phi_k^{(j)}(Z|\mathbf{x}) = \sum_{\mathbf{z} \in Z \cap \overset{j}{\mathbb{Z}}} \frac{g_k(\mathbf{z}|\mathbf{x})}{\kappa_k(\mathbf{z}) + \int_{\overset{j}{\mathbb{X}}} D_{k|k-1}(\mathbf{x}') p_{D,k}(\mathbf{x}'; \overset{j}{\mathcal{S}}) g_k(\mathbf{z}|\mathbf{x}') \mathrm{d}\mathbf{x}'} \tag{A.46}$$

Substituting (A.44) into (4.21) and noting that $L_Z^{(i)}(\mathbf{x}; \overset{j}{\mathcal{S}}) = L^{(i)}_{Z\cap\overset{i}{\mathbb{Z}}}(\mathbf{x}; \overset{j}{\mathcal{S}})$,

$$\mathcal{R}_k(Z; \mathcal{S}) = \sum_{j=1}^{P} \int D_{k|k-1}(\mathbf{x}) \left\{ 1 - L^{(j)}_{Z\cap\overset{j}{\mathbb{Z}}}(\mathbf{x}; \overset{j}{\mathcal{S}}) + L^{(j)}_{Z\cap\overset{j}{\mathbb{Z}}}(\mathbf{x}; \overset{j}{\mathcal{S}}) \log[L^{(j)}_{Z\cap\overset{j}{\mathbb{Z}}}(\mathbf{x}; \overset{j}{\mathcal{S}})] \right\} \mathrm{d}\mathbf{x} \tag{A.47}$$

A comparison of (A.47) to the form of (4.21) reveals that the information gain is, in fact, a sum of information gains over the cells:

$$\mathcal{R}_k(Z; \mathcal{S}) = \sum_{i=1}^{P} \mathcal{R}_k(Z \cap \overset{i}{\mathbb{Z}}; \overset{i}{\mathcal{S}}) \tag{A.48}$$

A.5 Quadrature of Single-Measurement Conditioned Information Gain Expectation

The quadrature approximation in (4.36) is most accurate when all measurement points within a given region yield a similar information gain. However, performing excessive information gain computations to determine the quadrature regions on the basis of information gain similarity would be counterproductive. Instead, the regions $\{\overset{j}{\Omega}_i\}$ and their representative quadrature points $\mathbf{z}_{j,i}$ are selected using discrete samples of the predicted measurement PHD.

Let $\{\bar{\mathbf{z}}_j[\ell]\}_{\ell=1}^{Q}$ be an array of $Q \gg R_j$ uniformly spaced measurement samples on $\overset{j}{\mathbb{Z}}$ and

$$\bar{D}_j[\ell] \triangleq D_{\mathrm{v},k|k-1}(\bar{\mathbf{z}}_j[\ell]; \mathcal{S}) \tag{A.49}$$

As illustrated in Fig. 4.2, the quadrature regions can be represented by sets of measurement points with similar log-PHD values; i.e.,

$$\overset{j}{\Omega}_i = \begin{cases} \{\bar{\mathbf{z}}_j[\ell] \,:\, 1 \leq \ell \leq Q,\, \bar{D}_j[\ell] \leq e^{\varepsilon_{j,i}}\} & i = 1 \\ \{\bar{\mathbf{z}}_j[\ell] \,:\, 1 \leq \ell \leq Q,\, e^{\varepsilon_{j,i-1}} < \bar{D}_j[\ell] \leq e^{\varepsilon_{j,i}}\} & i > 1 \end{cases} \tag{A.50}$$

where the discrete logarithmic bin edges are obtained as

$$\varepsilon_{j,i} = \varepsilon_0 + \frac{i}{R_j}(\varepsilon_{R_j} - \varepsilon_0), \quad 0 < i < R_j \tag{A.51}$$

$$\varepsilon_{j,0} = \max\left[\varepsilon_{\min}, \min_{1<\ell<Q}\left(\log\{\bar{D}_j[\ell]\}\right)\right] \tag{A.52}$$

$$\varepsilon_{j,R_j} = \max_{1\leq\ell\leq Q}\left(\log\{\bar{D}_j[\ell]\}\right) \tag{A.53}$$

In (A.52), the tunable parameter $\varepsilon_{\min}$ represents the lowest log-PHD that should be considered, so as to reduce unnecessary information gain computations in areas of extremely low probability. Then, a representative measurement is chosen from each region as

$$\mathbf{z}_{j,i} = \underset{\bar{\mathbf{z}}[\ell]\in\overset{j}{\Omega}_i}{\arg\min}\left[|\bar{D}_j[\ell] - \hat{D}_{j,i}|\right] \tag{A.54}$$

where, in (A.54), $|\cdot|$ represents the absolute value operator, and $\hat{D}_{j,i}$ is the average PHD value in region i of measurement cell j:

$$\hat{D}_{j,i} = \frac{1}{|\overset{j}{\Omega}_i|} \sum_{1\leq\ell\leq Q,\, \bar{\mathbf{z}}_j[\ell]\in\overset{j}{\Omega}_i} \bar{D}_j[\ell] \tag{A.55}$$

The volumes can be approximated by the proportion of discrete measurement samples that fall within each region as

$$A_{j,i} = \frac{|\overset{j}{\Omega}_i|}{Q} \cdot A(\overset{j}{\mathbb{Z}}) \tag{A.56}$$

A.6 Proof of Theorem 2

By the law of iterated expectations [7, p. 82],

$$\mathrm{E}_{Z^{(1)},Z^{(2)}}[\mathcal{R}(Z^{(1)},Z^{(2)};\mathcal{S})] = \mathrm{E}_{Z^{(2)}}\left[\mathrm{E}_{Z^{(1)}}\left[\mathcal{R}(Z^{(1)},Z^{(2)};\mathcal{S})|Z^{(2)}\right]\right] \tag{A.57}$$

$$= \int_{Z^{(2)}} \mathrm{E}_{Z^{(1)}}\left[\mathcal{R}(Z^{(1)},Z^{(2)};\mathcal{S})|Z^{(2)}\right] f(Z^{(2)};\mathcal{S})\delta Z^{(2)} \tag{A.58}$$

where $f(Z^{(2)};\mathcal{S})$ is the predicted density of $Z^{(2)}$ and

$$\mathrm{E}_{Z^{(1)}}\left[\mathcal{R}(Z^{(1)},Z^{(2)};\mathcal{S})|Z^{(2)}\right] = \int_{Z^{(1)}} \mathcal{R}(Z^{(1)},Z^{(2)};\mathcal{S}) f(Z^{(1)}|Z^{(2)};\mathcal{S})\delta Z^{(1)} \tag{A.59}$$

where $f(Z^{(1)}|Z^{(2)};\mathcal{S})$ is the predicted density of the first sensor's measurement conditioned on $Z^{(2)}$. By Theorem 1,

$$\mathrm{E}_{Z^{(1)},Z^{(2)}}[\mathcal{R}(Z^{(1)},Z^{(2)};\mathcal{S})] = \int_{Z^{(2)}} \mathrm{E}_{Z^{(1)}}\left[\mathcal{R}(Z^{(1)},Z^{(2)};\mathcal{S})\mid Z^{(2)}\right] f(Z^{(2)};\mathcal{S})\delta Z^{(2)} \tag{A.60}$$

$$\begin{aligned} = \sum_{i=1}^{P} & \mathrm{E}_{Z^{(1)}}\left[\mathcal{R}(Z^{(1)},\emptyset;\mu(\mathcal{S},i))|\emptyset\right](1-r^i) \\ & + r^i \int_{\overset{i}{\mathbb{Z}}} \mathrm{E}_{Z^{(1)}}\left[\mathcal{R}(Z^{(1)},\{\mathbf{z}\};\mu(\mathcal{S},i))|\{\mathbf{z}\}\right] p^i(\mathbf{z})\mathrm{d}\mathbf{z} \end{aligned} \tag{A.61}$$

where the shorthand $\overset{i}{\mathcal{S}}$ has been replaced with its explicit function definition (4.15) for careful bookkeeping. The conditional density $f(Z^{(1)}|Z^{(2)};\mathcal{S})$ is cell-MB and thus

$$\begin{aligned} \mathrm{E}_{Z^{(1)}}\left[\mathcal{R}(Z^{(1)},Z^{(2)};\mathcal{S})|Z^{(2)}\right] = \sum_{j=1}^{P} & \mathcal{R}(\emptyset,Z^{(2)};\overset{j}{\mathcal{S}})(1-\check{r}^j(Z^{(2)}\cap\overset{j}{\mathbb{Z}})) \\ & + \check{r}^j(Z^{(2)}\cap\overset{j}{\mathbb{Z}}) \int_{\overset{j}{\mathbb{Z}}} \mathcal{R}(\{\mathbf{z}'\},Z^{(2)};\overset{j}{\mathcal{S}})\check{p}^j(\mathbf{z}'|Z^{(2)}\cap\overset{j}{\mathbb{Z}})\mathrm{d}\mathbf{z}' \end{aligned} \tag{A.62}$$

The information gain expectation over $Z^{(1)}$, conditioned on $Z^{(2)} = \emptyset$ is, by Theorem 1,

$$
\begin{aligned}
&\mathrm{E}_{Z^{(1)}}\left[\mathcal{R}(Z^{(1)},\emptyset;\mu(\mathcal{S},i))|\emptyset\right] \\
&\quad = \sum_{j=1}^{P} \mathcal{R}(\emptyset,\emptyset;\mu(\mu(\mathcal{S},i),j))(1-\check{r}^j(\emptyset\cap\overset{j}{\mathbb{Z}})) \\
&\quad\quad + \check{r}^j(\emptyset\cap\overset{j}{\mathbb{Z}})\int_{\overset{j}{\mathbb{Z}}}\mathcal{R}(\{\mathbf{z}'\},\emptyset;\mu(\mu(\mathcal{S},i),j))\check{p}^j(\mathbf{z}'|\emptyset\cap\overset{j}{\mathbb{Z}})\mathrm{d}\mathbf{z}'
\end{aligned}
\tag{A.63}
$$

$$
= \sum_{j=1}^{P} \mathcal{R}(\emptyset,\emptyset;\overset{i,j}{\mathcal{S}})(1-\check{r}^j(\emptyset)) + \check{r}^j(\emptyset)\int_{\overset{j}{\mathbb{Z}}}\mathcal{R}(\{\mathbf{z}'\},\emptyset;\overset{i,j}{\mathcal{S}})\check{p}^j(\mathbf{z}'|\emptyset)\mathrm{d}\mathbf{z}' \tag{A.64}
$$

$$
= \mathcal{R}(\emptyset,\emptyset;\overset{i}{\mathcal{S}})(1-\check{r}^i(\emptyset)) + \check{r}^i(\emptyset)\int_{\overset{i}{\mathbb{Z}}}\mathcal{R}(\{\mathbf{z}'\},\emptyset;\overset{i}{\mathcal{S}})\check{p}^i(\mathbf{z}'|\emptyset)\mathrm{d}\mathbf{z}' \tag{A.65}
$$

where the abbreviation $\overset{i,j}{\mathcal{S}}$ denotes the nested FoV intersections

$$
\overset{i,j}{\mathcal{S}}_k \triangleq \mu(\mu(\mathcal{S},j),i) = \mathcal{S}\cap\overset{j}{\mathbb{X}}_s\cap\overset{i}{\mathbb{X}}_s = \begin{cases} \overset{j}{\mathcal{S}}_k & i=j \\ \emptyset & i\neq j \end{cases} \tag{A.66}
$$

Similarly, the information gain expectation taken over $Z^{(1)}$ conditioned on $Z^{(2)} = \{\mathbf{z}\}$ is

$$
\begin{aligned}
&\mathrm{E}_{Z^{(1)}}\left[\mathcal{R}(Z^{(1)}, \{\mathbf{z}\}; \mu(\mathcal{S}, i)) | \{\mathbf{z}\}\right] \\
&\quad = \sum_{j=1}^{P} \mathcal{R}(\emptyset, \{\mathbf{z}\}; \mu(\mu(\mathcal{S}, i), j))(1 - \check{r}^j(\{\mathbf{z}\} \cap \overset{j}{\mathbb{Z}})) \\
&\qquad + \check{r}^j(\{\mathbf{z}\} \cap \overset{j}{\mathbb{Z}}) \int_{\overset{j}{\mathbb{Z}}} \mathcal{R}(\{\mathbf{z}'\}, \{\mathbf{z}\}; \mu(\mu(\mathcal{S}, i), j))) \check{p}^j(\mathbf{z}' | \{\mathbf{z}\} \cap \overset{j}{\mathbb{Z}}) \mathrm{d}\mathbf{z}' \qquad \text{(A.67)} \\
&\quad = \sum_{j=1}^{P} \mathcal{R}(\emptyset, \{\mathbf{z}\}; \overset{i,j}{\mathcal{S}})(1 - \check{r}^j(\{\mathbf{z}\} \cap \overset{j}{\mathbb{Z}})) \\
&\qquad + \check{r}^j(\{\mathbf{z}\} \cap \overset{j}{\mathbb{Z}}) \int_{\overset{j}{\mathbb{Z}}} \mathcal{R}(\{\mathbf{z}'\}, \{\mathbf{z}\}; \overset{i,j}{\mathcal{S}}) \check{p}^j(\mathbf{z}' | \{\mathbf{z}\} \cap \overset{j}{\mathbb{Z}}) \mathrm{d}\mathbf{z}' \qquad \text{(A.68)} \\
&\quad = \mathcal{R}(\emptyset, \{\mathbf{z}\}; \overset{i}{\mathcal{S}})(1 - \check{r}^i(\{\mathbf{z}\} \cap \overset{i}{\mathbb{Z}})) \\
&\qquad + \check{r}^i(\{\mathbf{z}\} \cap \overset{i}{\mathbb{Z}}) \int_{\overset{i}{\mathbb{Z}}} \mathcal{R}(\{\mathbf{z}'\}, \{\mathbf{z}\}; \overset{i}{\mathcal{S}}) \check{p}^i(\mathbf{z}' | \{\mathbf{z}\} \cap \overset{i}{\mathbb{Z}}) \mathrm{d}\mathbf{z}' \qquad \text{(A.69)}
\end{aligned}
$$

Substitution of the simplified terms (A.65) and (A.69) into (A.61) gives (5.12), completing the proof. ■

A.7 Proof of Theorem 3

By the stated assumptions, the decomposition

$$
\mathbb{Z} = \overset{1}{\mathbb{Z}} \uplus \cdots \uplus \overset{P}{\mathbb{Z}}, \qquad \mathbb{X} = \overset{1}{\mathbb{X}} \uplus \cdots \uplus \overset{P}{\mathbb{X}} \qquad \text{(A.70)}
$$

is such that (4.16) and (4.24) hold. It follows then that

$$
\begin{aligned}
D_k(\mathbf{x} | Z^{(1)}; \mathcal{S}) g_k(\mathbf{z} | \mathbf{x}) &= L_{Z^{(1)}}(\mathbf{x}; \mathcal{S}, D_{k|k-1}) D_{k|k-1}(\mathbf{x}) g_k(\mathbf{z} | \mathbf{x}) \qquad \text{(A.71)} \\
&= 0 \qquad \forall\, \mathbf{x} \in \overset{j}{\mathbb{X}},\, \mathbf{z} \in \overset{j'}{\mathbb{Z}}, j \neq j' \qquad \text{(A.72)}
\end{aligned}
$$

Next note that, for $\mathbf{s} \notin \mathcal{S}_k$, $L_{Z^{(2)}}(\mathbf{x}; \mathcal{S}_k, D_k^{(1)}(\cdot|Z^{(1)}); \mathcal{S}_k) L_{Z^{(1)}}(\mathbf{x}; \mathcal{S}_k, D_{k|k-1}) = 1$, and thus the integral in (5.19) can be restricted to $\mathcal{S}_k \times \mathbb{X}_v$:

$$\begin{aligned}\mathcal{R}_k(Z^{(1)}, Z^{(2)}; \mathcal{S}_k, D_{k|k-1}) = \int_{\mathcal{S}_k \times \mathbb{X}_v} & D_{k|k-1}(\mathbf{x}) \cdot \\ & \Big[1 - L_{Z^{(2)}}(\mathbf{x}; \mathcal{S}_k, D_k^{(1)}(\cdot|Z^{(1)}; \mathcal{S})) \cdot L_{Z^{(1)}}(\mathbf{x}; \mathcal{S}_k, D_{k|k-1}) \\ & + L_{Z^{(2)}}(\mathbf{x}; \mathcal{S}_k, D_k^{(1)}(\cdot|Z^{(1)}; \mathcal{S})) \cdot L_{Z^{(1)}}(\mathbf{x}; \mathcal{S}_k, D_{k|k-1}) \\ & \cdot \log\left(L_{Z^{(2)}}(\mathbf{x}; \mathcal{S}_k, D_k^{(1)}(\cdot|Z^{(1)}; \mathcal{S})) \cdot L_{Z^{(1)}}(\mathbf{x}; \mathcal{S}_k, D_{k|k-1})\right)\Big] \mathrm{d}\mathbf{x} \end{aligned} \tag{A.73}$$

Furthermore, the integral can be re-expressed as a sum of integrals

$$\begin{aligned}\mathcal{R}_k(Z^{(1)}, Z^{(2)}; \mathcal{S}_k, D_{k|k-1}) = \sum_{j=1}^{P} \int_{\overset{j}{\mathcal{S}} \times \mathbb{X}_v} & D_{k|k-1}(\mathbf{x}) \cdot \\ & \Big[1 - L_{Z^{(2)}}(\mathbf{x}; \mathcal{S}_k, D_k^{(1)}(\cdot|Z^{(1)}; \mathcal{S}_k)) \cdot L_{Z^{(1)}}(\mathbf{x}; \mathcal{S}_k, D_{k|k-1}) \\ & + L_{Z^{(2)}}(\mathbf{x}; \mathcal{S}_k, D_k^{(1)}(\cdot|Z^{(1)}; \mathcal{S}_k)) \cdot L_{Z^{(1)}}(\mathbf{x}; \mathcal{S}_k, D_{k|k-1}) \\ & \cdot \log\left(L_{Z^{(2)}}(\mathbf{x}; \mathcal{S}_k, D_k^{(1)}(\cdot|Z^{(1)}; \mathcal{S}_k)) \cdot L_{Z^{(1)}}(\mathbf{x}; \mathcal{S}_k, D_{k|k-1})\right)\Big] \mathrm{d}\mathbf{x} \end{aligned} \tag{A.74}$$

As shown in Appendix (A.4), the pseudo-likelihood can be written terms of a sum of cell pseudo-likelihood functions

$$L_{Z^{(1)}}(\mathbf{x}; \mathcal{S}_k, D_{k|k-1}) = \begin{cases} \sum_{j=1}^{P} 1_{\overset{j}{\mathcal{S}}_k}(\mathbf{s}) L_{Z^{(1)}}^{(j)}(\mathbf{x}; \overset{j}{\mathcal{S}}_k) & \mathbf{s} \in \mathcal{S}_k \\ 1 & \mathbf{s} \notin \mathcal{S}_k \end{cases} \tag{A.75}$$

where by (A.44),

$$L_{Z^{(1)}}^{(j)}(\mathbf{x}; \overset{j}{\mathcal{S}}_k) = \begin{cases} 1 - p_{D,k}(\mathbf{x}, \overset{j}{\mathcal{S}}_k) + p_{D,k}(\mathbf{x}, \overset{j}{\mathcal{S}}_k) \Phi_k^{(j)}(Z^{(1)}|\mathbf{x}) & \mathbf{s} \in \overset{j}{\mathcal{S}}_k \\ 1 & \mathbf{s} \notin \overset{j}{\mathcal{S}}_k \end{cases} \tag{A.76}$$

$$\Phi_k^{(j)}(Z^{(1)}|\mathbf{x}) = \sum_{\mathbf{z} \in Z^{(1)} \cap \overset{j}{\mathbb{Z}}} \frac{g_k(\mathbf{z}|\mathbf{x})}{\kappa_k(\mathbf{z}) + \int_{\overset{j}{\mathbb{X}}} D_{k|k-1}(\mathbf{x}') p_{D,k}(\mathbf{x}'; \overset{j}{\mathcal{S}}_k) g_k(\mathbf{z}|\mathbf{x}') \mathrm{d}\mathbf{x}'} \tag{A.77}$$

where the implicit dependence on $D_{k|k-1}$ is omitted from the functions' arguments for brevity. Similarly,

$$L_{Z^{(2)}}(\mathbf{x}; \mathcal{S}_k, D_k^{(1)}(\cdot|Z^{(1)}; \mathcal{S}_k)) = \begin{cases} \sum_{j=1}^{P} 1_{\overset{j}{\mathcal{S}}_k}(\mathbf{s}) L_{Z^{(2)}}^{(j)}(\mathbf{x}; \overset{j}{\mathcal{S}}_k, D_k^{(1)}(\cdot|Z^{(1)}; \mathcal{S}_k)) & \mathbf{s} \in \mathcal{S}_k \\ 1 & \mathbf{s} \notin \mathcal{S}_k \end{cases} \tag{A.78}$$

$$\equiv \begin{cases} \sum_{j=1}^{P} 1_{\overset{j}{\mathcal{S}}_k}(\mathbf{s}) L_{Z^{(2)}}^{(j)}(\mathbf{x}; \overset{j}{\mathcal{S}}_k, D_k^{(1)}(\cdot|Z^{(1)}; \overset{j}{\mathcal{S}}_k)) & \mathbf{s} \in \mathcal{S}_k \\ 1 & \mathbf{s} \notin \mathcal{S}_k \end{cases} \tag{A.79}$$

where by (A.44),

$$\begin{aligned} &L_{Z^{(2)}}^{(j)}(\mathbf{x}; \overset{j}{\mathcal{S}}_k, D_k^{(1)}(\cdot|Z^{(1)}; \overset{j}{\mathcal{S}}_k)) \\ &\quad = \begin{cases} 1 - p_{D,k}(\mathbf{x}, \overset{j}{\mathcal{S}}) + p_{D,k}(\mathbf{x}, \overset{j}{\mathcal{S}}) \Phi_k^{(j)}(Z^{(2)}|\mathbf{x}; D_k^{(1)}(\cdot|Z^{(1)}; \overset{j}{\mathcal{S}}_k)) & \mathbf{s} \in \overset{j}{\mathcal{S}}_k \\ 1 & \mathbf{s} \notin \overset{j}{\mathcal{S}}_k \end{cases} \end{aligned} \tag{A.80}$$

$$\Phi_k^{(j)}(Z^{(2)}|\mathbf{x}; D_k^{(1)}(\cdot|Z^{(1)}; \overset{j}{\mathcal{S}}_k)) = \sum_{\mathbf{z} \in Z^{(2)} \cap \overset{j}{\mathbb{Z}}} \frac{g_k(\mathbf{z}|\mathbf{x})}{\kappa_k(\mathbf{z}) + \int_{\overset{j}{\mathbb{X}}} D_k^{(1)}(\mathbf{x}'|Z^{(1)}; \overset{j}{\mathcal{S}}_k) p_D(\mathbf{x}') g_k(\mathbf{z}|\mathbf{x}') d\mathbf{x}'} \tag{A.81}$$

and where the equivalence of (A.78) to (A.79) is due to the equivalence $\Phi_k^{(j)}(Z^{(2)}|\mathbf{x}; D_k^{(1)}(\cdot|Z^{(1)}; \mathcal{S}_k)) \equiv \Phi_k^{(j)}(Z^{(2)}|\mathbf{x}; D_k^{(1)}(\cdot|Z^{(1)}; \overset{j}{\mathcal{S}}_k))$. Also note that the integral in the denominator of (A.81) is restricted to $\overset{j}{\mathbb{X}}$ as a result of (A.72).

The product of (A.44) and (A.79) gives

$$L_{Z^{(2)}}(\mathbf{x};\mathcal{S}_k,D_k^{(1)}(\cdot|Z^{(1)});\mathcal{S}_k)L_{Z^{(1)}}(\mathbf{x};\mathcal{S}_k,D_{k|k-1}) \tag{A.82}$$

$$= \begin{cases} \sum_{j=1}^{P}\sum_{i=1}^{P} 1_{\overset{j}{\mathcal{S}}_k}(\mathbf{s})1_{\overset{i}{\mathcal{S}}_k}(\mathbf{s})L^{(j)}_{Z^{(1)}}(\mathbf{x};\overset{j}{\mathcal{S}}_k)L^{(i)}_{Z^{(2)}}(\mathbf{x};\overset{i}{\mathcal{S}}_k,D_k^{(1)}(\cdot|Z^{(1)};\overset{i}{\mathcal{S}}_k)) & \mathbf{s}\in\mathcal{S}_k \\ 1 & \mathbf{s}\notin\mathcal{S}_k \end{cases} \tag{A.83}$$

$$= \begin{cases} \sum_{j=1}^{P} 1_{\overset{j}{\mathcal{S}}_k}(\mathbf{s})L^{(j)}_{Z^{(2)}}(\mathbf{x};\overset{j}{\mathcal{S}}_k,D_k^{(1)}(\cdot|Z^{(1)};\overset{j}{\mathcal{S}}_k))L^{(j)}_{Z^{(1)}}(\mathbf{x};\overset{j}{\mathcal{S}}_k) & \mathbf{s}\in\mathcal{S}_k \\ 1 & \mathbf{s}\notin\mathcal{S}_k \end{cases} \tag{A.84}$$

Substituting this product into (A.74),

$$
\begin{aligned}
&\mathcal{R}_k(Z^{(1)}, Z^{(2)}; \mathcal{S}_k, D_{k|k-1}) \\
&\quad = \sum_{j=1}^{P} \int_{\overset{j}{\mathcal{S}}_k \times \mathbb{X}_v} D_{k|k-1}(\mathbf{x}) \qquad \text{(A.85)} \\
&\qquad \cdot \Bigg[1 - \Bigg(\sum_{i=1}^{P} 1_{\overset{i}{\mathcal{S}}_k}(\mathbf{s}) L^{(i)}_{Z^{(2)}}(\mathbf{x}; \overset{j}{\mathcal{S}}_k, D^{(1)}_k(\cdot|Z^{(1)}; \overset{i}{\mathcal{S}}_k)) L^{(i)}_{Z^{(1)}}(\mathbf{x}; \overset{i}{\mathcal{S}}_k) \Bigg) \\
&\qquad + \Bigg(\sum_{i=1}^{P} 1_{\overset{i}{\mathcal{S}}_k}(\mathbf{s}) L^{(i)}_{Z^{(2)}}(\mathbf{x}; \overset{j}{\mathcal{S}}_k, D^{(1)}_k(\cdot|Z^{(1)}; \overset{i}{\mathcal{S}}_k)) L^{(i)}_{Z^{(1)}}(\mathbf{x}; \overset{i}{\mathcal{S}}_k) \Bigg) \\
&\qquad \cdot \log \Bigg(\sum_{i=1}^{P} 1_{\overset{i}{\mathcal{S}}_k}(\mathbf{s}) L^{(i)}_{Z^{(2)}}(\mathbf{x}; \overset{j}{\mathcal{S}}_k, D^{(1)}_k(\cdot|Z^{(1)}; \overset{i}{\mathcal{S}}_k)) L^{(i)}_{Z^{(1)}}(\mathbf{x}; \overset{i}{\mathcal{S}}_k) \Bigg) \Bigg] \mathrm{d}\mathbf{x}
\end{aligned}
$$

$$
\begin{aligned}
&\quad = \sum_{j=1}^{P} \int_{\overset{j}{\mathcal{S}}_k \times \mathbb{X}_v} D_{k|k-1}(\mathbf{x}) \qquad \text{(A.86)} \\
&\qquad \cdot \Bigg[1 - \Bigg(\sum_{i=1}^{P} 1_{\overset{i}{\mathcal{S}}_k}(\mathbf{s}) L^{(i)}_{Z^{(2)}}(\mathbf{x}; \overset{i}{\mathcal{S}}_k, D^{(1)}_k(\cdot|Z^{(1)}; \overset{i}{\mathcal{S}}_k)) L^{(i)}_{Z^{(1)}}(\mathbf{x}; \overset{i}{\mathcal{S}}_k) \Bigg) \\
&\qquad + \Bigg(\sum_{i=1}^{P} 1_{\overset{i}{\mathcal{S}}_k}(\mathbf{s}) L^{(i)}_{Z^{(2)}}(\mathbf{x}; \overset{i}{\mathcal{S}}_k, D^{(1)}_k(\cdot|Z^{(1)}; \overset{i}{\mathcal{S}}_k)) L^{(i)}_{Z^{(1)}}(\mathbf{x}; \overset{i}{\mathcal{S}}_k) \\
&\qquad \cdot \log \Big(1_{\overset{i}{\mathcal{S}}_k}(\mathbf{s}) L^{(i)}_{Z^{(2)}}(\mathbf{x}; \overset{i}{\mathcal{S}}_k, D^{(1)}_k(\cdot|Z^{(1)}; \overset{i}{\mathcal{S}}_k)) L^{(i)}_{Z^{(1)}}(\mathbf{x}; \overset{i}{\mathcal{S}}_k) \Big) \Bigg) \Bigg] \mathrm{d}\mathbf{x}
\end{aligned}
$$

$$
\begin{aligned}
&\quad = \sum_{j=1}^{P} \int_{\overset{j}{\mathcal{S}}_k \times \mathbb{X}_v} D_{k|k-1}(\mathbf{x}) \cdot \Big[1 - 1_{\overset{j}{\mathcal{S}}_k}(\mathbf{s}) L^{(j)}_{Z^{(2)}}(\mathbf{x}; \overset{j}{\mathcal{S}}_k, D^{(1)}_k(\cdot|Z^{(1)}; \overset{j}{\mathcal{S}}_k)) L^{(j)}_{Z^{(1)}}(\mathbf{x}; \overset{j}{\mathcal{S}}_k) \\
&\qquad + 1_{\overset{j}{\mathcal{S}}_k}(\mathbf{s}) L^{(j)}_{Z^{(2)}}(\mathbf{x}; \overset{j}{\mathcal{S}}_k, D^{(1)}_k(\cdot|Z^{(1)}; \overset{j}{\mathcal{S}}_k)) L^{(j)}_{Z^{(1)}}(\mathbf{x}; \overset{j}{\mathcal{S}}_k) \\
&\qquad \cdot \log \Big(1_{\overset{j}{\mathcal{S}}_k}(\mathbf{s}) L^{(j)}_{Z^{(2)}}(\mathbf{x}; \overset{j}{\mathcal{S}}_k, D^{(1)}_k(\cdot|Z^{(1)}; \overset{j}{\mathcal{S}}_k)) L^{(j)}_{Z^{(1)}}(\mathbf{x}; \overset{j}{\mathcal{S}}_k) \Big) \Big] \mathrm{d}\mathbf{x} \qquad \text{(A.87)}
\end{aligned}
$$

From (A.87), the final result of (5.21) is obtained by noting that $L^{(j)}_{Z^{(1)}}(\cdot) = L^{(j)}_{Z^{(1)} \cap \overset{j}{\mathbb{Z}}}(\cdot)$ and $L^{(j)}_{Z^{(2)}}(\cdot) = L^{(j)}_{Z^{(2)} \cap \overset{j}{\mathbb{Z}}}(\cdot)$, completing the proof. ■

A.8 Proof of Theorem 4

The result is proven by induction. The base case of $b = \mathrm{M}$ follows directly from Theorem 1 as follows:

$$\mathrm{E}_{Z^{(\mathrm{M})}}[\mathcal{R}(Z^{(\mathrm{M})}; \mathcal{S}^{(\mathrm{M})})] = \sum_{j=1}^{P} \mathcal{R}(\emptyset; \overset{j}{\mathcal{S}})(1 - r^j) + \hat{\mathcal{R}}_{\mathrm{z}}^{j} \cdot r^j \tag{A.88}$$

$$= \sum_{j=1}^{P} \mathrm{E}_{Z^{(\mathrm{M})} \cap \overset{j}{\mathbb{Z}}}[\mathcal{R}(Z^{(\mathrm{M})} \cap \overset{j}{\mathbb{Z}}; \overset{j}{\mathcal{S}})] \tag{A.89}$$

$$= \sum_{j=1}^{P} \mathcal{E}(j, Z^{(\mathrm{M})}, \mathcal{S}^{(\mathrm{M})}) \tag{A.90}$$

For the inductive step, assume (5.24) holds for $b = \ell$. Now consider the case of $b = \ell - 1$. By the law of iterated expectation,

$$\mathrm{E}_{Z^{(\ell-1:\mathrm{M})}}[\mathcal{R}(Z^{(\ell-1:\mathrm{M})}; \mathcal{S}^{(\ell-1:\mathrm{M})})] = \mathrm{E}_{Z^{(\ell-1)}} \left\{ \mathrm{E}_{Z^{(\ell:\mathrm{M})}} \left[\mathcal{R}(Z^{(\ell-1:\mathrm{M})}; \mathcal{S}^{(\ell-1:\mathrm{M})}) \right] \mid Z^{(\ell-1)} \right\} \tag{A.91}$$

Because the conditional distribution $f(Z^{(\ell-1)}|Z^{(\ell:\mathrm{M})})$ is cell-MB with parameters $\{\check{r}^j(Z^{(\ell:\mathrm{M})} \cap \overset{j}{\mathbb{Z}}),\, \check{p}^j(\mathbf{z}|Z^{(\ell:\mathrm{M})} \cap \overset{j}{\mathbb{Z}})\}_{j=1}^{P}$, Theorem 1 can be applied to find

$$\begin{aligned}
&\mathrm{E}_{Z^{(\ell-1:\mathrm{M})}}[\mathcal{R}(Z^{(\ell-1:\mathrm{M})}; \mathcal{S}^{(\ell-1:\mathrm{M})})] \\
&= \sum_{j=1}^{P} (1 - \check{r}^j(\cdot)) \mathrm{E}_{Z^{(\ell:\mathrm{M})}} \left[\mathcal{R}(\emptyset, Z^{(\ell:\mathrm{M})} \cap \overset{j}{\mathbb{Z}}; \overset{j}{\mathcal{S}}{}^{(\ell-1:\mathrm{M})}) \right] \\
&\quad + \sum_{j=1}^{P} \int_{\overset{j}{\mathbb{Z}}} \check{r}^j(\cdot) \check{p}^j(\mathbf{z}'|\cdot) \mathrm{E}_{Z^{(\ell:\mathrm{M})}} \left[\mathcal{R}(\{\mathbf{z}'\}, Z^{(\ell:\mathrm{M})} \cap \overset{j}{\mathbb{Z}}; \overset{j}{\mathcal{S}}{}^{(\ell:\mathrm{M})}) \right] \mathrm{d}\mathbf{z}'
\end{aligned} \tag{A.92}$$

$$
\begin{aligned}
&\mathrm{E}_{Z^{(\ell-1:\mathrm{M})}}[\mathcal{R}(Z^{(\ell-1:\mathrm{M})};\mathcal{S}^{(\ell-1:\mathrm{M})})] \qquad \text{(A.93)}\\
&\quad=\sum_{j=1}^{P}[1-\check{r}^j(\cdot)]1_{\emptyset}(\overset{j}{\mathcal{S}}{}^{(\ell-1)})\mathrm{E}_{Z^{(\ell:\mathrm{M})}\cap\overset{j}{\mathbb{Z}}}\big[\mathcal{R}(Z^{(\ell:\mathrm{M})}\cap\overset{j}{\mathbb{Z}};\overset{j}{\mathcal{S}}{}^{(\ell:\mathrm{M})})\big]\\
&\qquad+\sum_{j=1}^{P}[1-\check{r}^j(\cdot)]\big[1-1_{\emptyset}(\overset{j}{\mathcal{S}}{}^{(\ell-1)})\big]\mathrm{E}_{Z^{(\ell:\mathrm{M})}\cap\overset{j}{\mathbb{Z}}}\big[\mathcal{R}(\emptyset,Z^{(\ell:\mathrm{M})}\cap\overset{j}{\mathbb{Z}};\overset{j}{\mathcal{S}}{}^{(\ell-1:\mathrm{M})})\big]\\
&\qquad+\sum_{j=1}^{P}\int_{\overset{j}{\mathbb{Z}}}\check{r}^j(\cdot)\check{p}^j(\mathbf{z}'|\cdot)1_{\emptyset}(\overset{j}{\mathcal{S}}{}^{(\ell-1)})\mathrm{E}_{Z^{(\ell:\mathrm{M})}\cap\overset{j}{\mathbb{Z}}}\left[\mathcal{R}(Z^{(\ell:\mathrm{M})}\cap\overset{j}{\mathbb{Z}};\overset{j}{\mathcal{S}}{}^{(\ell:\mathrm{M})})\right]\mathrm{d}\mathbf{z}'\\
&\qquad+\sum_{j=1}^{P}\int_{\overset{j}{\mathbb{Z}}}\check{r}^j(\cdot)\check{p}^j(\mathbf{z}'|\cdot)\big[1-1_{\emptyset}(\overset{j}{\mathcal{S}}{}^{(\ell-1)})\big]\mathrm{E}_{Z^{(\ell:\mathrm{M})}\cap\overset{j}{\mathbb{Z}}}\left[\mathcal{R}(\{\mathbf{z}'\},Z^{(\ell:\mathrm{M})}\cap\overset{j}{\mathbb{Z}};\overset{j}{\mathcal{S}}{}^{(\ell-1:\mathrm{M})})\right]\mathrm{d}\mathbf{z}'
\end{aligned}
$$

Note that $\overset{j}{\mathcal{S}}{}^{(\ell-1)}=\emptyset \implies \check{r}^j(\cdot)=0$, and thus

$$
\begin{aligned}
&\mathrm{E}_{Z^{(\ell-1:\mathrm{M})}}[\mathcal{R}(Z^{(\ell-1:\mathrm{M})};\mathcal{S}^{(\ell-1:\mathrm{M})})] \qquad \text{(A.94)}\\
&\quad=\sum_{j=1}^{P}1_{\emptyset}(\overset{j}{\mathcal{S}}{}^{(\ell-1)})\mathrm{E}_{Z^{(\ell:\mathrm{M})}\cap\overset{j}{\mathbb{Z}}}\big[\mathcal{R}(Z^{(\ell:\mathrm{M})}\cap\overset{j}{\mathbb{Z}};\overset{j}{\mathcal{S}}{}^{(\ell:\mathrm{M})})\big]\\
&\qquad+\sum_{j=1}^{P}\big[1-1_{\emptyset}(\overset{j}{\mathcal{S}}{}^{(\ell-1)})\big][1-\check{r}^j(\cdot)]\mathrm{E}_{Z^{(\ell:\mathrm{M})}\cap\overset{j}{\mathbb{Z}}}\big[\mathcal{R}(\emptyset,Z^{(\ell:\mathrm{M})}\cap\overset{j}{\mathbb{Z}};\overset{j}{\mathcal{S}}{}^{(\ell-1:\mathrm{M})})\big]\\
&\qquad+\sum_{j=1}^{P}\big[1-1_{\emptyset}(\overset{j}{\mathcal{S}}{}^{(\ell-1)})\big]\int_{\overset{j}{\mathbb{Z}}}\check{r}^j(\cdot)\check{p}^j(\mathbf{z}'|\cdot)\mathrm{E}_{Z^{(\ell:\mathrm{M})}\cap\overset{j}{\mathbb{Z}}}\big[\mathcal{R}(\{\mathbf{z}'\},Z^{(\ell:\mathrm{M})}\cap\overset{j}{\mathbb{Z}};\overset{j}{\mathcal{S}}{}^{(\ell-1:\mathrm{M})})\big]\mathrm{d}\mathbf{z}'
\end{aligned}
$$

By reverse application of Theorem 1,

$$
\begin{aligned}
&\mathrm{E}_{Z^{(\ell-1:\mathrm{M})}}[\mathcal{R}(Z^{(\ell-1:\mathrm{M})};\mathcal{S}^{(\ell-1:\mathrm{M})})] \qquad \text{(A.95)}\\
&\quad=\sum_{j=1}^{P}1_{\emptyset}(\overset{j}{\mathcal{S}}{}^{(\ell-1)})\mathrm{E}_{Z^{(\ell:\mathrm{M})}\cap\overset{j}{\mathbb{Z}}}\big[\mathcal{R}(Z^{(\ell:\mathrm{M})}\cap\overset{j}{\mathbb{Z}};\overset{j}{\mathcal{S}}{}^{(\ell:\mathrm{M})})\big]\\
&\qquad+\sum_{j=1}^{P}\big[1-1_{\emptyset}(\overset{j}{\mathcal{S}}{}^{(\ell-1)})\big]\mathrm{E}_{Z^{(\ell-1:\mathrm{M})}\cap\overset{j}{\mathbb{Z}}}\big[\mathcal{R}(Z^{(\ell-1:\mathrm{M})}\cap\overset{j}{\mathbb{Z}};\overset{j}{\mathcal{S}}{}^{(\ell-1:\mathrm{M})})\big]
\end{aligned}
$$

For $\overset{j}{\mathcal{S}}{}^{(\ell-1)}\neq\emptyset$, Assumption 1 asserts that there is at most one other FoV that covers $\overset{j}{\mathbb{X}}_s$, and thus

$$
\begin{aligned}
&\mathrm{E}_{Z^{(\ell-1:\mathrm{M})}\cap\overset{j}{\mathbb{Z}}}\big[\mathcal{R}(Z^{(\ell-1:\mathrm{M})}\cap\overset{j}{\mathbb{Z}},\overset{j}{\mathcal{S}}^{(\ell-1:\mathrm{M})})\big] \qquad\qquad \text{(A.96)}\\
&=\begin{cases}
\mathrm{E}\big[\mathcal{R}(Z^{(\ell-1)}\cap\overset{j}{\mathbb{Z}},\overset{j}{\mathcal{S}}^{(\ell-1)})\big] & \overset{j}{\mathcal{S}}^{(\ell-1)}\neq\emptyset,\ \overset{j}{\mathbb{X}}_s\nsubseteq\mathcal{S}^{(t)}\,\forall\, t>\ell-1, t\leq\mathrm{M}\\
\mathrm{E}\big[\mathcal{R}(Z^{(\ell-1)}\cap\overset{j}{\mathbb{Z}},Z^{(t)}\cap\overset{j}{\mathbb{Z}},\overset{j}{\mathcal{S}}^{(\ell-1)},\overset{j}{\mathcal{S}}^{(t)})\big] & \overset{j}{\mathbb{X}}_s\subseteq\mathcal{S}^{(\ell-1)}\cap\mathcal{S}^{(t)},\ t>\ell-1
\end{cases}
\end{aligned}
$$

for all j such that $\overset{j}{\mathcal{S}}^{(\ell-1)}\neq\emptyset$, and where the expectation subscripts have been dropped for brevity. By (A.96) it follows that

$$
\mathrm{E}_{Z^{(\ell-1:\mathrm{M})}}[\mathcal{R}(Z^{(\ell-1:\mathrm{M})};\mathcal{S}^{(\ell-1:\mathrm{M})})]=\sum_{j=1}^{P}\tilde{\mathcal{E}}(j,Z^{(\ell-1:\mathrm{M})},\mathcal{S}^{(\ell-1:\mathrm{M})}) \qquad \text{(A.97)}
$$

where

$$
\begin{aligned}
&\tilde{\mathcal{E}}(j,Z^{(\ell-1:\mathrm{M})},\mathcal{S}^{(\ell-1:\mathrm{M})}) \qquad\qquad \text{(A.98)}\\
&\triangleq\begin{cases}
\mathrm{E}\big[\mathcal{R}(Z^{(\ell:\mathrm{M})}\cap\overset{j}{\mathbb{Z}};\overset{j}{\mathcal{S}}^{(\ell:\mathrm{M})})\big] & \overset{j}{\mathcal{S}}^{(\ell-1)}=\emptyset\\
\mathrm{E}\big[\mathcal{R}(Z^{(\ell-1)}\cap\overset{j}{\mathbb{Z}},\overset{j}{\mathcal{S}}^{(\ell-1)})\big] & \overset{j}{\mathbb{X}}_s\subseteq\mathcal{S}^{(\ell-1)},\ \overset{j}{\mathbb{X}}_s\nsubseteq\overset{j}{\mathcal{S}}^{(t)}\,\forall\, t>\ell-1, t\leq\mathrm{M}\\
\mathrm{E}\big[\mathcal{R}(Z^{(\ell-1)}\cap\overset{j}{\mathbb{Z}},Z^{(t)}\cap\overset{j}{\mathbb{Z}},\overset{j}{\mathcal{S}}^{(\ell-1)},\overset{j}{\mathcal{S}}^{(t)})\big] & \overset{j}{\mathbb{X}}_s\subseteq\mathcal{S}^{(\ell-1)}\cap\mathcal{S}^{(t)},\ t>\ell-1
\end{cases}
\end{aligned}
$$

By the induction hypothesis,

$$
\begin{aligned}
&\tilde{\mathcal{E}}(j,Z^{(\ell-1:\mathrm{M})},\mathcal{S}^{(\ell-1:\mathrm{M})}) \qquad\qquad \text{(A.99)}\\
&=\begin{cases}
\mathcal{E}(j,Z^{(\ell:\mathrm{M})},\mathcal{S}^{(\ell:\mathrm{M})}) & \overset{j}{\mathcal{S}}^{(\ell-1)}=\emptyset\\
\mathrm{E}\big[\mathcal{R}(Z^{(\ell-1)}\cap\overset{j}{\mathbb{Z}},\overset{j}{\mathcal{S}}^{(\ell-1)})\big] & \overset{j}{\mathbb{X}}_s\subseteq\mathcal{S}^{(\ell-1)},\ \overset{j}{\mathbb{X}}_s\nsubseteq\overset{j}{\mathcal{S}}^{(t)}\,\forall\, t>\ell-1, t\leq\mathrm{M}\\
\mathrm{E}\big[\mathcal{R}(Z^{(\ell-1)}\cap\overset{j}{\mathbb{Z}},Z^{(t)}\cap\overset{j}{\mathbb{Z}},\overset{j}{\mathcal{S}}^{(\ell-1)},\overset{j}{\mathcal{S}}^{(t)})\big] & \overset{j}{\mathbb{X}}_s\subseteq\mathcal{S}^{(\ell-1)}\cap\mathcal{S}^{(t)},\ t>\ell-1
\end{cases}
\end{aligned}
$$

which, when expanded gives

$$\tilde{\mathcal{E}}(j, Z^{(\ell-1:\mathrm{M})}, \mathcal{S}^{(\ell-1:\mathrm{M})}) \tag{A.100}$$

$$= \begin{cases} \mathrm{E}\big[\mathcal{R}(Z^{(i)} \cap \overset{j}{\mathbb{Z}}, \overset{j}{\mathcal{S}}^{(i)})\big] & \overset{j}{\mathcal{S}}^{(\ell-1)} = \emptyset,\ \overset{j}{\mathbb{X}}_s \subseteq \mathcal{S}^{(i)}, \\ & \overset{j}{\mathbb{X}}_s \nsubseteq \overset{j}{\mathcal{S}}^{(t)}\ \forall\, \ell \leq t \leq \mathrm{M},\ t \neq i \\ \mathrm{E}\big[\mathcal{R}(Z^{(i)} \cap \overset{j}{\mathbb{Z}}, Z^{(t)} \cap \overset{j}{\mathbb{Z}}, \overset{j}{\mathcal{S}}^{(i)}, \overset{j}{\mathcal{S}}^{(t)})\big] & \overset{j}{\mathcal{S}}^{(\ell-1)} = \emptyset,\ \overset{j}{\mathbb{X}}_s \subseteq \mathcal{S}^{(i)} \cap \mathcal{S}^{(t)}, \\ & \ell \leq i < t \leq \mathrm{M} \\ \mathrm{E}\big[\mathcal{R}(Z^{(\ell-1)} \cap \overset{j}{\mathbb{Z}}, \overset{j}{\mathcal{S}}^{(\ell-1)})\big] & \overset{j}{\mathbb{X}}_s \subseteq \mathcal{S}^{(\ell-1)}, \\ & \overset{j}{\mathbb{X}}_s \nsubseteq \overset{j}{\mathcal{S}}^{(t)}\ \forall\, \ell-1 < t \leq \mathrm{M} \\ \mathrm{E}\big[\mathcal{R}(Z^{(\ell-1)} \cap \overset{j}{\mathbb{Z}}, Z^{(t)} \cap \overset{j}{\mathbb{Z}}, \overset{j}{\mathcal{S}}^{(\ell-1)}, \overset{j}{\mathcal{S}}^{(t)})\big] & \overset{j}{\mathbb{X}}_s \subseteq \mathcal{S}^{(\ell-1)} \cap \mathcal{S}^{(t)},\ t > \ell - 1 \\ 0 & \text{otherwise} \end{cases}$$

$$= \begin{cases} \mathrm{E}\big[\mathcal{R}(Z^{(i)} \cap \overset{j}{\mathbb{Z}}, \overset{j}{\mathcal{S}}^{(i)})\big] & \overset{j}{\mathbb{X}}_s \subseteq \mathcal{S}^{(i)},\ \overset{j}{\mathbb{X}}_s \nsubseteq \overset{j}{\mathcal{S}}^{(t)}\ \forall\, \ell-1 \leq t \leq \mathrm{M},\ t \neq i \\ \mathrm{E}\big[\mathcal{R}(Z^{(i)} \cap \overset{j}{\mathbb{Z}}, Z^{(t)} \cap \overset{j}{\mathbb{Z}}, \overset{j}{\mathcal{S}}^{(i)}, \overset{j}{\mathcal{S}}^{(t)})\big] & \overset{j}{\mathbb{X}}_s \subseteq \mathcal{S}^{(i)} \cap \mathcal{S}^{(t)},\ \ell-1 \leq i < t \leq \mathrm{M} \\ 0 & \text{otherwise} \end{cases}$$

$$= \mathcal{E}(j, Z^{(\ell-1:\mathrm{M})}, \mathcal{S}^{(\ell-1:\mathrm{M})}) \tag{A.101}$$

Substitution of this result in (A.97) completes the proof. ∎

BIBLIOGRAPHY

[1] Nisar R. Ahmed, Eric M. Sample, and Mark Campbell. Bayesian multicategorical soft data fusion for human-robot collaboration. *IEEE Transactions on Robotics*, 29(1):189–206, 2013.

[2] Daniel L. Alspach and Harold W. Sorenson. Nonlinear bayesian estimation using Gaussian sum approximations. *IEEE Transactions on Automatic Control*, 17(4):439–448, 1972.

[3] Giuseppe Anastasi, Marco Conti, Mario Di Francesco, and Andrea Passarella. Energy conservation in wireless sensor networks: A survey. *Ad Hoc Networks*, 7(3):537–568, 2009.

[4] Brian Anderson and John B Moore. *Optimal Filtering*. Prentice-Hall Information and System Sciences Series, Englewood Cliffs: Prentice-Hall, 1979.

[5] M. Sangeev Arulampalam, Simon Maskell, Neil Gordon, and Tim Clapp. A tutorial on particle filters for online nonlinear/non-Gaussian Bayesian tracking. *IEEE Transactions on Signal Processing*, 50(2):174–188, 2002.

[6] Roland Badeau, Bertrand David, and Gael Richard. Fast approximated power iteration subspace tracking. *IEEE Transactions on Signal Processing*, 53(8):2931–2941, 2005.

[7] Yaakov Bar-Shalom, X-Rong Li, and Thiagalingam Kirubarajan. *Estimation with Applications To Tracking and Navigation*. John Wiley & Sons, 2001.

[8] Yaakov Bar-Shalom and Edison Tse. Tracking in a cluttered environment with probabilistic data association. *Automatica*, 11(5):451–460, 1975.

[9] Yaakov Bar-Shalom, Peter K Willett, and Xin Tian. *Tracking and Data Fusion*. YBS publishing, 2011.

[10] Kelli A.C. Baumgartner, Silvia Ferrari, and Anil V. Rao. Optimal control of an underwater sensor network for cooperative target tracking. *IEEE Journal of Oceanic Engineering*, 34(4):678–697, 2009.

[11] Michael Beard, Ba-Tuong Vo, Ba-Ngu Vo, and Sanjeev Arulampalam. Sensor control for multi-target tracking using Cauchy-Schwarz divergence. In *18th International Conference on Information Fusion*, pages 937–944, Washington, DC, 2015.

[12] Michael Beard, Ba-Tuong Vo, Ba-Ngu Vo, and Sanjeev Arulampalam. Void probabilities and Cauchy-Schwarz divergence for generalized labeled multi-Bernoulli models. *IEEE Transactions on Signal Processing*, 65(19):5047–5061, 2017.

[13] Christopher Berry and Donald J. Bucci. Obstructed target tracking in urban environments. 2019.

[14] Adrian N Bishop and Branko Ristic. Fusion of spatially referring natural language statements with random set theoretic likelihoods. *IEEE Transactions on Aerospace and Electronic Systems*, 49(2):932–944, 2013.

[15] Samuel Blackman and Robert Popoli. *Design and Analysis of Modern Tracking Systems*. Artech House, 1999.

[16] Samuel S Blackman. Multiple-target tracking with radar applications. *Dedham, MA, Artech House, Inc., 1986, 463 p.*, 1, 1986.

[17] Per Bostrom-Rost, Daniel Axehill, and Gustaf Hendeby. Sensor management for search and track using the Poisson multi-Bernoulli mixture filter. *IEEE Transactions on Aerospace and Electronic Systems*, 2021.

[18] Augustus Buonviri, Matthew York, Keith A. LeGrand, and James Meub. Survey of challenges in labeled random finite set based distributed multi-sensor multi-object tracking. In *2019 IEEE Aerospace Conference*, 2019.

[19] Chenghui Cai and Silvia Ferrari. Information-driven sensor path planning by approximate cell decomposition. *IEEE Transactions on Systems, Man, and Cybernetics - Part B*, 39(3):672–689, 2009.

[20] Han Cai, Steve Gehly, Yang Yang, Reza Hoseinnezhad, Robert Norman, and Kefei Zhang. Multisensor tasking using analytical Rényi divergence in labeled multi-Bernoulli filtering. *Journal of Guidance, Control, and Dynamics*, 49(2):1–8, apr 2019.

[21] David Castañón and Lawrence Carin. Stochastic control theory for sensor management. In Alfred Olivier Hero, David Castañón, Doug Cochran, and Keith Kastella, editors, *Foundations and Applications of Sensor Management*, chapter 2. Springer Science & Business Media, 2007.

[22] Daniel Clark, Ali Taylan Cemgil, Paul Peeling, and Simon Godsill. Multi-object tracking of sinusoidal components in audio with the Gaussian mixture

probability hypothesis density filter. In *IEEE Workshop on Applications of Signal Processing to Audio and Acoustics*, pages 339–342, 2007.

[23] Thomas M. Cover and Joy A. Thomas. *Elements of Information Theory*. John Wiley & Sons, 1999.

[24] David F. Crouse, Peter Willett, Krishna R. Pattipati, and Lennart Svensson. A look at Gaussian mixture reduction algorithms. In *Proceedings of the 2011 14th International Conference on Information Fusion*, pages 1–8, 2011.

[25] Kyle J. DeMars, Robert H. Bishop, and Moriba K. Jah. Entropy-based approach for uncertainty propagation of nonlinear dynamical systems. *Journal of Guidance, Control, and Dynamics*, 36(4):1047–1057, 2013.

[26] Kyle J. DeMars, Islam I. Hussein, Carolin Frueh, Moriba K. Jah, and R. Scott Erwin. Multiple object space surveillance tracking using finite set statistics. *Journal of Guidance, Control, and Dynamics*, pages 1741–1756, 2015.

[27] Cong-Thanh Do and Hoa Van Nguyen. Multistatic Doppler-based marine ships tracking. In *2018 International Conference on Control, Automation and Information Sciences (ICCAIS)*, pages 151–156, 2018.

[28] Bryce Doerr and Richard Linares. Decentralized control of large collaborative swarms using random finite set theory. *IEEE Transactions on Control of Network Systems*, 8(2):587–597, 2021.

[29] Adel El-Fallah, Aleksandar Zatezalo, Ronald P.S. Mahler, Raman K. Mehra, and Khanh D. Pham. Situational awareness sensor management of space-based EO/IR and airborne GMTI radar for road targets tracking. In *Proc. SPIE 7697, Signal Processing, Sensor Fusion, and Target Recognition XIX*, volume 7697, pages 7697 – 7697, 2010.

[30] Ozgur Erdinc, Peter Willett, and Stefano Coraluppi. The Gaussian mixture cardinalized PHD tracker on MSTWG and SEABAR'07 datasets. In *FUSION*, pages 1–8, 2008.

[31] Maryam Fatemi, Karl Granström, Lennart Svensson, Francisco J R Ruiz, and Lars Hammarstrand. Poisson multi-Bernoulli mapping using Gibbs sampling. *IEEE Transactions on Signal Processing*, 65(11):2814–2827, 2017.

[32] Manuel Fernandez and Stuart Williams. Closed-form expression for the

Poisson-Binomial probability density function. *IEEE Transactions on Aerospace and Electronic Systems*, 46(2):803–817, 2010.

[33] Silvia Ferrari, Rafael Fierro, Brent Perteet, Chenghui Cai, and Kelli Baumgartner. A geometric optimization approach to detecting and intercepting dynamic targets using a mobile sensor network. *SIAM Journal on Control and Optimization*, 48(1):292–320, January 2009.

[34] Silvia Ferrari and Thomas A. Wettergren. *Information-driven Planning and Control*. MIT Press, 2021.

[35] Silvia Ferrari, Thomas A. Wettergren, Richard Linares, and Keith A. LeGrand. Guest editorial special issue on control of very-large scale robotic (VLSR) networks. *IEEE Transactions on Control of Network Systems*, 8(2):527–529, 2021.

[36] Nicola Forti, Giorgio Battistelli, Luigi Chisci, Suqi Li, Bailu Wang, and Bruno Sinopoli. Distributed joint attack detection and secure state estimation. *IEEE Transactions on Signal and Information Processing over Networks*, 4(1):96–110, 2018.

[37] Ángel F. García-Fernández, Yuxuan Xia, Karl Granström, Lennart Svensson, and Jason L Williams. Gaussian implementation of the multi-Bernoulli mixture filter. In *2019 22nd International Conference on Information Fusion (FUSION)*, 2019.

[38] Steven Gehly, Brandon Jones, and Penina Axelrad. Sensor allocation for tracking geosynchronous space objects. *Journal of Guidance, Control, and Dynamics*, pages 1–15, 2016.

[39] Steven Gehly, Brandon A. Jones, and Penina Axelrad. Search-detect-track sensor allocation for geosynchronous space objects. *IEEE Transactions on Aerospace and Electronic Systems*, 54(6):2788–2808, 2018.

[40] Amadou Gning, Branko Ristic, and Lyudmila Mihaylova. Bernoulli particle/box-particle filters for detection and tracking in the presence of triple measurement uncertainty. *IEEE Transactions on Signal Processing*, 60(5):2138–2151, 2012.

[41] Irwin R. Goodman, Ronald P.S. Mahler, and Hung T. Nguyen. *Mathematics of Data Fusion*. Kluwer Academic Publishers, 1997.

[42] Amirali K. Gostar, Reza Hoseinnezhad, and Alireza Bab-Hadiashar. Sensor control for multi-object tracking using labeled multi-Bernoulli filter. In *Proceedings of the 17th International Conference on Information Fusion (FUSION)*, 2014.

[43] Amirali Khodadadian Gostar, Reza Hoseinnezhad, and Alireza Bab-Hadiashar. Multi-Bernoulli sensor control using Cauchy-Schwarz divergence. In *Proceedings of the 19th International Conference on Information Fusion (Fusion 2016)*, Heidelberg, Germany, 2016.

[44] Karl Granström. *Extended Target Tracking Using PHD Filters*. PhD thesis, Linköping University, 2012.

[45] Matthew J. Gualdoni and Kyle J. DeMars. Utilizing information statistics in multi-observation sensor tasking. In *2018 Space Flight Mechanics Meeting*, number January, pages 1–17, 2018.

[46] Matthew J. Gualdoni and Kyle J. DeMars. Impartial sensor tasking via forecasted information content quantification. *Journal of Guidance, Control, and Dynamics*, 43(11):2031–2045, aug 2020.

[47] Marcel L. Hernandez, Thia Kirubarajan, and Yaakov Bar-Shalom. Multisensor resource deployment using posterior Cramér-Rao bounds. *IEEE Transactions on Aerospace and Electronic Systems*, 40(2):399–416, 2004.

[48] Alfred Olivier Hero, III, Christopher M. Kreucher, and Doron Blatt. Stochastic control theory for sensor management. In Alfred Olivier Hero, David Castañón, Doug Cochran, and Keith Kastella, editors, *Foundations and Applications of Sensor Management*, chapter 3. Springer Science & Business Media, 2007.

[49] Kenneth J. Hintz. A measure of the information gain attributable to cueing. *IEEE Transactions on Systems, Man and Cybernetics*, 21:237–244, 1991.

[50] Hung Gia Hoang, Ba-Ngu Vo, Ba-Tuong Vo, and Ronald P.S. Mahler. The Cauchy-Schwarz divergence for Poisson point processes. *IEEE Transactions on Information Theory*, 61(8):4475–4485, 2015.

[51] Hung Gia Hoang and Ba-Tuong Vo. Sensor management for multi-target tracking via multi-Bernoulli filtering. *Automatica*, 50(4):1135–1142, 2014.

[52] Mohammed I. Hossain, Amirali Khodadadian Gostar, Alireza Bab-

Hadiashar, and Reza Hoseinnezhad. Visual mitosis detection and cell tracking using labeled multi-Bernoulli filter. In *2018 21st International Conference on Information Fusion (FUSION)*, pages 1–5, 2018.

[53] Biao Hu, Uzair Sharif, Rajat Koner, Guang Chen, Kai Huang, Feihu Zhang, Walter Stechele, and Alois Knoll. Random finite set based Bayesian filtering with OpenCL in a heterogeneous platform. *Sensors*, 17(4):1–19, 2017.

[54] Marco F. Huber. Adaptive Gaussian mixture filter based on statistical linearization. In *Proceedings of the 2011 14th International Conference on Information Fusion*, pages 1–8, 2011.

[55] Marco F. Huber, Tim Bailey, Hugh Durrant-Whyte, and Uwe D. Hanebeck. On entropy approximation for Gaussian mixture random vectors. *IEEE International Conference on Multisensor Fusion and Integration for Intelligent Systems*, pages 181–188, 2008.

[56] Andrew H. Jazwinski. *Stochastic Processes and Filtering Theory.* Courier Corporation, 2007.

[57] Meng Jiang, Wei Yi, and Lingjiang Kong. Multi-sensor control for multi-target tracking using Cauchy-Schwarz divergence. In *Proceedings of the 2016 19th International Conference on Information Fusion (FUSION)*, 2016.

[58] Michael Kalandros, Lucy Y. Pao, and Yu-Chi Ho. Randomization and super-heuristics in choosing sensor sets for target tracking applications. In *Proceedings of the 38th IEEE Conference on Decision and Control (Cat. No.99CH36304)*, volume 2, pages 1803–1808 vol.2, 1999.

[59] Rudolph Emil Kalman. A new approach to linear filtering and prediction problems. *Transactions of the ASME–Journal of Basic Engineering*, 82(Series D):35–45, 1960.

[60] Wolfgang Koch. On exploiting 'negative' sensor evidence for target tracking and sensor data fusion. *Information Fusion*, 2007.

[61] Chris Kreucher, Alfred Olivier Hero, III, and Keith Kastella. A comparison of task driven and information driven sensor management for target tracking. In *Proceedings of the 44th IEEE Conference on Decision and Control, and the European Control Conference, CDC-ECC '05*, volume 2005, pages 4004–4009, 2005.

[62] Vikram Krishnamurthy. *Partially Observed Markov Decision Processes: From Filtering to Controlled Sensing*. Cambridge University Press, Cambridge, 2016.

[63] Keith A. LeGrand. *Space-Based Relative Multitarget Tracking*. Master's thesis, Missouri University of Science and Technology, 2015.

[64] Keith A. LeGrand and Kyle J. DeMars. Relative multiple space object tracking using intensity filters. In *Proceedings of the 2015 18th International Conference on Information Fusion (FUSION)*, pages 1253–1261, 2015.

[65] Keith A. LeGrand and Kyle J. DeMars. The data-driven δ-generalized labeled multi-Bernoulli tracker for automatic birth initialization. In *Signal Processing, Sensor/Information Fusion, and Target Recognition XXVII*, volume 10646, page 1064606. International Society for Optics and Photonics, 2018.

[66] Keith A. LeGrand, Kyle J. DeMars, and Henry J. Pernicka. Bearing-only initial relative orbit determination. *Journal of Guidance, Control, and Dynamics*, 38:1699–1713, 2015.

[67] Keith A. LeGrand and Silvia Ferrari. The role of bounded fields-of-view and negative information in finite set statistics (FISST). In *Proceedings of the 2020 23rd International Conference on Information Fusion (FUSION)*, pages 1–9, July 2020.

[68] Keith A. LeGrand, Pingping Zhu, and Silvia Ferrari. Cell multi-Bernoulli (cell-MB) sensor control for multi-object search-while-tracking (SWT). 2021.

[69] Keith A. LeGrand, Pingping Zhu, and Silvia Ferrari. A random finite set sensor control approach for vision-based multi-object search-while-tracking. In *2021 24th International Conference on Information Fusion (FUSION)*, 2021.

[70] Friedrich Liese and Igor Vajda. On divergences and informations in statistics and information theory. *IEEE Transactions on Information Theory*, 52(10):4394–4412, 2006.

[71] Bryan D. Little and Carolin E. Frueh. Multiple heterogeneous sensor tasking optimization in the absence of measurement feedback. *The Journal of the Astronautical Sciences*, 67(4):1678–1707, 2020.

[72] Ronald P.S. Mahler. Multitarget Bayes filtering via first-order multitarget moments. *IEEE Transactions on Aerospace and Electronic Systems*, 39(4):1152–1178, 2003.

[73] Ronald P.S. Mahler. PHD filters of higher order in target number. *IEEE Transactions on Aerospace and Electronic Systems*, 43(4):1523–1543, October 2007.

[74] Ronald P.S. Mahler. *Statistical Multisource-Multitarget Information Fusion*. Artech House Boston, 2007.

[75] Ronald P.S. Mahler. *Advances in Statistical Multisource-Multitarget Information Fusion*. Artech House, 2014.

[76] Ronald P.S. Mahler and Tim R. Zajic. Probabilistic objective functions for sensor management. In *Signal Processing, Sensor Fusion, and Target Recognition XIII*, volume 5429, pages 233–244, aug 2004.

[77] James S. McCabe. *Multitarget Tracking and Terrain-Aided Navigation Using Square-Root Consider Filters*. Dissertation, Missouri University of Science and Technology, 2018.

[78] James S. McCabe and Kyle J. DeMars. Anonymous feature-based terrain relative navigation. *Journal of Guidance, Control, and Dynamics*, 43(3):410–421, aug 2019.

[79] Hoa Van Nguyen, Hamid Rezatofighi, Ba-Ngu Vo, and Damith C Ranasinghe. Multi-objective multi-agent planning for jointly discovering and tracking mobile objects. In *Proceedings of the AAAI Conference on Artificial Intelligence*, volume 34, pages 7227–7235, apr 2020.

[80] Dominik Nuss, Stephan Reuter, Markus Thom, Ting Yuan, Gunther Krehl, Michael Maile, Axel Gern, and Klaus Dietmayer. A random finite set approach for dynamic occupancy grid maps with real-time application. *The International Journal of Robotics Research*, 37(8):841–866, jul 2018.

[81] Jonatan Olofsson, Gustaf Hendeby, Tom Rune Lauknes, and Tor Arne Johansen. Multi-agent informed path-planning using the probability hypothesis density. *Autonomous Robots*, 2020.

[82] Jonah Ong, Ba-Tuong Vo, Ba-Ngu Vo, Du Yong Kim, and Sven Nordholm. A Bayesian 3D multi-view multi-object tracking filter. pages 1–14, 2020.

[83] Sabita Panicker, Amirali Khodadadian Gostar, Alireza Bab-Hadiashar, and Reza Hoseinnezhad. Tracking of targets of interest using labeled multi-Bernoulli filter with multi-sensor control. *Signal Processing*, 171, 2020.

[84] Neal Patwari, Joshua N. Ash, Spyros Kyperountas, Alfred O. Hero, Randolph L. Moses, and Neiyer S. Correal. Locating the nodes: cooperative localization in wireless sensor networks. *IEEE Signal Processing Magazine*, 22(4):54–69, 2005.

[85] Abu Sajana Rahmathullah, Ángel F. García-Fernández, and Lennart Svensson. Generalized optimal sub-pattern assignment metric. In *2017 20th International Conference on Information Fusion (Fusion)*, pages 1–8, 2017.

[86] Carl E. Rasmussen and Christopher K. I. Williams. *Gaussian Processes for Machine Learning*, volume 14. The MIT Press, 2004.

[87] Tharindu Rathnayake, Amirali Khodadadian Gostar, Reza Hoseinnezhad, Ruwan Tennakoon, and Alireza Bab-Hadiashar. On-line visual tracking with occlusion handling. *Sensors*, 20(3):929, feb 2020.

[88] Donald B. Reid. An algorithm for tracking multiple targets. *Automatic Control, IEEE Transactions on*, 24(6):843–854, 1979.

[89] Stephan Reuter, Ba-Tuong Vo, Ba-Ngu Vo, and Klaus Dietmayer. The labeled multi-Bernoulli filter. *IEEE Transactions on Signal Processing*, 62(12):3246–3260, 2014.

[90] Branko Ristic. *Particle Filters for Random Set Models*. Springer, New York, NY, 2013.

[91] Branko Ristic and Ba-Ngu Vo. Sensor control for multi-object state-space estimation using random finite sets. *Automatica*, 46(11):1812–1818, 2010.

[92] Branko Ristic, Ba-Ngu Vo, and Daniel Clark. A note on the reward function for PHD filters with sensor control. *IEEE Transactions on Aerospace and Electronic Systems*, pages 1521 – 1529, 2011.

[93] Branko Ristic, Ba-Tuong Vo, Ba-Ngu Vo, and Alfonso Farina. A tutorial on Bernoulli filters: Theory, implementation and applications. *IEEE Transactions on Signal Processing*, 61(13):3406–3430, 2013.

[94] Andrew R. Runnalls. Kullback-Leibler approach to Gaussian mixture

reduction. *IEEE Transactions on Aerospace and Electronic Systems*, 43(3):989–999, 2007.

[95] David J. Salmond. Mixture reduction algorithms for point and extended object tracking in clutter. *IEEE Transactions on Aerospace and Electronic Systems*, 45(2):667–686, 2009.

[96] Simo Särkkä. *Bayesian Filtering and Smoothing*. Cambridge University Press, 2013.

[97] Hedvig Sidenbladh. Multi-target particle filtering for the probability hypothesis density. In *Sixth International Conference of Information Fusion, 2003. Proceedings of the*, volume 2, pages 800–806, 2003.

[98] Peng Mun Siew, Daniel Jang, and Richard Linares. Sensor tasking for space situational awareness using deep reinforcement learning. In *2021 AAS/AIAA Astrodynamics Specialist Conference*, number August, 2021.

[99] Katherine M. Simonson and Tian J. Ma. Robust real-time change detection in high jitter. Technical report, Sandia National Laboratories, 8 2009.

[100] Per Skoglar. *Planning Methods for Aerial Exploration and Ground Target Tracking*. PhD thesis, Linköping University, 2009.

[101] Taek Lyul Song, Darko Musicki, and Kim Da Sol. Target tracking with target state dependent detection. *IEEE Transactions on Signal Processing*, 59(3):1063–1074, 2011.

[102] Harold W. Sorenson and Daniel L. Alspach. Recursive Bayesian estimation using Gaussian sums. *Automatica*, 7(4):465–479, 1971.

[103] Steven J. Spencer, Anup Parikh, Daniel R. McArthur, Carol C. Young, Timothy J. Blada, Jonathan E. Slightam, and Stephen P. Buerger. Autonomous detection and assessment with moving sensors. In *2020 IEEE/RSJ International Conference on Intelligent Robots and Systems (IROS)*, pages 8231–8238, 2020.

[104] Ratnasingham Tharmarasa and Thia Kirubarajan. Sensor management for large-scale multisensor-multitarget tracking. In Mahendra Mallick, Vikram Krishnamurthy, and Ba-Ngu Vo, editors, *Integrated Tracking, Classification, and Sensor Management*, chapter 12, pages 447–520. John Wiley & Sons, Inc., Hoboken, New Jersey, 2013.

[105] Martin Tobias and Aaron D. Lanterman. Probability hypothesis density-based multitarget tracking with bistatic range and doppler observations. *IEEE Proceedings-Radar, Sonar and Navigation*, 152(3):195–205, 2005.

[106] Rina Tse and Mark Campbell. Human-robot communications of probabilistic beliefs via a Dirichlet process mixture of statements. *IEEE Transactions on Robotics*, 34(5):1280–1298, 2018.

[107] Kirsten Tuggle and Renato Zanetti. Automated splitting Gaussian mixture nonlinear measurement update. *Journal of Guidance, Control, and Dynamics*, 41(3):1–10, 2018.

[108] Rudolph van der Merwe. *Sigma-point Kalman Filters for Probabilistic Inference in Dynamic State-space Models*. PhD thesis, Oregon Health & Science University, 2004.

[109] Iuliu Vasilescu, Keith D. Kotay, Daniela L. Rus, Matthew Dunbabin, and Peter I. Corke. Data collection, storage, and retrieval with an underwater sensor network. In *Proceedings of the 3rd International Conference on Embedded Networked Sensor Systems*, SenSys '05, pages 154–165, New York, NY, USA, 2005. Association for Computing Machinery.

[110] Ba-Ngu Vo and Wing-Kin Ma. The Gaussian mixture probability hypothesis density filter. *IEEE Transactions on Signal Processing*, 54(11):4091–4104, Nov 2006.

[111] Ba-Ngu Vo, Sumeetpal Singh, and Arnaud Doucet. Sequential Monte Carlo methods for multitarget filtering with random finite sets. *IEEE Transactions on Aerospace and Electronic Systems*, 41(4):1224–1245, 2005.

[112] Ba-Ngu Vo, Ba-Tuong Vo, and Dinh Phung. Labeled random finite sets and the Bayes multi-target tracking filter. *IEEE Transactions on Signal Processing*, 62(24):6554–6567, 2014.

[113] Ba-Tuong Vo and Ba-Ngu Vo. Labeled random finite sets and multi-object conjugate priors. *IEEE Transactions on Signal Processing*, 61(13):3460–3475, 2013.

[114] Ba-Tuong Vo, Ba-Ngu Vo, and Antonio Cantoni. The cardinalized probability hypothesis density filter for linear gaussian multi-target models. In *Information Sciences and Systems, 2006 40th Annual Conference on*, pages 681–686, March 2006.

[115] Ba-Tuong Vo, Ba-Ngu Vo, and Antonio Cantoni. Analytic implementations of the cardinalized probability hypothesis density filter. *IEEE Transactions on Signal Processing*, 55(7):3553–3567, July 2007.

[116] Ba-Tuong Vo, Ba-Ngu Vo, and Antonio Cantoni. The cardinality balanced multi-target multi-Bernoulli filter and its implementations. *IEEE Transactions on Signal Processing*, 57(2):409–423, 2009.

[117] Xiaoying Wang, Reza Hoseinnezhad, Amirali K. Gostar, Tharindu Rathnayake, Benlian Xu, and Alireza Bab-Hadiashar. Multi-sensor control for multi-object Bayes filters. *Signal Processing*, 142:260–270, 2018.

[118] Baishen Wei and Brett Nener. Distributed space debris tracking with consensus labeled random finite set filtering. *Sensors*, 18:1–26, 2018.

[119] Hongchuan Wei and Silvia Ferrari. A geometric transversals approach to sensor motion planning for tracking maneuvering targets. *IEEE Transactions on Automatic Control*, 60(10):2773–2778, 2015.

[120] Hongchuan Wei, Keith A. LeGrand, Andre A. Paradise, and Silvia Ferrari. Real-time communication control in decentralized autonomous. *Journal of Aerospace Information Systems*, 2022.

[121] Hongchuan Wei, Wenjie Lu, Pingping Zhu, Silvia Ferrari, Miao Liu, Robert H. Klein, Shayegan Omidshafiei, and Jonathan P. How. Information value in nonparametric Dirichlet-process Gaussian-process (DPGP) mixture models. *Automatica*, 74(June):360–368, 2016.

[122] Hongchuan Wei, Pingping Zhu, Miao Liu, Jonathan P. How, and Silvia Ferrari. Automatic pan-tilt camera control for learning Dirichlet process Gaussian process (DPGP) mixture models of multiple moving targets. *IEEE Transactions on Automatic Control*, 64(1):159–173, 2019.

[123] Peng Wei, Quanquan Gu, and Dengfeng Sun. Wireless sensor network data collection by connected cooperative UAVs. In *2013 American Control Conference*, pages 5911–5916, 2013.

[124] Mike West. Approximating posterior distributions by mixtures. *Journal of the Royal Statistical Society: Series B (Methodological)*, 55(2):409–422, jan 1993.

[125] Jason L. Williams. Marginal multi-Bernoulli filters: RFS derivation of MHT,

JIPDA, and association-based MeMBer. *IEEE Transactions on Aerospace and Electronic Systems*, 51(3):1664–1687, 2015.

[126] Ning Xiong and Per Svensson. Multi-sensor management for information fusion: issues and approaches. *Information Fusion*, 3(2):163–186, 2002.

[127] Murali Yeddanapudi, Yaakov Bar-Shalom, and Krishna R. Pattipati. IMM estimation for multitarget-multisensor air traffic surveillance. *Proceedings of the IEEE*, 85(1):80–96, 1997.

[128] Guoxian Zhang, Silvia Ferrari, and Chenghui Cai. A comparison of information functions and search strategies for sensor planning in target classification. *IEEE Transactions on Systems, Man, and Cybernetics - Part B*, 42(1):2–16, 2012.

[129] Yun Zhu, Li Zhao, Yumei Zhang, and Xiaojun Wu. Receiver selection for multi-target tracking in multi-static Doppler radar systems. *EURASIP Journal on Advances in Signal Processing*, 2021(1):118, 2021.